M. ABDUESSLAM

THEORETICAL INVESTIGATION OF CARBONYL SULFIDE CAPTURE BY ORGANIC SOLVENTS

THE GRADUATE SCHOOL OF NATURAL AND APPLIED SCIENCES
OF
ATILIM UNIVERSITY

MAHMOUD ABDUESSLAM

DOCTOR OF PHILOSOPHY THESIS
IN
THE DEPARTMENT OF MODELING AND DESIGN OF ENGINEERING SYSTEMS (MAIN FIELD OF STUDY: CHEMICAL ENGINEERING)

JULY 2021

ATILIM UNIVERSITY 2021

THEORETICAL INVESTIGATION OF CARBONYL SULFIDE CAPTURE BY ORGANIC SOLVENTS

A THESIS SUBMITTED TO
THE GRADUATE SCHOOL OF NATURAL AND APPLIED SCIENCES
OF
ATILIM UNIVERSITY

BY

MAHMOUD ABDUESSLAM

IN PARTIAL FULFILLMENT OF THE REQUIREMENTS
FOR
THE DEGREE OF DOCTOR OF PHILOSOPHY
IN
THE DEPARTMENT OF MODELING AND DESIGN OF ENGINEERING SYSTEMS (MAIN FIELD OF STUDY: CHEMICAL ENGINEERING)

JULY 2021

Approval of the Graduate School of Natural and Applied Sciences, Atilim University.

Prof. Ender KESKINKILIC
Director

I certify that this thesis satisfies all the requirements as a thesis for the degree of **Doctor of Philosophy in Modeling and Design of Engineering Systems. Main field of study: Chemical Engineering Department, Atilim University.**

Prof. Ender KESKINKILIC
Head of Department

This is to certify that we have read the thesis THEORETICAL INVESTIGATION OF CARBONYL SULFIDE CAPTURE BY ORGANIC SOLVENTS submitted by Mahmoud Abduesslam and that in our opinion it is fully adequate, in scope and quality, as a thesis for the degree of Doctor of Philosophy.

Assoc. Prof. Dr. Hakan KAYI
Co-Supervisor

Prof. Dr. Şeniz ÖZALP YAMAN
Supervisor

Examining Committee Members:

Prof. Dr. Şeniz ÖZALP YAMAN
Chemical Eng. Department, Atılım University

Prof. Dr. Yılser DEVRİM
Energy Systems Eng. Department, Atılım University

Assoc. Prof. Dr. Eylem GÜVEN
Nanotechnology and Nanomedicine Division,
Hacettepe University

Assoc. Prof. Dr. Murat TORUN
Hacettepe University

Asst. Prof. Dr. Enver GÜLER
Chemical Eng. Department, Atılım University

Date: July 07, 2021

I hereby declare that all information in this document has been obtained and presented in accordance with academic rules and ethical conduct. I also declare that, as required by these rules and conduct, I have fully cited and referenced all material and results that are not original to this work.

Mahmoud ABDUESSLAM:

Signature:

ABSTRACT

THEORETICAL INVESTIGATION OF CARBONYL SULFIDE CAPTURE BY ORGANIC SOLVENTS

Mahmoud Abduesslam

PhD, Modeling and Design of Engineering Systems (MODES) Department

Supervisor: Prof. Dr. Şeniz Özalp Yaman

Co-Supervisor: Assoc. Prof. Dr. Hakan Kayı

July 2021, 94 pages

Chemical engineers focus on the presence of carbonyl sulfide (COS) in industrial gases, and also consider natural occurrences of COS in liquefied petroleum gas. To comply with the environmental regulations and meet the strict environmental requirements of gas delivery industries, all impurities in gas streams that are toxic and have corrosive properties should be cleaned. Reactive absorption is a technique that is typically used for removing acids through the use of amines and alcohol mixtures, since it is considered as one of the most reliable ways to remove acid gases. In this study, capture of COS was investigated using the density functional theory (DFT) calculations at the theory level of ωB97X-D3/6-311++G(d,p) with the use of organic liquid mixtures. These mixtures consisted of amines, i.e., 1,8-diazabicyclo[5.4.0]undec-7-ene (DBU), 1,5-diazabicyclo[4.3.0]-non-5-ene (DBN), 2-tert-butyl-1,1,3,3-tetramethylguanidine (BTMG) and 1, 5, 7-triazabicyclo [4.4.0] dec-5-ene (TBD), as well as a number of linear alcohols, i.e., methanol, ethanol, 1-propanol, 1-butanol, 1-pentanol, and 1-hexanol. Throughout the study, a termolecular reaction mechanism of a modified single-step for 4 types of amines with 6 types of alcohol in the capture of COS was examined. In total eighteen different systems have been investigated, and the structural properties along with the thermodynamics and kinetics of the suggested COS capture reactions have been revealed in detail. The results showed that the suggested termolecular reaction mechanisms were thermodynamically feasible for the 18 different systems being tested, and the organic liquid combination of the BTMG and methanol

resulted in an energy barrier that was the lowest and a rate of reaction that was the highest in the capture of COS.

Keywords: Carbonyl sulfide capture, Density functional theory, Single-step reaction mechanism.

ÖZ

ORGANİK ÇÖZÜCÜLERLE KARBONİL SÜLFİT YAKALAMANIN TEORİK OLARAK İNCELENMESİ

Mahmoud Abduesslam
Doktora, Mühendislik Sistemlerinin Modellenmesi ve Tasarımı (MODES) Bölümü
Tez Yöneticisi: Prof. Dr. Şeniz Özalp Yaman
Ortak Tez Yöneticisi: Doç. Dr. Hakan Kayı

Temmuz 2021, 94 sayfa

Kimya mühendisleri, endüstriyel gazlardaki karbonil sülfitin (COS) varlığına odaklanırlar ve ayrıca sıvılaştırılmış petrol gazında COS'nin doğal oluşumlarını dikkate alırlar. Çevresel düzenlemelere uymak ve gaz dağıtım endüstrilerinin katı çevresel gereksinimlerini karşılamak için gaz akışlarındaki zehirli ve aşındırıcı özelliklere sahip tüm safsızlıklar temizlenmelidir. Reaktif soğurma, asit gazlarını gidermenin en güvenilir yollarından biri olarak kabul edildiğinden, aminler ve alkol karışımları kullanılarak asitleri gidermek için tipik olarak kullanılan bir tekniktir. Bu çalışmada, organik sıvı karışımları kullanılarak ωB97X-D3/6-311++G(d,p) teori düzeyinde yoğunluk fonksiyonel teorisi (DFT) hesaplamaları kullanılarak COS'nin yakalanması araştırılmıştır. Bu karışımlar, aminlerden, 1,8-diazabisiklo[5.4.0]undek-7-en (DBU), 1,5-diazabisiklo[4.3.0]non-5-en (DBN) ve 2-tert-bütil-1,1,3,3-tetrametilguanidin (BTMG) and 1, 5, 7-triazabicyclo [4.4.0] dec-5-ene (TBD)'den oluşmakta ve ayrıca bir dizi lineer alkol, yani metanol, etanol, 1-propanol, 1-butanol, 1-pentanol ve 1-hekzanol içermektedir. Çalışma boyunca, COS'un yakalanmasında 4 tip amin ile 6 tip alkol için modifiye edilmiş tek basamaklı bir termoleküler tepkime mekanizması incelenmiştir. Toplamda on sekiz farklı sistem araştırılmış ve önerilen COS yakalama tepkimelerinin termodinamiği ve kinetiği ile birlikte yapısal özellikleri ayrıntılı olarak ortaya konulmuştur. Sonuçlar, önerilen termoleküler tepkime mekanizmalarının test edilen 18 farklı sistem için termodinamik olarak uygulanabilir olduğunu ve BTMG ile

metanolden oluşan organik sıvı kombinasyonunun, COS yakalamada en düşük enerji bariyeri ve en yüksek tepkime hızı ile sonuçlandığını gösterdi.

Anahtar Kelimeler: Karbonil sülfit yakalama, Yoğunluk fonksiyoneli teorisi, Tek basamaklı tepkime mekanizması.

To My Family

{Father, Mother, Wife and Kids}

ACKNOWLEDGMENTS

I would like to express appreciation and gratitude to supervisor Prof. Dr. Şeniz Özalp Yaman and co-supervisor Assoc. Prof. Dr. Hakan Kayi for providing advice, guidance, and assistance throughout the research period, I am really grateful to you.

I shall also thank to all academic staff in the Chemical Engineering department of Atilim University.

I would like to thank my parents for their life-time care and encouragement, and how much I wished to see your faces on this day, and I hope God to be proud of me.

I would like to express my deep gratitude to my family (my wife, my kids, my brothers and my sisters) for their endless and continuous encouragement and support throughout the years.

Finally, I would like to thank everyone supported me, even if this support was a word.

TABLE OF CONTENTS

LIST OF TABLES

LIST OF FIGURES

LIST OF ABBREVIATIONS

ρ	Electron density
AO	Atomic orbital
B3LYP	Becke 3-term correlation functional; Lee, Yang, and Parr
BTMG	2-tert-butyl-1,1,3,3-tetrame thylguanidine
TBD	1, 5, 7-triazabicyclo [4.4.0] dec-5-ene
COS-BOLs	Carbonyl sulfide-binding organic liquids
DBN	1,5- diazabicyclo[4.3.0]non-5-ene
DBU	1,8-diazabicyclo [5.4.0] undec-7-ene
DFT	Density functional theory
E	Energy
E_a	Activation energy
E_{el}	Electronic energy Eigenvalue
E_{XC}	Exchange correlation energy
GTO	Gaussian-type orbitals
H	Hamiltonian operator
HF-SCF	Hartree-Fock self-consistent field
HK	Hohenberg and Kohn
IEF-PCM	Polarizable continuum model
k	Reaction rate constant
LCAO	Linear combination of atomic orbitals
MO	Molecular orbital
N	Number of electrons
PES	Potential energy surface concept
R	Position
STO	Slater-type orbitals
T	Time
V	Potential energy
V_{ext}	External potential
Z	Atomic number

$\Delta^{\ddagger}G^{\circ}$	Standard Gibbs free energy of activation
ΔG_{rxn}°	Standard Gibbs free energy of reaction
Ψ	Wave function
ωB97X-D3	Hybrid functionals

CHAPTER 1

INTRODUCTION

1.1. Problem Statement

Natural gas has grown in importance in the global energy matrix during the previous few decades, and its importance has been steadily increasing over time. The reason for this rise is that natural gas has gradually replaced coal and fuel oil as a more convenient and environmentally friendly alternative. Regardless, gas processing technologies play a part in its development since they can help with the extraction of inaccessible deposits [1]. Most gas fields contain considerable amounts of acid, carbon dioxide (CO_2), and sulfur compounds, such as hydrogen sulfide (H_2S) gas. It is true that sulfur compounds sour the gas, and if H_2S concentrations in natural gas exceed 5.7 mg/m^3, it is difficult to use [2]. There are some procedures that have been utilized in the removal of H_2S and other acid gases. A process such as this is what is known as a "sweetening process". This is because this process aids in the process of removing the acid gas.

In recent decades, acid gas treatment has grown in popularity. Since the implementation of increasingly rigors environmental rules, the efficiency of acid gas removal (CO_2 and H_2S) has greatly increased; thus, greater research work in this field is required. Because much recent research has concentrated on CO_2 and H_2S removal, specialists have paid little attention to the removal of less reactive sulfur compounds such as carbon disulfide (CS_2), mercaptans, and carbonyl sulfide (COS), despite the fact that they are also present in several industrial gases. Normally, environmental specifications are stated in terms of total sulfur content rather than merely H_2S; however, eliminating other sulfur compounds is equally critical [3, 4]. Such sulfuric compounds are very toxic; hence, they can poison catalysts and they are extremely detrimental to industrial equipment and pipelines [3, 5].

To comply with environmental pollution prevention requirements, it is necessary that these contaminants in the gas streams, which were mentioned previously above, are removed and then handled in an environmentally appropriate manner. Reactive absorption, which frequently employs alkanolamines as absorbents, is likely the most commonly chosen technology that is used in the removal of acid gas in gas processing operations [5–7].

1.2. Purpose of the Study

The present thesis focused on achieving the following goals:

- Understanding the process of removing COS using organic solvent mixtures.
- Investigating and revealing kinetics of the reaction when COS absorption takes place in an organic solvent mixture.
- Finding an effective organic solvent to remove COS.

1.3. Aims and Objectives

The aims of this study included investigating the COS absorption and its reaction kinetics in organic liquids [COS-binding organic liquids (COS-BOLs)], as well as evaluating their potential for the COS removal. To achieve these aims, specific objectives were set:

- Conducting a performance evaluation of a one-step reaction with the aim of obtaining reaction rate constants for the reaction that occurs between amidine or guanidine organic bases, which, in this research, comprised 1,8-diazabicyclo [5.4.0] undec-7-ene (DBU), 1,5-diazabicyclo [4.3.0]-non-5-ene (DBN), and 2-tert-butyl-1,1,3,3-tetramethylguanidine (BTMG), 1, 5, 7-triazabicyclo [4.4.0] dec-5-ene (TBD) and COS in the presence of linear alcohols.
- Conducting an evaluation of the dominant base effect that was observed while conducting the kinetic calculations of the termolecular reaction, as well as the effect that each of the alcohols had during the reactions.

1.4. Scope of the Study

The main scope of the current research study is to obtain first-hand knowledge about the new COS-BOL, as well as to understand its behavior in removing COS.

1.5. Thesis Outline

This design of this thesis was organized in the following manner:

It starts with an introduction section, as described above in Chapter One. Chapter Two provides a literature survey on capturing COS by applying organic solvents. Chapter Three explains the research methodology to represent the work in detail and the steps supporting the work by reviewing the previous literature, as well as the use of modeling to simulate and reveal the details of the structural and energetic interactions that occur for a single-step termolecular reaction. Chapter Four mainly presents the results and discusses them. Finally, Chapter Five presents the conclusions and recommends the future course of action.

CHAPTER 2

LITERATURE SURVEY

2.1. Chapter Overview

Now, the acid gas removal process will be introduced.

This chapter mentions several processes, such as acid gas removal, and explains the best available technology for removing acid gas from natural gas through amine treatment and reactive absorption, which are popular industrial processes.

2.2. Reasons for Acid Gas Removal

As mentioned previously, natural gas that has been extracted from gas and oil wells comprises a significant quantity of carbon dioxide (CO_2) and sulfur compounds. Normally the acid gas proportion in natural gas is different for almost every gas field, and the impurities of acidic gases deter the properties of natural gas.

In the cryogenic conversion of natural gas to CO_2 and LNG, for instance, the substances are transformed into solid state, which stops the liquid transportation in pipes. Sometimes, the corrosiveness of H_2S decreases the service time that is necessary for these transportation pipes. Furthermore, H_2S is very harmful and dangerous to humans and CO_2 has no heating value. As a consequence of this, the acid gas impurities that are found in natural gas are concentrated; thus resulting in the necessity for this concentration to be decreased down to a specific level prior to the initiation of any further processes [8–10].

2.3. Acid Gas Removal Technologies

Traditional technologies for removing acid gas are given below [8]:

- **Physical Absorption:** This process physically absorbs acidic gases in a specific organic solvent without the need chemical processes. Since acid gases are highly soluble, they are absorbed by the solvent. Their solubility increases when the temperature is reduced and pressure is increased; hence, the cost of physical absorption and operational procedures is higher when compared to amine processes, because it requires refrigerating units and high-pressure exerting equipment. Although the application of a physical solvent for bulk acid gas removal removes large quantities of gas, when a chemical solvent is used, the concentration of acid gas will be much lower. Since some physical solvents are cheaper, choosing either an amine solvent or a physical one depends on the requirements involved. However, anime absorbing chemicals are more popular.
- **Chemical Absorption:** When chemical absorption is initiated, the components of acidic gases chemically react in a solvent, which transforms them into dissolved chemicals. A stripper column is used to apply heat and regenerate the solvent. When heat is applied, it removes the chemical bond between the solvent and the acid gases, and therefore, the solvent gases are removed. Alkanolamine is the most commonly used solvent to absorb acidic gases, and it is used in the amine process.
- **Hybrid Process:** When a hybrid process is chosen, it combines the use of both chemical and physical solvents so as to be able to benefit from the advantages provided by both of these processes.
- **Membrane Separation Process:** In this process, membrane separation is performed for CO_2 removal in bulk; thus, it is commonly chosen when there is high concentration of CO_2.

2.4. Amine Process

The gas industry utilizes chemical solvent absorption on a commercial scale to remove acid gas impurities, and, as mentioned earlier, chemical solvent technology is currently used for this purpose (amine-based absorbents). Popular amine chemical solvents include alkanolamines, which have been used in many industries to remove CO_2. For

natural gas treatment, ammonia and H_2 production, and capturing CO_2 from combustible gases, alkanolamines are commonly used [8]. This process was first developed in the 1930s [8], but now, methyldiethanolamine (MDEA) and monoethanolamine (MEA) aqueous solutions are popular gas sweetening solvents. Some industries use blended amines to improve gas quality and reduce operating costs [10]. It should be kept in mind that MDEA is better due to its selective H_2S removal from the mixture. This happens as a result of the higher reaction rate between MDEA and H_2S, which is certainly greater than its reaction rate with CO_2 [11]. This happens because H_2S gas has H^+ ions, so they shift to MDEA through speedy and spontaneous proton transfer. When compared to the rest of the amines, MDEA has better stability, lower volatility, and is less corrosive. Moreover, it has a higher absorption capacity and lower reaction to heat [11].

2.5. Amine Type

Commercially, four amine types are used for acidic gas removal, which include MEA (primary amines), diethanolamine (DEA) (secondary amines), MDEA (tertiary amines) and piperazine (PZ) (cyclic amines). Figures 2.1 and 2.2 show the chemical structures of these different amines [8].

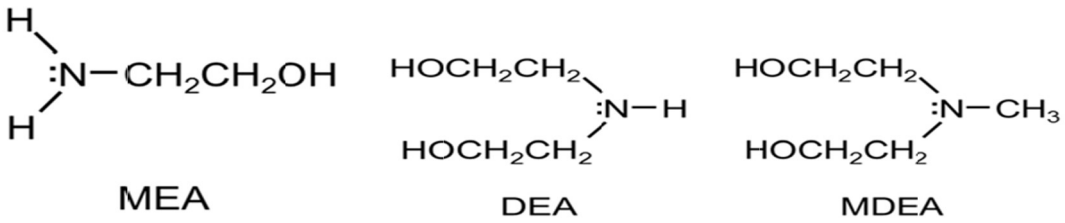

Figure 2.1. Representation of the chemical structure of the primary amine, secondary amine, and tertiary amine [8].

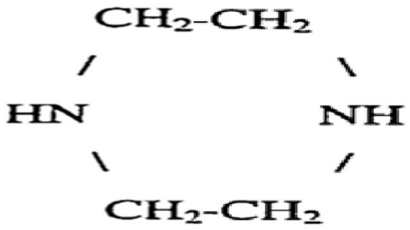

Figure 2.2. Representation of the chemical structure of the cyclic amine PZ [8].

2.5.1. Amidine and Guanidine Catalysts

The past decade has witnessed a massive increase in the usage and development of organo-catalysis, which require a catalyst to act like a nucleophile. Both amidines and guanidines are strong organic bases, but their small molecules with fundamental functional groups also function like nucleophilic catalysts.

Guanidines and amidines are significant compound classes, which exist in nature, and they are used in organic chemistry [12–17].

Guanidines and amidines are commonly used as organic alkalis. They are strong organic bases, and they have protonated forms, which delocalize charge in a couple of nitrogen atoms. The structures of common amidines and guanidines are shown (Figure 2.3) [15, 18]. Such alkalis are widely used in several organic reactions; hence, they have definitive advantages when compared to other organic alkalis, such as the bicyclic amidines DBU and DBN are commonly used for dehydrohalogenation reactions, because they allow alkene bonds to form under mild conditions, so they are better than other nitrogenous bases [19]. Both guanidines and amidines have useful physical coordination properties [13].

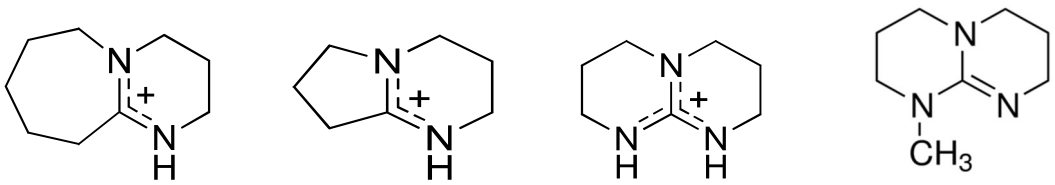

Figure 2.3. Structure of some commonly used amidine and guanidine bases.

Amidines and guanidines have been conventionally considered as non-nucleophilic alkalis, but when interest in organo-catalysis [14] increased, researchers declared some amidines and guanidines as nucleophilic catalysts, which were suitable for a wide range of reactions. Several structurally related derivatives of isothiourea have been prepared due to the amazing potential that amidines and guanidines have as acyl transfer catalysts [13, 20, 21]. Nucleophilic catalysts have structural diversity, which is based on isothiourea, guanidine cores, and amidines, which include structures with

stereo-centers, and that makes this type of catalyst useful for large numbers of stereo-selective and achiral reactions.

2.6. Carbonyl Sulfide Removal

2.6.1. Chemical Properties of Carbonyl Sulfide

COS is a linear molecule with the structure of O=C=S. As COS and CO_2 are structurally similar and have the same number of valence electrons, they share some similarities in their chemical properties and reactions. The boiling point of COS is −50 °C at 1 atm [22]; hence, COS exists in the gas phase on the earth's surface. COS is soluble in water, even though it has lower solubility than CO_2 [23]. Due to the difference between the electro-negativities of oxygen and sulfur, the length of the C-S bond is significantly longer than that of the C-O bond (1.56 vs. 1.16 Å) [22]. Thus, unlike CO_2, COS is a polar molecule (dipole moment 0.715 D) [24]. Its hydrolysis in water differs from the hydrolysis of CO_2. The asymmetry of the COS molecule gives rise to a more complicated rotational and vibrational spectrum than that of CO_2 [25].

2.6.2. COS Effect on the Environment

COS is a very tiny environmental component, because the atmosphere only has approximately 0.5 ppb of it, and its lifetime is just a few years [26]. Hence, if we consider its oxidation, which takes place by hydroxyl ion, it is above 9 years; however, since it is a chemically stable compound, it survives in the atmosphere for almost 4 years [26–28].

The major source of COS is the ocean, which has direct, indirect (CS_2), and dimethyl-sulfide (DMS) emissions, which immediately oxidize to form COS [29].

Different industrial plants and refineries operating in the energy sector are sources of COS, as well as other sulfur compounds, which all have serious environmental impact.

2.6.3. Health and Safety

Since COS irritates the eyes, skin, throat, lungs, and nose, which results in sneezing and coughing, it has the ability to form H_2S through hydrolysis [30]. For low or moderate concentrations of vapors, a highly noticeable irritant action appears in the form of painful and severe conjunctivitis, which leads to tears or lachrymation, and light sensitivity or photophobia [30, 31]. If the concentrations are either low or moderate, it results in diarrhea, nausea, headache, mental confusion, and profuse salivation, but the response is different for different people; therefore, precisely limiting the concentration is impossible and inadvisable. In the event that a person is exposed to a high vapor concentration, it might lead to tremors, sudden collapse, tachycardia, or blurred vision, while prolonged exposure results in coma, death, or unconsciousness due to respiratory paralysis [31]. Sub-lethal exposure to high concentrations might lead to slow recovery, low pulse rate, amnesia, or even cardiac dilation. Normally, complete recovery takes place when there is a nonfatal case. As mentioned previously, it is impossible to exactly define a high vapor concentration [32, 33], but generally, a concentration of 0.1% $^{vol}/_{vol}$ or more can cause death within 2 h.

2.6.4. Carbonyl Sulfide in Petroleum and Natural Gas

In petroleum, COS is found in tiny fractions, which makes it an issue in different petrochemical procedures. Since both COS and propane have almost same boiling points (–50.2 °C for COS and –44.5 °C for propane), after separation, only 10% COS is found in ethane, while 90% exists in propane.

When COS occurs in natural gas, it is generally saturated with water, and before processing, this COS is mostly hydrolyzed into H_2S. The frequency of COS in the downstream has been identified. COS quantitative trapping should be undertaken using a cryogenic trapping process, which is performed at –150 °C without the use of liquid cryogens [35].

2.6.5. Uses of Carbonyl Sulfide

COS has been used for the industrial synthesis of sulfur-trisubstituted carbinols, thio acids, substituted thiocarbamic acids, and substituted thiazoles (pharmaceutical anti-inflammatory drugs, flavors, and fragrances). Particularly when dealing with substituted thiazoles, high yields are obtained.

2.6.6. Carbonyl Sulfide Chemistry, the Claus Reaction

Recently, experts have realized the importance and benefits of COS for different industries when environmental concerns were raised. For example, the Claus reaction is very important for gas desulfurization, and obtains sulfur at high temperatures through the oxidization of H_2S at almost 850 °C. Using Eqs. (2.2) and (2.3), it was possible to obtain Eq. (2.4), which is given below:

$$3H_2S + 3/2O_2 \rightarrow 2H_2S + SO_2 + H_2O \quad (2.1)$$

$$2H_2S + SO_2 \rightarrow 3S + 2H_2O \quad (2.2)$$

$$3H_2S + 3/2O_2 \rightarrow 3S + 3H_2O \quad (2.3)$$

Here, it is obvious that H_2S combustion first leads to SO_2 formation and water is also obtained [Eq. (2.2)]. The obtained SO_2 further reacts with the H_2S and expels condensed sulfur, and water is also obtained [Eq. (2.3)]. Moreover, CO_2 also forms during the combustion process, which yields CS_2 and COS when it reacts with H_2S, as shown in Eqs. (2.5) and (2.6).

$$CO_2 + H_2S \rightarrow COS + H_2O \quad (2.4)$$

$$CO_2 + 2H_2S \rightarrow CS_2 + 2H_2O \quad (2.5)$$

In the Claus reaction, COS is a pollutant because it yields H_2S and CO_2 [34] when it undergoes hydrolysis, which is given in Eq. (2.7):

$$COS + H_2O \rightarrow CO_2 + H_2S \quad (2.6)$$

Generally, H_2S and CO_2 are the hydrolysis products, which are easier to remove from refinery gases when compared to COS; therefore, the downstream removal of COS through a Claus converter requires costly treatments [36].

Reactive absorption is perhaps the best acid gas removal technology in gas processing industries [5–7].

Several studies have been conducted using a wide range of solvents to investigate COS absorption over the last few decades [37–45], and both single-step and two-step (zwitterion) molecular reaction mechanisms have been proposed. Now, most researchers are attempting to find the best solvents for absorption capacity enhancement, improve the reaction rate, and reduce the heating needs for COS and CO_2 absorption. An alternative approach to capture COS is the application of organic alcoholic liquids that have a strong guanidine or amidine base rather than the use of aqueous solutions. This was proposed due to the fact that CO_2 and COS have structural similarity, because both of them are linear compounds; hence, this similarity is reflected in their reactions [37, 40, 41]. Many researchers have used this assumption to build theories specifically on reaction mechanisms. They proposed the reaction mechanism as: the reaction between COS and organic alcohol-based mixtures of amine, and the formation of zwitterion has been observed, which increased the system polarity. This means that at low temperatures, desorption is possible because of a reduction in the COS binding enthalpy [7, 46]. Moreover, the alcohol type or amine affects the reaction rate during the capturing process, which means that it is a tunable property of organic mixtures.

An approach to using alcohol-based COS is the binding of organic liquids (COS-BOLs) and using a strong guanidine/amidine base rather than using amines [46, 47].

After reviewing the literature, it was noticed that COS removal requires an in-depth understanding regarding kinetics and reaction mechanisms when it is immersed and dissolved in alkanolamines.

2.6.7. Reaction Mechanism for COS Capture

Organic liquid mixtures react using COS and primary/secondary amines, which have been explained in the studies by termolecular and zwitterion reaction processes [37, 41]. Caplow [48] was the first to propose the zwitterion mechanism for CO_2 absorption reaction. Later, Danckwerts [49] discussed it again. There are two sequential reactionary steps in a zwitterion mechanism. Zwitterion formation is the first step in COS-amine reaction, and the second step is thiocarbamate ion formation when a protonated base in the zwitterion reacts with another base [5, 41, 43–45, 50–51]. A study was conducted by Crooks and Donnellan [52], which was regarding the reaction that occurred between CO_2 and amines within aqueous solutions. Alper and Bouhamra [37] suggested that in aqueous solutions, COS reacts just like CO_2, which is shown in Eq. (2.7).

$$COS + R_2NH\ldots B \rightleftarrows R_2NCOS^{-}\ldots BH^{+} \tag{2.7}$$

For COS absorption reactions, amidine bases, such as DBU or DBN, are used. A guanidine base BTMG is also used with an alcohol. After this, a termolecular reaction mechanism that has been modified can then be initiated, which is similar to CO_2-binding organic liquids (CO_2-BOLs) [53–55], as is given below:

$$COS_{(g)} + amine_{(l)} + ROH_{(l)} \rightleftarrows [amine - H^{+}]\,[R - O - COS^{-}]_{(l)} \tag{2.8}$$

$$COS_{(g)} + DBU_{(l)} + ROH_{(l)} \rightleftarrows [DBUH^{+}]\,[ROCOS^{-}]_{(l)} \tag{2.9}$$

$$COS_{(g)} + DBN_{(l)} + ROH_{(l)} \rightleftarrows [DBNH^{+}]\,[ROCOS^{-}]_{(l)} \tag{2.10}$$

$$COS_{(g)} + BTMG_{(l)} + ROH_{(l)} \rightleftarrows [BTMGH^{+}]\,[ROCOS^{-}]_{(l)} \tag{2.11}$$

$$COS_{(g)} + TBD_{(l)} + ROH_{(l)} \rightleftarrows [TBDH^{+}]\,[ROCOS^{-}]_{(l)} \tag{2.12}$$

In these reactions mentioned above, the H atom that is in the alcohol included in the hydroxyl group. The atom also has a link to the nitrogen atom that is in the DBN, DBU, or BTMG, TBD and they then have a further link to a couple of carbon atoms.

Thus, a covalent bond is formed between the carbon atom in the COS and the O atom in the alcohol, and this thus brings about the formation of zwitterionic products, which are shown in Figure 2.4, 2.5, 2.6, 2.7 and Eq. (2.8).

Figure 2.4. Representatives of the mechanism of reaction by means of COS/DBU/methanol, which consists of reactant (on the left), transition state (in the center), and product (on the right).

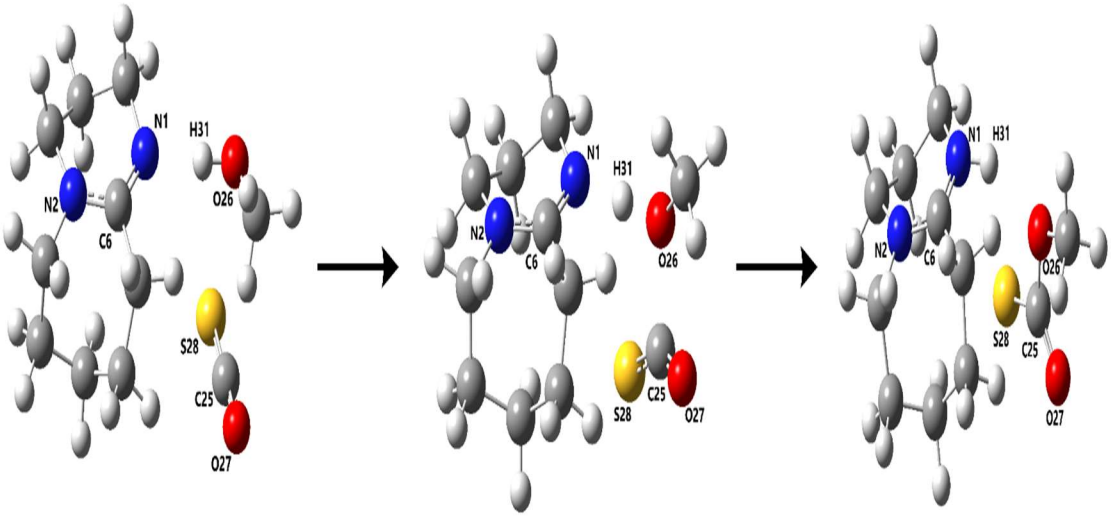

Figure 2.5. Representatives of the mechanism of reaction by means of COS/DBN/methanol, which consists of reactant (on the left), transition state (in the center), and product (on the right).

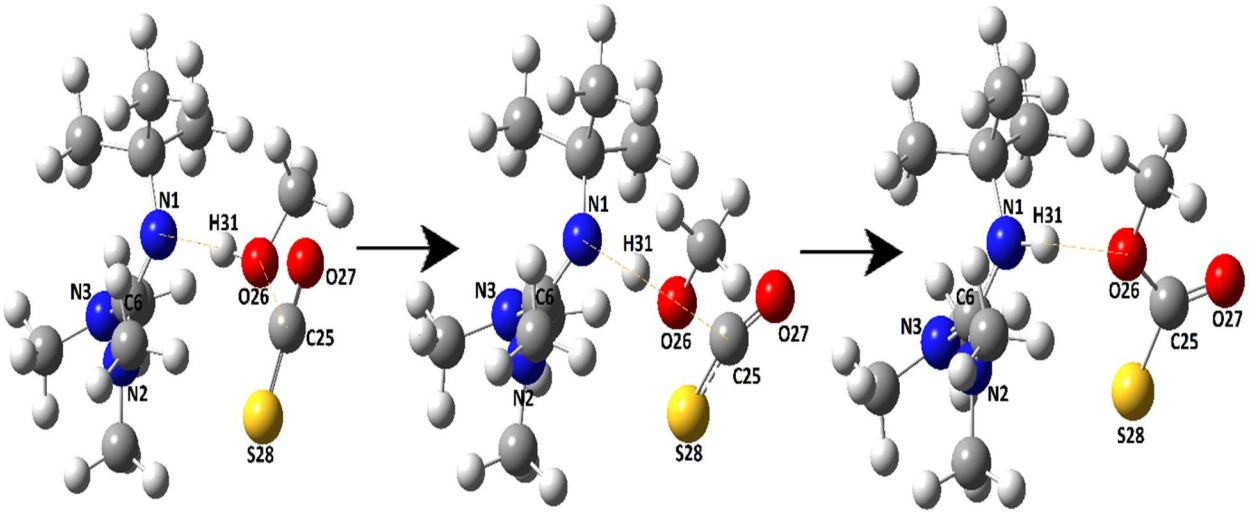

Figure 2.6. Representatives of the mechanism of reaction by means of COS/BTMG/methanol, which consists of reactant (on the left), transition state (in the center), and product (on the right).

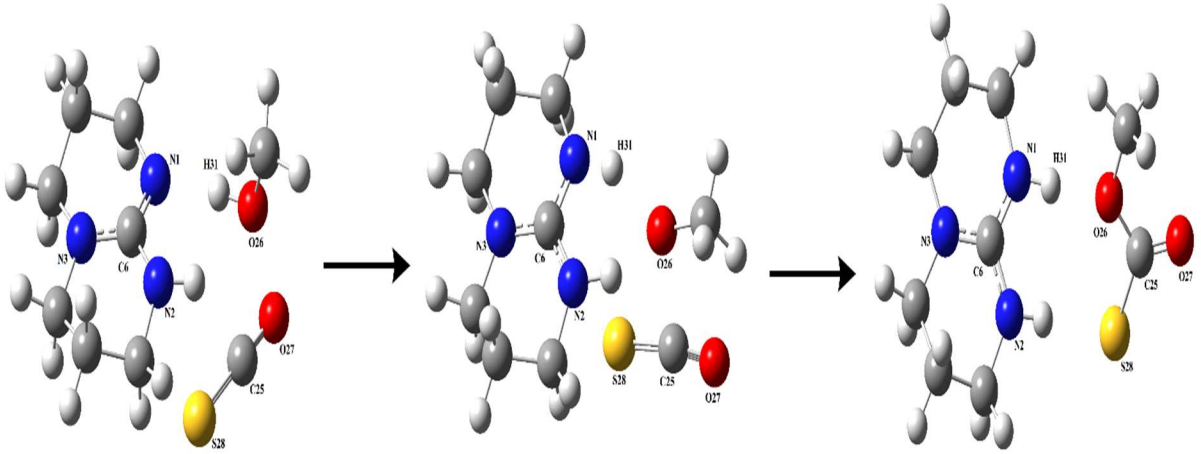

Figure 2.7. Representatives of the mechanism of reaction by means of COS/TBD/methanol, which consists of reactant (on the left), transition state (in the center), and product (on the right).

The observed forward reaction rate is shown in Eq. (2.13) using pseudo first-order conditions when there is an excessive amount of organic liquid, which comprises a mixture of the amine and the alcohol.

$$r_o = k_o[COS] \tag{2.13}$$

The COS capture systems containing DBU, DBN BTMG and TBD are shown in Eq. (2.14), where it can be seen that k_o (mechanism 2.8) resembles the COS-BOL systems [53–55].

$$k_o = \{k_{amine}\,[amine] + k_{ROH}\,[ROH]\}\,[amine] \quad (2.14)$$

$$k_o = \{k_{DBU}\,[DBU] + k_{ROH}\,[ROH]\}\,[DBU] \quad (2.15)$$

$$k_o = \{k_{DBN}\,[DBN] + k_{ROH}\,[ROH]\}\,[DBN] \quad (2.16)$$

$$k_o = \{k_{BTMG}\,[BTMG] + k_{ROH}\,[ROH]\}\,[BTMG] \quad (2.17)$$

$$k_o = \{k_{TBD}\,[TBD] + k_{ROH}\,[ROH]\}\,[TBD] \quad (2.18)$$

In the event that there is an excessive volume of alcohol, Eq. (2.19) shows the rate constant, k, with a constant concentration of alcohol:

$$k = k_{ROH}\,[ROH], \quad (2.19)$$

and then k_o, which includes k, becomes:

$$k_o = \{k_{amine}\,[amine] + k\}\,[amine] \quad (2.20)$$

$$k_o = \{k_{DBU}\,[DBU] + k\}\,[DBU] \quad (2.21)$$

$$k_o = \{k_{DBN}\,[DBN] + k\}\,[DBN] \quad (2.22)$$

$$k_o = \{k_{BTMG}\,[BTMG] + k\}\,[BTMG] \quad (2.23)$$

$$k_o = \{k_{TBD}\,[TBD] + k\}\,[TBD] \quad (2.24)$$

The reaction order for the systems used to capture the COS equals one. This is because the alcohol is the dominant base; therefore, for (mechanism 2.8), the k_o expressions are given below:

$$k_o = k\,[\text{amine}] \tag{2.25}$$

$$k_o = k\,[\text{DBU}] \tag{2.26}$$

$$k_o = k\,[\text{DBN}] \tag{2.27}$$

$$k_o = k\,[\text{BTMG}] \tag{2.28}$$

$$k_o = k\,[\text{TBD}] \tag{2.29}$$

Now, it is appropriate to mention that the reaction order is two when the amine is a dominant base. Moreover, recent studies on capturing CO_2 through CO_2-BOLs [53–55] have shown that the pseudo first-order conditions were focused on for the forward reaction rate. The kinetics and thermodynamics of COS capturing reactions have been investigated when organic liquids were used as suitable solvents. For simulating the dominant base effect of the alcohols that were under study herein, so as to be able to determine the kinetics of the termolecular reaction, in these mentioned studies, the researchers used the integral equation formalism-polarizable continuum model (IEF-PCM) [56–58]; hence, the alcohols implicitly affected the reaction.

CHAPTER 3

METHODOLOGY COMPUTATIONAL CHEMISTRY

3.1. Introduction

A few decades ago, several alkanolamines were studied to dissolve COS and CO_2. However, some shortages or limited clarifications pertaining to the molecule structures and their chemical equilibrium still exist [59].

The researchers pondered how a theory could be proven through an experiment, and how to solve the experimental problems using theoretical systems.

The search for the answers to these questions led the research community towards computational modeling [60].

Chemical engineering and applied chemistry require specific processes, costs, or trials to understand the accompanying risks, which aid in achieving the best performances in the studied system.

Another question was: Why should computers be used to do molecular modeling?

A model was prepared to be specifically applied in a definitive area or chemical space [60].

Molecular modeling aids researchers in understanding the details of molecules, and it has the following benefits [61]:

- It is more appropriate than the classic methods.
- The models are like actual molecules.
- Rotating the model is possible using a computer, so as to observe it from different angles.

- Atomic positions can be seen in several ways.
- Corrections can be made to incorrect drawings.
- For unstable molecules, modeling is better than hand drawings.
- It is possible to display and predict various properties, such as energies, attractive forces, frequency properties, and spectra.

Based on the mentioned benefits, computer-aided molecular modeling is more appropriate because it involves imagination, study, research, and the optimization of chemical processes.

Improvements in chemical theories and computational and software/hardware are inter-related. The inability to solve equations leads to difficulties in testing a theory; however, computational and technological improvements make such theories relevant and applicable, despite the fact that they have complex systems [60].

Theories are drafted to assure the generality of a finding. Most theories can be applied in the case of macroscopic systems, but that is not the case with small systems. For example, Quantum theory is defined through intractable equations; however, it is ideal for small systems because the mentioned model simplifies quantum calculations and gives them the form of a general theory [60].

This model applies to a definite volume, also termed as chemical space, through calculations to simplify the approximations, which are needed to generalize a theory [60].

Theoretical chemistry illustrates the following [62]:

- The structural geometries of molecules.
- Advanced properties like energies, wave functions, polarization, IR vibrations, nuclear magnetic resonance (NMR), and dipole moments.
- The inter-molecular interaction and potential energies of different reactions.

The field of computational chemistry has been growing very fast, as it is a form of theoretical chemistry, which focuses on solving chemical problems through calculations [62].

The capability to create data and analyze the wave function is one of the greatest effects of computational chemistry, which provides a better understanding into gain insight and highlights. In this way, the behaviors of different molecular groups can be justified [62].

Computational chemistry is new and old at the same time; old because it has existed since the development phase of quantum mechanics, during the early twentieth century, and young because it is based on the latest technology, including computers and software [60].

Mathematical procedures are extensively used in the two-particle system, but they are not as effective for multi-particle systems. Many computational processes can solve such problems to obtain approximated solutions [62].

Now it is necessary to review the background of particle theories before going deeper in the computational methodologies.

3.2. Quantum Mechanics

Quantum mechanics calculations are used for clarifying the reaction mechanism, and highlighting the processes involved in it [59].

This is a benefit because it allows the opportunity to calculate chemical properties with or without experimental data. Recently, quantum mechanics has improved in terms of calculations and applications pertaining to computational chemistry, and such calculations have been successfully applied to research for assessing the molecular structures, reaction mechanisms, and spectroscopic characterizations and thermodynamics of the studied systems [59].

The mathematical expression for dynamical equations for particle velocity and mass are subdivided into four regimes (Figure 3.1).

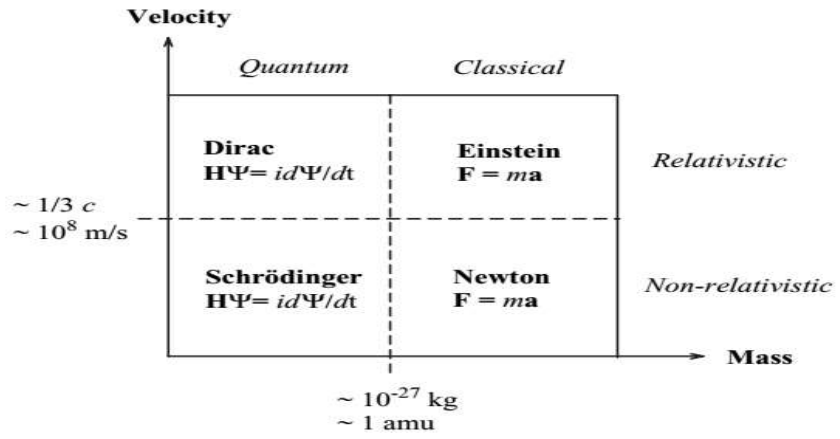

Figure 3.1. Domains of the dynamical equations [62].

The classic approach is very different when compared to quantum mechanics, because the later just explains approximations or probabilities, while the former is thought to be deterministic [62].

Classical/deterministic mechanics is based on the integration of Newton's equations, which define the locations of the particles at certain times. Using this type of mechanics, it is possible to predict the location and time of solar eclipses with remarkable accuracy; however, quantum mechanics calculates both the time and location in terms of probability, and the probability function is determined by taking the square of the wave function, as shown below:

$$P\,(\mathbf{r},t) = \Psi^2\,(\mathbf{r},t). \tag{3.1}$$

Here, **r** represents the location/position, while *t* shows the time, and the wave function is denoted by Ψ, which is computed by solving the Schrödinger or Dirac equation (Figure 3.1) [62].

The electronic Schrödinger equation (time-independent) for an *N*-electron atomic or molecular system can be given as in the following equation:

$$H\Psi = E\Psi. \quad (3.2)$$

In this equation, the Hamilton operator (H) sums up the potential as well as kinetic energies, which can be termed as electronic energy [63].

The target is approximated in the quantum chemical approaches. The Schrödinger equation is given below:

$$H\,\Psi_i(X_1, X_2, \dots, X_N, R_1, R_2, \dots, R_M) = E_i\Psi_i(X_1, X_2, \dots, X_N, R_1, R_2, \dots, R_M). \quad (3.3)$$

Here, H represents the Hamiltonian operator of a molecular system, which has N electrons and M nuclei. In this case, the wave function, Ψ_i, possesses all possible information regarding the ith state of the quantum system that is under study. It relies on X_M, which are the spatial coordinates of the nuclei) and X_N (spatial and spin coordinates). Here, Ψ_i describes E_i, which is a numerical value of energy. Moreover, H is a differential operator as well, which shows the total energy, as shown below:

$$H = -\frac{1}{2}\sum_{i=1}^{N}\nabla_i^2 - \frac{1}{2}\sum_{A=1}^{M}\frac{1}{M_A}\nabla_A^2 - \sum_{i=1}^{N}\sum_{A=1}^{M}\frac{Z_A}{r_{iA}} + \sum_{i=1}^{N}\sum_{j>i}^{N}\frac{1}{r_{ij}} + \sum_{A=1}^{M}\sum_{B>A}^{M}\frac{Z_A Z_{AB}}{R_{AB}}. \quad (3.4)$$

In this equation, i and j denote the system electrons; A and B both run over the M nuclei; A, r, and R denote the inter-particle distances; and M_A denotes the mass of the nucleus. In the Eq. (3.4), the term 1 depicts the electron's kinetic energy, term 2 depicts the electron's nucleic kinetic energy, and the restof the equation depicts the electron's potential energy. Term 3 depicts the electron-nucleus electrostatic interaction, while terms 4 and 5, respectively, depict the repulsiveness because of the electron-electron and nucleus-nucleus interactions [64].

According to the variational principle, the energy determined through a wave function will always be equal to or more than the exact energy [62].

This principle is important for every quantum chemical application. Standard quantum mechanics show that observable operator O has the expected value of wave function Ψ_{trial}, as demonstrated by Koch and Holthausen [64]:

$$\langle O \rangle = \int \ldots \int \Psi^*_{trial}\, O\, \Psi_{trial}\, \mathrm{d}\vec{\mathrm{x}}_1 \mathrm{d}\vec{\mathrm{x}}_1 \ldots \mathrm{d}\vec{\mathrm{x}}_1 \equiv \langle \Psi_{trial} | O | \Psi_{trial} \rangle. \quad (3.5)$$

Both the Dirac and Schrödinger equations (Figure 3.1) look similar; however, their difference is based on factor *H*. In the case of small mass particles, for example, electrons, the Schrödinger equation will be applied [62], as follows:

$$H\Psi = i\frac{\partial \Psi}{\partial t}. \quad (3.6)$$

The Hamiltonian operator sums up all kinetic (*T*) and potential (*V*) energies.

$$H_{Schrodinger} = T + V \quad (3.7)$$

The Schrödinger equation shows results in the form of Eq. (1), which finds a the probability of a particle at time *t* and position **r**.

Light particles move at a mere fraction of the speed of light, and the Dirac equation is used in this case.

$$H\Psi = i\frac{\partial \Psi}{\partial t} \quad (3.8)$$

Here, the Hamiltonian operator is more complex.

$$H_{Dirac} = (c\boldsymbol{\alpha}.\mathbf{p} + \boldsymbol{\beta}mc^2) + V \quad (3.9)$$

Both **α** and **β** exist in the form of 4 × 4 matrices, while the relativistic wave function is made up of 4 components that are both large and small, and each one of them has α and β spin functions that differ from the **α** and **β** matrices. Here, wave functions have two components: electronic (large components) and positronic (small components), wheras the **α** and **β** matrices couple components such as these. When the limit $c \rightarrow \infty$, the Schrödinger equation forms when Dirac equation is reduced; hence, the wave function components are reduced into the α and β spin orbitals [62].

The physical properties of the system are described through a wave function; thus, factors (operators) are applied in quantum mechanics according to the studied physical

properties. The probabilities and expectations allow a system to give a certain value/values for the physical property/properties [60].

Both atoms and molecules have more weight when compared to electrons; hence, they basically behave like classical particles. Quantum mechanics, on the other hand, describes electrons as lighter and also mentions their particle properties [62].

Defining a wave function or giving it a physical explanation is not possible. There is no possibility of directly deriving a wave function [65].

When trying to solve the electronic Schrödinger equation for a molecule; in that case, every electron function will become a molecular orbital (MO) [62].

A spin quantum number describes electrons, but it cannot be assigned to two electrons. Then, in the opposite spin, the MO is fixed for two electrons [65].

Although the Schrödinger equation is accurate, it is over-complicated, that a H_2 atom is the greatest system it can analytically solve. For calculating the multi-particle system, Dirac and others conducted several approximations [65].

In the next sections, some of these approximations have been summarized.

3.3. Ab Initio Computation Methods

These methods require no approximation other than the one that was mathematically tested. In this context, a useful approximation for molecules is the Born-Oppenheimer approximation.

3.3.1. Born-Oppenheimer Approximation

This study theoretically deals with multi-molecular systems, which means that the wave functions for these systems are excessively complicated because the movements of the species are affected by both repulsion and attraction forces, which means that the particles are unable to travel independently [60].

It is common knowledge that nuclei move remarkably slower when compared to electrons because electrons are lighter; thus, separating electronic energies in fixed nucleic positions will be appropriate [60].

Nucleic kinetic energy is independent of electrons, and the potential energy of electron-nuclear attraction is ignored; hence, nuclear-nuclear repulsion has constant potential energy [60].

The term Born-Oppenheimer approximation is alternatively termed as clamped nuclei approximation because electrons move towards a fixed nuclei field; thus, H reduces into electronic Hamiltonian, H_{elec} [Eq. (3.4)].

$$H_{elec} = -\frac{1}{2}\sum_{i=1}^{N}\nabla_i^2 - \sum_{i=1}^{N}\sum_{A=1}^{M}\frac{Z_A}{r_{iA}} + \sum_{i=1}^{N}\sum_{j>i}^{N}\frac{1}{r_{ij}} = T + V_{Ne} + V_{ee} \quad (3.10)$$

The Schrödinger equation is solved using H_{elec}, which has electronic energy E_{elec} and electronic wave function Ψ_{elec} [64].

$$H_{elec}\,\Psi_{elec} = E_{elec}\,\Psi_{elec} \quad (3.11)$$

The total energy, E_{tot}, is the summation of replulsion energy and E_{elec}:

$$E_{nuc} = \sum_{A=1}^{M}\sum_{B>A}^{M}\frac{Z_A Z_{AB}}{R_{AB}},$$

which given as [64]:

$$E_{tot} = E_{elec} + E_{nuc}. \quad (3.12)$$

The concept of potential energy surface (PES) has been illustrated through Born-Oppenheimer approximation. Here, E_{elec} determines the PES by finding the total possible coordinates of the nucleus [60].

This approximation has improved the concepts of transition state geometry and equilibrium geometry, which are sensitive in the case of PES [60].

The Hartree-Fock self-consistent field (HF-SCF) method is considered as the easiest Ab initio procedure, which was developed by the Nobel Laureate John A. Pople, [66], to perform calculations regarding atoms and other microstructures is described below:

3.3.2. Hartree-Fock Self-Consistent Field Method

There are some difficulties in solving and analyzing a Schrödinger equation, because defining the energy of a single electron is required, which exists in a field with all of the other electrons [65].

The HF-SCF process deals with this difficulty because it computes the energy of each electron. Initially, it estimates the total energies of the electrons, which are later used to compute the energy that exists in each electron. Then, the repitition of this recursive routine continues until convergence is assured [65].

Correlation energy needs to be defined because it is the energy difference between the Hartree-Fock calculations and the Schrödinger equation [65].

Since the HF-SCF calculations are sufficiently accurate, and they adequately highlight the issues, they are applied in different problems. Moreover, the correlation energy is significant in defining the properties of the system [65].

3.4. Electron Correlation Methods

The HF-SCF process has a major deficiency, in which it assumes that every electron is under the average effect of the energy for the movement; hence, finding the particular position of a specific electron is not dependent on the other electrons' positions. However, this approach is unable to take into account the inter-electron Coulombic interactions that cause them to repel each other. This means that the motion of the electrons is correlated, which makes them move apart, which is contrary to the HF-SCF concept [67, 68]. In quantum chemical calculations, electron correlation can be handled using multiple approaches, of which the density functional theory (DFT) and Møller-Plesset perturbation theory are very important.

DFT is explained in detail in the next section because it is applied in this research.

3.4.1. Density Functional Theory

3.4.1.1. Introduction

For the sake of simplicity and ease in processes, rather than working on wave functions, it is possibile to work on physical observables to determine energy; moreover, this possibility existed in classical mechanics as well [60].

Studying the Hamiltonian operator is sufficient to find the physical observable because it is dependent on both the nuclei's atomic number and its position (**r**). On the other hand, the Hamiltonian operator depends on the total number of electrons, which makes it a useful choice for physical observation because it aids in computing the electron density (ρ) [60].

3.4.1.2. Electron Density

The given electronic system has a specific electron density, $\rho(\mathbf{r})$, in the given state. Its formula in terms of wave function is given below [63]:

$$\rho(\mathbf{r_1}) = N \int_1 \dots \int_N |\Psi(X_1, X_2, \dots, X_N)|^2 ds_1 dx_2 \dots dx_N. \tag{3.13}$$

The non-negative simple function shows the total number of electrons (N) [66]:

$$N = \int \rho(\mathbf{r}) d\mathbf{r}. \tag{3.14}$$

The local maxima, in terms of electron density, is according to the positions of the nuclei; hence, the Hamiltonian operator can be defined by the atomic number. The density shows this information because the maximum electron density ($\mathbf{r}_\mathrm{A}$) is the location of each nucleus (A).

$$\frac{\partial \bar{\rho}(r_\mathrm{A})}{\partial r_\mathrm{A}}\Big|_{r_\mathrm{A}=0} = -2Z_\mathrm{A}\rho(\mathbf{r}_\mathrm{A}) \tag{3.15}$$

Here, r_A is the radial distance from A, $\bar{\rho}$ represents the spherically-averaged density, and Z_A is the atomic number of A.

The DFT of the electronic structure allows for replacing the complex *N*-electron wave function $\Psi \ (X_1, X_2, \ldots, X_N)$, which is linked with the Schrodinger equation, through calculations that include the simple electron density $\rho(\mathbf{r})$.

The main target of the DFT method is to design functions to connect the electron energy and density [63, 64], while that of the former can be totally defined as the ground state using the electron density (ρ) [62].

Hohenberg and Kohn [72] presented two fundamental but crucial theorems that established the DFT as a logical quantum chemical methodology [60].

3.4.1.3. First Hohenberg-Kohn Theorem: Proof of Existence

For *N*-electron system, Hohenberg and Kohn [69] reported that the Hamiltonian operator can be completely fixed by the external potential (V_{ext}); hence, all of the ground state density ρ(r) properties can be determined using *N* and the V_{ext} [63].

In this case, the Hamiltonian operator is determined through $\rho(\mathbf{r})$. Moreover, the density integration shows a specific number of electrons, and the remainder of the process involves defining an operator to determine the V_{ext} in terms of the positions and charges of the nuclei [60].

In this case, ρ shows V_{ext}, and it is assumed that the V_{exts} (V_a and V_b) are consistent and have a similar ground state density (ρ_0) [60].

In this case, the ground state wave functions are Ψ_a and Ψ_b, and H_a and H_b belong to them. The wave functions correspond to E_{0a} and E_{0b}, given that $E_{0a} \neq E_{0b}$. The only difference between H_a and H_b is the V_{ext}, so $H_a = T + V_{ee} + V_a$ and $H_b = T + V_{ee} + V_b$ [64].

With Hamiltonian operators H_a and H_b, V_a and V_b appear, while every Hamiltonian operator associates with the ground state Ψ_0. It is further associated with the ground state E_0. H_a is the expected value through Ψ_b, but it should be more than E_a, as given below [60]:

$$E_{0a} < \langle \Psi_{0b} | H_a | \Psi_{0b} \rangle. \tag{3.16}$$

Rewriting this expression:

$$E_{0a} < \langle \Psi_{0b} | H_a - H_b + H_b | \Psi_{0b} \rangle$$

$$< \langle \Psi_{0b} | H_a - H_b | \Psi_{0b} \rangle + \langle \Psi_{0b} | H_b | \Psi_{0b} \rangle$$

$$< \langle \Psi_{0b} | \mathrm{V_a} - \mathrm{V_b} | \Psi_{0b} \rangle + \mathrm{E_{0b}}. \tag{3.17}$$

The last line integral in Eq. (3.17), in terms of the ground-state density, is given below. Here, V is a single-electron operator:

$$E_{0a} < \int (\mathrm{V_a}(\mathbf{r}) - \mathrm{V_b}(\mathbf{r}))\, \rho_0(\mathbf{r}) d\mathbf{r} + \mathrm{E_{0b}}. \tag{3.18}$$

Here, no difference exists between a and b, so Eq. (18) will become:

$$E_{0b} < \int (\mathrm{V}_b(\mathbf{r}) - \mathrm{V}_a(\mathbf{r}))\, \rho_0(\mathbf{r}) d\mathbf{r} + \mathrm{E}_{0a}. \tag{3.19}$$

Adding the inequalities given in Eqs. (3.18) and (3.19), will give:

$$E_{0a} + E_{0b} < \int (\mathrm{V}_b(\mathbf{r}) - \mathrm{V}_a(\mathbf{r}))\, \rho_0(\mathbf{r}) d\mathbf{r} + \int (\mathrm{V}_a(\mathbf{r}) - \mathrm{V}_b(\mathbf{r}))\, \rho_0(\mathbf{r}) d\mathbf{r} + E_{0b} + \mathrm{E}_{0a}$$

$$< \int (\mathrm{V}_b(\mathbf{r}) - \mathrm{V}_a(\mathbf{r}) + \mathrm{V}_a(\mathbf{r}) - \mathrm{V}_b(\mathbf{r})) \rho_0(\mathbf{r}) d\mathbf{r} + E_{0b} + \mathrm{E}_{0a}$$

$$< E_{0b} + \mathrm{E}_{0a}. \tag{3.20}$$

This means that there is a contradiction [64]:

$$E_{0a} + \mathrm{E}_{0b} < E_{0b} + \mathrm{E}_{0a}\ or\ 0 < 0. \tag{3.21}$$

This clearly indicates that two V_{ext} cannot yield the same density. To state it a different way, the density of the ground state is specifically specified by the V_{ext}. If Eq. (3.4) is recalled, ρ_0 is added, which has certain information $\{N, Z_A, R_A\}$; thus, after summarizing, $\rho_0 \Rightarrow \{N, Z_A, R_A\} \Rightarrow \mathrm{H} \Rightarrow \Psi_0 \Rightarrow E_0$ is obtained (with other properties). Since there is a functional relationship between the electron density of the ground state and the full ground state energy, *Ne* shows the V_{ext}, which is defined by the nucleic attraction [64].

$$E_0(\rho_0) = T(\rho_0) + E_{ee}(\rho_0) + E_{Ne}(\rho_0) \tag{3.22}$$

The nuclei-electron attraction of the system has potential energy; hence, N, R_A, and Z_A can be expressed in the universal form, as given below:

$$E_0(\rho_0) = \int \rho_0(\vec{r}) V_{Ne} d\vec{r} + T(\rho_0) + E_{ee}(\rho_0). \tag{3.23}$$

Here, $T(\rho_0) + E_{ee}(\rho_0)$ is the universally valid part, while the system-dependent part is shown by $\rho_0(\vec{r}) V_{Ne} d\vec{r}$ [64].

If the system-independent parts in a Hohenberg-Kohn (HK) function, $F_{HK}(\rho_0)$, are combined:

$$E_0(\rho_0) = \int \rho_0(\vec{r}) V_{Ne} d\vec{r} + F_{HK}(\rho_0). \tag{3.24}$$

At first, functional $F_{HK}(\rho_0)$ seems like a desired formula for DFT, but if it is known exactly, the Schrodinger equation can be solved. Since it is system-independent, a H_2 atom can be used to find the exact solution for the system, but it is impossible to find $T(\rho_0)$ in the exact forms and $E_{ee}(\rho_0)$ [64].

Up until now, it can be stated that the density of the ground state is sufficient to obtain every one of the system properties. However, it is important to understand if the

density that has been defined is in actuality the density of the ground state that is required.

3.4.1.4. Second Hohenberg-Kohn Theorem: Variational Principle

In this theorem, at the ground state, the functional $F_{HK}(\rho_0)$ drives the system energy, and it also drives the least energy when there is real ground state density ρ_0 [64]. The variational principle can be written in the following form:

$$E_0 \leq E(\tilde{\rho}) = T(\tilde{\rho}) + E_{Ne}(\tilde{\rho}) + E_{ee}(\tilde{\rho}). \tag{3.25}$$

The trial density $\tilde{\rho}(\mathbf{r})$ has its specific H and $\widetilde{\Psi}$. Now, this wave function is taken as Ψ_{trial}. The true V_{ext} generates H. The desired results are achieved from the equation below [64]:

$$\langle\widetilde{\Psi}|\widetilde{H}|\widetilde{\Psi}\rangle = T(\tilde{\rho})\, V_{ee}(\tilde{\rho}) + \int \tilde{\rho}(\vec{\mathbf{r}})V_{ext}\mathrm{d}\vec{\mathbf{r}} = E(\tilde{\rho}) \geq E_0(\rho_0) = \langle\Psi_0|H|\Psi_0\rangle. \tag{3.26}$$

3.4.1.5. The Kohn-Sham Approach

Kohn and Sham (KS) [70] used the HF theory to bring the HK theorems into reality, and performed its calculations. It is necessary to develop the required imaginary system for N non-interacting electrons with the density of a real system. This system has a ground state wave function Ψ_0 that has been expressed through a single-slater determinant. This slater determinant is formed by the KS orbital (ϕKS) to solve N single-particle equations. The ϕKS variations determine the energy and density of the ground state on the basis of the variational principle [71].

The single-electron KS operator is given below [60]:

$$h_i^{KS} = -\frac{1}{2}\nabla_i^2 - \sum_k^{nuclei}\frac{Z_k}{|r_i - r_k|} + \int\frac{\rho(r')}{|r_i - r'|}dr' + V_{xc} \tag{3.27}$$

and

$$V_{xc} = \frac{\delta E_{xc}}{\delta \rho}. \quad (3.28)$$

Here, E_{xc} is the V_{xc} expectation value and V_{xc} is a single-electron operator. The KS-energy contribution comes from the exchange correlation energy (E_{XC}), which includes the kinetic energy corrections, which emerge because of electron-electron repulsions, while the interaction correlations need corrections [71].

3.5. Basis Sets

This is actually a set of mathematical functions used for constructing wave functions [60]. The computations of its electronic structure require molecular wave functions in the linear combination of atomic orbitals (LCAOs), while the AO function solves the Schrödinger equations for the H_2 atoms [67].

For defining MOs, LCAOs are used, while every MO is itself a single-electron wave function. The *N* electrons of the MO combine and make the *N* electron wave function. MOs or AOs cannot describe systems that have two or more electrons. For describing this kind of system, it is necessary to have specific *N*-body wave functions, while the MOs construct good approximates to the mentioned *N*-electron wave functions [72].

Each single-electron function is considered as a MO to solve the electronic Schrödinger equation for a molecule produced from a spin function (α, β) and a spatial orbital [62].

Many approximation methods are available to solve the Schrödinger equation and to select a method, its performance is compared to the values given in the experimental data, which is certainly better than directly proceeding with the computation [62].

A basis set approximates ab initio methods. In this case, there is a complete basis set, it is not an approximation if the known function is expanded as an MO. In this case, a complete basis set is based on an unlimited number of functions. Moreover, in real calculations, they are considered to be impossible [62].

The expansion of the MO leads to the integration of the QM operators over the basis function, but making the calculations easier depends on the form of the basis function [62].

3.5.1. Slater and Gaussian Type Orbitals Basis Set

There is a need to simplify ab initio MO calculations to apply them to large molecules. A widely used method is termed as the linear combination of the AOs self-consistent field (LCAO-SCF), which uses a minimal-basis slater-type orbital (STO) set [73].

H_2 wave functions acquire the following form: $\psi nlm(\mathrm{r},\theta,\varphi) = \mathrm{R}nl(\mathrm{r})\mathrm{Y}ml(\theta,\varphi)$. $\mathrm{R}nl(\mathrm{r})$ as the radial part of the H_2 wave function, which is a polynomial of r that represents the distance from the origin. The polynomial drives the STOs and it is a simplified form, which is given below [72]:

$$\varphi_{STO}(\mathrm{r}_A,\theta,\varphi;\ n,m,l,\zeta) = N\mathrm{r}_A^{n-1}\exp(-\zeta\ \mathrm{r}_A)Y_{ml}(\theta,\varphi). \tag{3.29}$$

In this case, a spherical coordinate system (r_A,θ,φ) is defined around atom A, while parameter Zeta (ζ) represents the orbital exponent and N is a normalization constant.

It takes long time to calculate full STOs because this requires a two-electron integral evaluation. The Gaussian function integrals can be analyzed, so replacing each STO is possible through a small number of linear combinations in the Gaussian-type orbitals (GTOs) [73].

The following spherical Gaussian form was obtained when the GTOs replaced $\exp(-\zeta\ \mathrm{r})$ by $\exp(-\alpha\ r^2)$ [72]:

$$\varphi_{sGTO}(\mathrm{r},\theta,\varphi;\ n,m,l,\alpha) = N\mathrm{r}_A^{n-1}\exp(-\alpha\ \mathrm{r}^2)Y_{ml}(\theta,\varphi). \tag{3.30}$$

The form of Cartesian Gaussians is:

$$\varphi_{GTO}(r;\ i,j,k,\alpha) = N\ X_A^i\ Y_A^j Z_A^k\exp(-\alpha\ |\mathbf{R}A\ -\ r|^2). \tag{3.31}$$

In Eq. (3.31), the coordinate $\mathbf{R}_A$ = (X_A,Y_A,Z_A) defines the GTO center, N is the normalization constant, and r = (x,y,z) expresses the Cartesian coordinate when the GTO is evaluated. The integers i, j, and k show the angular momentum of the GTOs [72],

and

$$L = i + j + k. \tag{3.32}$$

When the STO and GTO are compared, the STO cusps are correct when the distance from the center reduces to zero, and as the distance increases, it decays, like H_2. At a decreased r, the GTOs have an incorrect behavior, and they rapidly decay when r is increased. GTOs are more practical because in this and faster evaluations of the integrals is possible [72].

The long-range decay and incorrect cusp of the GTOs can be fixed when Gaussian functions are applied in a linear combination with a unique orbital exponent for each of them to make a contracted Gaussian basis function (CGTO) [72].

$$\varphi_{CGTO}(r) = \sum_k d_k \, \varphi_{GTO}(r; \alpha_k) \tag{3.33}$$

3.5.2. Minimal Basis Set

There is a single function STO, GTO, or CGTO, which is used for the AO. The STO-nG, generally represents this basis, for example, the STO-3G basis set means that three primitive GTOs have combined into a single CGTO [64].

The nomenclature implies that every orbital core through valence is only defined by a single basis function; thus, H and He only have a single function, while five functions exist for Li to Ne. Elements from Na to Ar have four functions, which are added to the five second-row functions to make a total of nine functions [60].

3.5.3. Split-Valence (Pople) Basis Sets

It is possible to construct two basic functions in the STO-3G basis set for each AO, without doubling the size of a basis set, but it will certainly increase the size of equation. Thus, it is likely to double ζ with two functions, so it is called a 'double-ζ ' basis [60].

The electronic wave function changes take place in a valence space. If it is possible to limit the set doubling of the functions while still keeping the inert core electrons in a minimal set, it will define a split-valence set [64].

Split-valence basis sets were developed by Pople et al. [66], in which the Pople basis sets have the following typical notation: X-YZg, while X shows the Gaussian primitive number that has been used in the inert core functions. The valence orbitals primitives are denoted by Y and Z, and when there are two basis functions, it is written as a double-ζ basis. In this case, it has three functions, so it has a triple-ζ valence [60].

In this notation, * shows the polarization functions for all of the atoms other than H_2, while ** shows that the atoms, including the H_2 atom, have polarization functions. Here, + means that there are diffused functions for all of the atoms, other than H_2, while ++ means that the H_2 also has diffusion functions [72].

Table 3.1 shows some Pople-style basis sets with their compositions for contracted as well as primitive basis functions, and Table 3.2 shows the designation of a 6-311++G(d,p) basis set.

Table 3.1. The composition of the basis sets with regard to the primitive and contracted basis functions for some of the Pople style basis sets [62].

Basis	Hydrogen		First row elements		Second row elements	
	Contracted	Primitive	Contracted	Primitive	Contracted	Primitive
STO-3G	*1s*	*3s*	*2s1p*	*6s3p*	*3s2p*	*9s6p*
3-21G	*2s*	*3s*	*3s2p*	*6s3p*	*4s3p*	*9s6p*
6-31G(d,p)	*2s1p*	*4s*	*3s2p1d*	*10s4p*	*4s3p1d*	*16s10p*
6-311G(2df,2pd)	*3s2p1d*	*5s*	*4s3p2d1f*	*11s5p*	*6s4p2d1f*a	*13s9p*a*

*McLean-Chandler basis set [74]

Table 3.2. 6-311++G(d,p) designation [62].

6-311++G(d,P)	6 primitive GTOs
-	Split valence
311	AOs
G	GTOs
+ +	Diffuse functions
(d,p)	Polarization functions d- type orbitals for heavy atoms d- type orbitals for H atom

3.5.4. Correlation-Consistent Basis Sets

For optimizing correlated Post-Hartree-Fock methods, Dunning [75] used extrapolation techniques to design the correlation-consistent polarized valence. This function is included in the basis set, which has the abbreviated form cc-pVxZ, while VxZ shows the number of functions for each valence AO. Here, x is the zeta basis that denotes double and triple as: D = double, T = triple [72].

Dunning [75] established that primitive Gaussian functions describe correlation in case the functions' exponents are then optimized using atomic correlated calculations. They established this after studying correlation effects on the O_2 atom. Calculations such as this guide the first-row atoms from B to Ne. For all of these atoms, the *spdfg* sets are used for correlated molecular calculations.

Due to the addition of correlation functions, the incremental energy reduces; hence, the *1d* function and *1s1p* set reduce the correlation energy. Moreover, the incremental energy reduces for the *2s2p*, *2d*, and *1f* sets. Table 3.3 shows the *sp* set for the first-row atoms [75].

Table 3.3. The sp set [75].

	Primitive	Contracted	Polarization set
cc-pVDZ	*(9s4p)*	*(3s2p)*	(1d)
cc-pVTZ	*(10s5p)*	*(4s3p)*	(2d 11)
cc-pVQZ	*(12s6p)*	*(5s4p)*	(3d2/1g)

3.5.5. Exchange-Correlation Functional

Eq. (28) shows the E_{XC}, which comprises differences in kinetic energy between the real and imaginary systems. The E_{xc} has functional and energy densities (ε_{XC}), which depend on the electron density [60].

$$E_{XC}(\rho(r)) = \int \rho(r)\varepsilon_{XC}(\rho(r))dr \tag{3.34}$$

3.5.6. B3LYP Hybrid Functional

The Becke 3-Term Correlation Functional; Lee, Yang, and Parr (B3LYP) functional method, which is pronounced B-three-lip, combines the B88 functional [76], LYP functional [77], and local density approximation. It also combines the generalized gradient approximation (GGA) correlation function by Lee et al. [77] with the GGA exchange of Becke [72].

This method uses the following formula to show the KS DFT based on the exchange-correlation energy (E_{xc}) [78]:

$$\mathrm{E_{XC}} = \int_0^1 \mathrm{U_{XC}^{\lambda}}\, \mathrm{d}\lambda. \tag{3.35}$$

Here, $U_{XC}^{\boldsymbol{\lambda}}$ represents the potential energy of the exchange correlation and λ represents a parameter that shows the inter-electronic coupling-strength.

In Eq. (3.35), when limit λ = 0 is applied to the coupling-strength integration in the exact exchange, the exact exchange energy is highly accurate in terms of DFTs; hence, the following exchange-correlation approximation was proposed [78]:

$$E_{XC} = E_{XC}^{LSDA} + a_0(E_X^{exact} - E_X^{LSDA}) + a_X\Delta E_X^{B88} + a_C\Delta E_C^{PW91}. \tag{3.36}$$

Eq. (3.36) has semi-empirical coefficients (a_0, a_X, a_C) that are determined using experimental data. In this equation, ΔE_X^{B8} denotes Becke's gradient correction, E_X^{exact} stands for the exact exchange energy, and ΔE_C^{PW91} represents the 1991 gradient correlation correction (Perdew and Wang) [76, 79].

3.6. Computational Method

When the COS interacted with the amidine, i.e., the DBN and the DBU, and the guanidine, i.e. the BTMG and TBD bases, in the presence of the linear alcohols, i.e., methanol, ethanol, 1-propanol, 1-butanol, 1-pentanol and 1-hexanol, they were theoretically investigated by applying quantum mechanics. Initially, the minimum energy structures of linear alcohols, DBU, DBN, BTMG, TBD and the COS were obtained by optimizing their geometries, and then vibrational frequency analyses were performed to ensure that, at the same level, they were appropriate minima on the potential energy surface. A flowchart is given in Figure 3.2 that shows the different steps of the geometric optimization. When minimum energy structures were obtained for the COS, DBU, DBN, BTMG and TBD as well as the linear alcohols, as the next step, both the products and the reactants were prepared by considering the termolecular reaction mechanisms that were discussed previously.

Following the geometry optimizations for both systems of the reactants (R) and products (P), the vibrational frequency was calculated by applying the same process for both, to verify that neither of the systems had imaginary vibrational frequency values, and that both had a proper minimum value. When both systems of the reactants and products, which were located at the surface, had sufficient potential energy, then the transition state calculations were done to determine the saddle point. At this time, the transition state (TS) structure was also determined. Vibrational frequency calculations and intrinsic reaction coordinates verified the attained transition state structures. The calculations done by ωB97X-D3 hybrid functional [80] that included Grimme's empirical dispersion corrections in the D3 version.

According to Goerigk et al. [80], large database utilization is focused on the kinetics, thermochemistry, and non-covalent interactions of the general main-group. It was found that ωB97X-D3 was one of the 3 best-performing hybrid functionals. Next, Pople's contracted Gaussian triple-zeta-quality basis set, 6-311++G (d,p), was applied, which includes diffusion and polarization functions for H_2, as well as other heavier atoms [81]. Throughout this study, all of these calculations were done at a level of ωB97X-D3/6-311++G(d,p), utilizing the IEF-PCM when there was a self-consistent reaction field [56-58]. The dominant base effect of each alcohol was considered. What

this means is that the effects of the bulk solvent were taken into consideration while the calculations were being performed. The thermodynamic analysis and the kinetic analysis of these suggested reactions were all then done at 298.15 K below 1 atm of pressure, when, at the same time, the Gibbs free-energy of reaction and activation values were calculated. Gaussian software version 09 Rev.D.0.1 [82] was used to calculate all of the density functions and Gauss View 5.0.9 [83] was used for the molecular visualizations. Figures 3.2 and 3.3 give an overview of a theoretical model, and how molecular structures and properties are measured for quantum calculations.

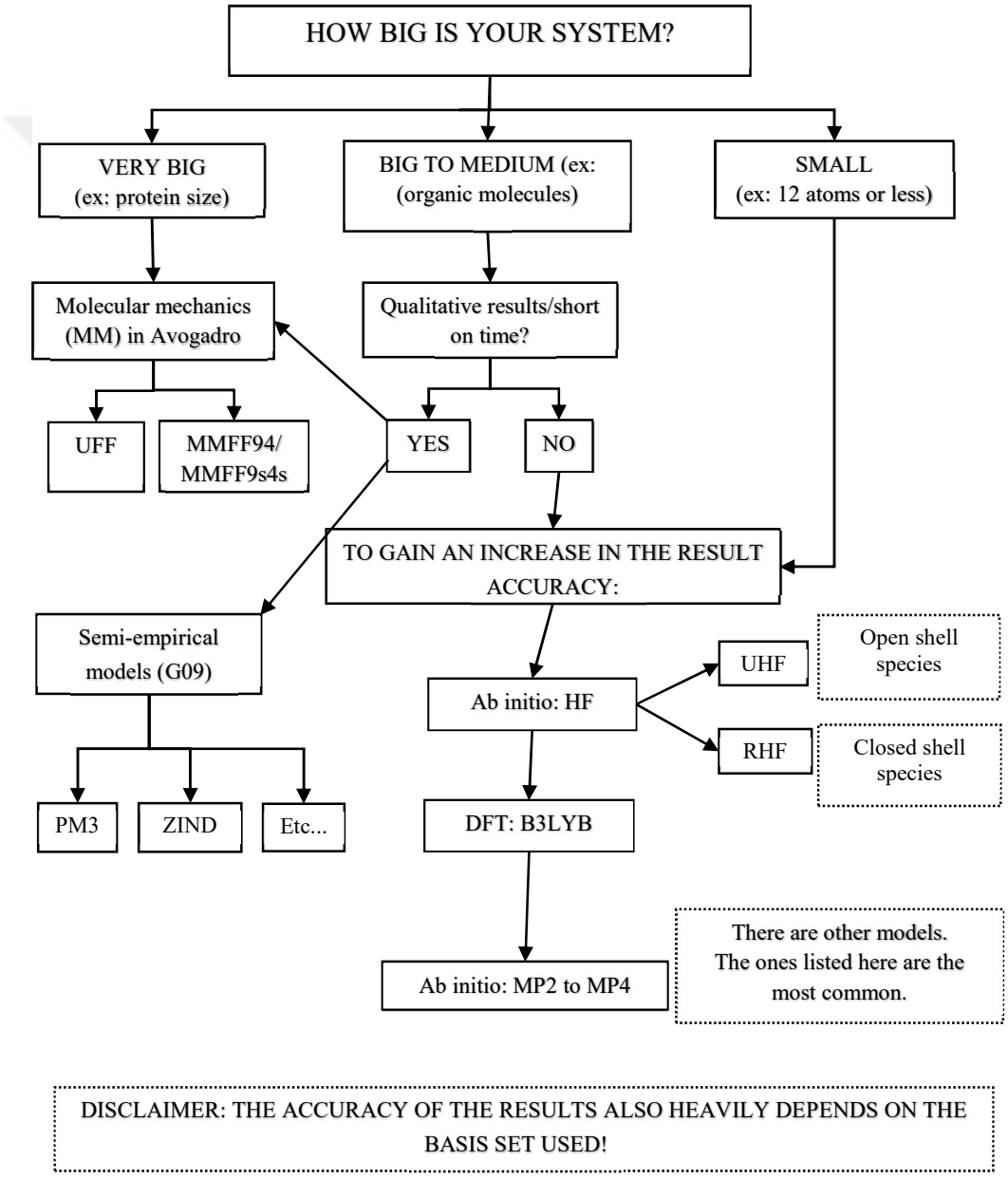

Figure 3.2. Flowcharts demonstrating how to choose the right theoretical model.

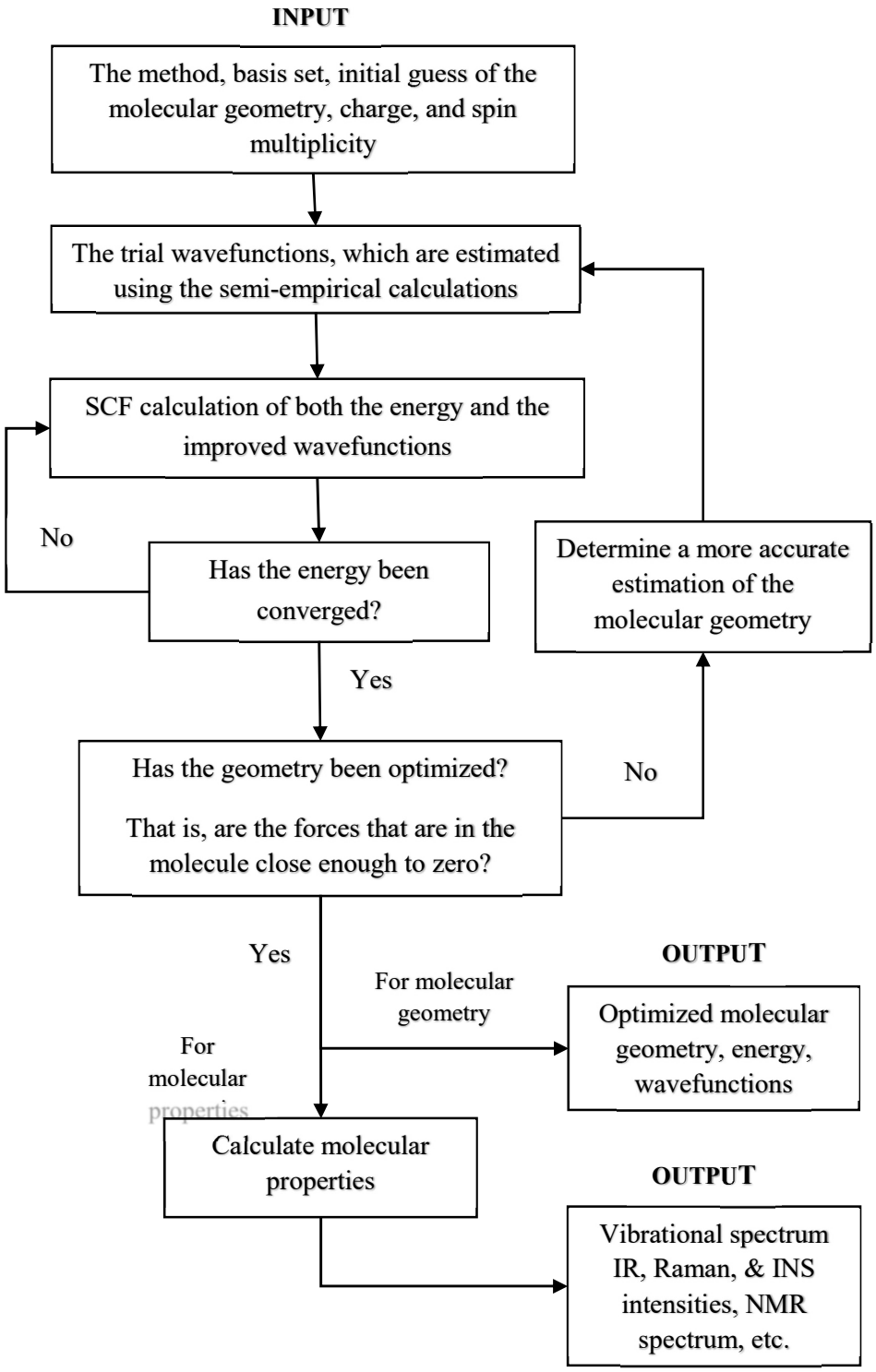

Figure 3.3. Flowcharts demonstrating how molecular configurations and properties are calculated in quantum mechanical calculations.

CHAPTER 4

RESULTS AND DISCUSSION

The chapter herein will present the theoretical findings with regard to the charge distribution, the structure, and the kinetic and the thermochemical properties. Moreover, descriptions of all of the details of the geometries that were optimized are given and discussed for the termolecular reaction mechanisms.

In the current research study, a single-step mechanism was both considered and utilized, and through this mechanism, interactions between organic bases, comprising DBU, DBN, BTMG and TBD and COS, as well as linear alcohols, which comprised ethanol, methanol, 1-propanol, 1-butanol, 1-pentanol and 1-hexanol took place. The transition state, the product structures, and the reactant were all obtained by utilizing calculations that were performed at the level of ωB97X-D3/6-311++G(d,p). These included empirical dispersion corrections as well as implicit solvent effects, as can be seen in Figures 4.2−4.25. Furthermore, an atom labeling scheme can also be seen in Figures 4.2−4.25, that shows the most significant structural parameters for the transition states, the products, and the reactants, which were changed substantially when the reactions occurred. The geometrical parameters as well as their values for the COS-binding organic liquids, which comprised the COS/DBU/linear alcohols, COS/DBN/linear alcohols, COS/BTMG/linear alcohols and COS/TBD/linear alcohols are given in Table 4.1 below.

The H31-O26 distance depicts the lengths of the H-O bonds in the hydroxyl groups of all of the linear alcohols. Table 4.1 shows the bond lengths for H31-O26 for the product and the reactant structures for the COS/DBU/methanol system, which can be seen in Figure 4.2; the COS/DBN/methanol system, which can be seen in Figure 4.8; the COS/BTMG/methanol system, which can be seen in Figure 4.14 and the COS/TBD/methanol system, which can be seen in Figure 4.20. The determined values for the systems comprised 0.989, 0.986, 0.990 and 0.992 Å, and 1.972, 1.882, 1.927 and 1.887 Å for the reactants and the products of

COS/DBU/methanol, COS/DBN/methanol COS/BTMG/methanol, and COS/TBD/methanol, respectively. For the structures of the transition state for the COS/DBU/methanol system, COS/DBN/methanol system, COS/BTMG/methanol and COS/TBD/methanol system, the determined geometrical parameter values comprised 1.109, 1.101, 1.090 and 1.716 Å, respectively. The distance of the H-O bond for the methanol was determined as 0.956 Å in its isolated form [84], while the same distance for the COS/BTMG/methanol system was 0.990 Å. When a comparison was performed of the experimental data with the values that were calculated, it appeared that they had been overestimated. It is true that there existed methanol within the COS/BTMG/methanol reactant system, and it was observed to interact with the COS and the BTMG. Moreover, it was not determined to be stand-alone. In both the BTMG and the H31 atom in the methanol, the weak interactions that took place between the un-paired electrons in the N1 atoms thus resulted in a slight elongation in the length of the H31-O26 bond. This was additionally confirmed by the observed reductions in the distances of the H31-N1 reactant-product for all of the systems that were investigated. The H31-N1 distances that were calculated comprised 1.801, 1.438, and 1.018 Å, when again taking into consideration the COS-BTMG-methanol system. Moreover, the H31-O26 distances comprised 0.990, 1.090, and 1.927 Å for the reactant, the transition state, and the product of COS/BTMG/methanol, respectively. Findings such as these ones clearly proved that the H31-O26 bond had been broken as a result of the very strong attraction forces that existed within the H31 and N1 atoms. In the hydroxyl group on the N1 atom in the BTMG, the methanol donated the H31 atom, and then later on, a new covalent bond was formed on the product, between the N1 and H31 atoms. This is reflected in Figure 4.1. In a similar manner, a reduction was observed in distances of the H31-N1 reactant-product from 1.806 to 1.025 in the COS/BTMG/1-propanol system, 1.799 to 1.018 in the COS/BTMG/ethanol system, 1.747 to 1.019 in the COS/BTMG/1-pentanol system, 1.796 to 1.019 in the COS/BTMG/1-butanol system, and 1.752 to 1.019 Å in the COS/BTMG/1-hexanol system. The H31-N1 reactant-product distances reduced from 1.765 to 1.018 in the COS/DBU/ethanol system, 1.763 to 1.017 in the COS/DBU/methanol system, 1.803 to 1.018 in the COS/DBU/1-butanol system, 1.780 to 1.017 in the COS/DBU/1-propanol system, 0.816 to 1.019 in the COS/DBU/1-hexanol system, and 1.809 to 1.018 Å in the COS/DBU/1-pentanol system. For all of the investigated systems, it was observed that the alcohol-amine interactions took place through H atoms (H31) in the hydroxyl alcohols and the same was true for the nitrogen atoms (N1) in the amines.

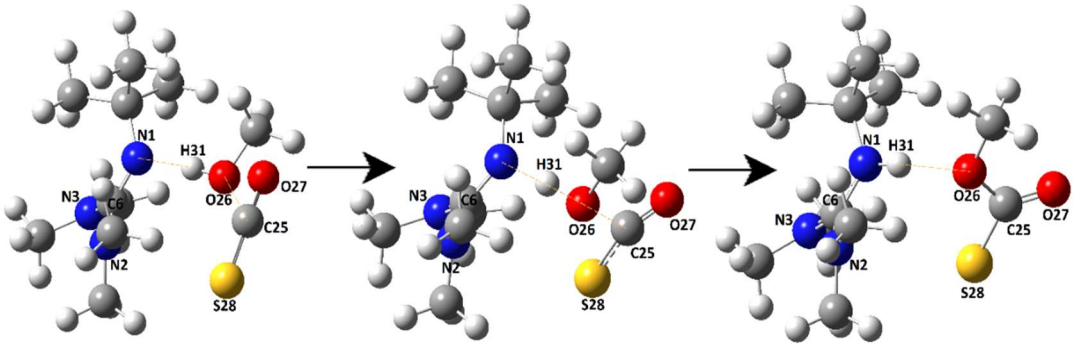

Figure 4.1. Representatives of the mechanism of reaction by means of the COS/BTMG/methanol system, which consists of the reactant (on the left), the transition state (in the center), and the product (on the right).

The single-step termolecular process that has been proposed shows that the concurrent alcohol-COS interactions and alcohol-amine interactions should be elaborately examined. For the reactant, the transition state, and the product structures, all of the C25-O26 bond lengths were calculated in 4 groups: (3.041, 1.917, and 1.382 Å), (2.997, 1.900, and 1.378 Å), (2.987, 1.902, and 1.379 Å) and (3.818, 2.382, and 1.373 Å). They were, respectively, computed for the COS-DBU-methanol system, the COS/DBN/methanol system, the COS/BTMG/methanol and the COS/TBD/methanol system. The angle values of the O27-C25-S28 bond, on the other hand, for similar systems were "177.88°, 150.02°, and 128.17°", "177.94°, 149.39°, and 128.45°", "177.69°, 149.82°, and 128.21°" and "178.78°, 164.28°, and 127.86°". The COS was located at 2.987Å at a distance of C25-O26 from the methanol. However, for the COS, the angle value of the O27-C25-S28 bond was 177.69°. The isolated COS molecules had linear structures, like CO_2 [85]. The COS had slightly bent geometry for all of the reactant systems, which showed very weak alcohol-COS interaction by means of the O25 and O26 atoms, which bent the COS structure almost 2°–2.3°. In the COS-DBU-butanol system, the COS/DBU/1-pentanol system, and the COS/DBU/1-hexanol system, the process of the COS bending was, quite interestingly, obtained at just 0.3°, which was an exception. Elucidating a large (above 4.3 Å) distance of C25-O26 for these 4 systems actually diminished the interactions that took place COS between the butanol, the hexanol, and the pentanol. With regard to the COS/BTMG/methanol system, the transition state structure bending was intense because it reached 149.82°. Moreover, for the same system, the length of the C25-O26 bond and angle of the O27-C25-S28 bond were determined as 1.379 Å and 128.21° in the product structure. In the same way, the O27-C25-S28 bond angle decreased from 177.56 to 128.23° and the C25-O26 reactant-product distance reduced from 2.920 to 1.385 Å. In the

COS/BTMG/1-hexanol system, it showed that a deprotonated alcohol-COS covalent bond had formed, which was obvious from the values. For all of the other systems, the same trend was observed, which is obvious in Table 4.1.

Table 4.1. Geometrical parameters, which comprise the bond lengths in Å and the bond angles in degrees, for the reactant, the transition state (TS), and the product structures of the systems used to capture the COS. The numbering scheme for these atoms is given in Figures 4.2–4.25).

System		Geometric parameter					
		H31-N1	H31-O26	C25-O26	C25-O27	C25-S28	O27-C25-S28
COS/DBU/methanol	R	1.763	0.989	3.041	1.152	1.563	177.883
	TS	1.386	1.109	1.917	1.170	1.621	150.022
	P	1.017	1.972	1.382	1.220	1.723	128.166
COS/DBU/ethanol	R	1.765	0.989	3.076	1.152	1.563	178.034
	TS	1.427	1.087	1.893	1.171	1.624	149.246
	P	1.018	1.937	1.384	1.220	1.723	127.956
COS/DBU/1-propanol	R	1.780	0.988	3.160	1.152	1.562	178.101
	TS	1.424	1.089	1.891	1.171	1.624	149.257
	P	1.017	1.951	1.386	1.220	1.722	127.978
COS/DBU/1-butanol	R	1.803	0.987	4.333	1.153	1.560	179.723
	TS	1.428	1.087	1.890	1.171	1.171	149.226
	P	1.018	1.935	1.386	1.219	1.722	128.030
COS/DBU/1-pentanol	R	1.809	0.987	4.341	1.153	1.560	179.689
	TS	1.423	1.090	1.888	1.171	1.624	149.005
	P	1.018	1.910	1.387	1.219	1.722	128.148
COS/DBU/1-hexanol	R	1.816	0.986	4.333	1.153	1.560	179.667
	TS	1.450	1.081	1.865	1.172	1.627	148.196
	P	1.019	1.909	1.388	1.219	1.722	128.228
Geometric parameter		H31-N1	H31-O26	C25-O26	C25-O27	C25-S28	O27-C25-S28
COS/DBN/methanol	R	1.778	0.986	2.997	1.152	1.562	177.938
	TS	1.399	1.101	1.900	1.170	1.624	149.391
	P	1.019	1.882	1.378	1.218	1.726	128.447
COS/DBN/ethanol	R	1.790	0.985	2.992	1.152	1.562	177.984
	TS	1.462	1.069	1.876	1.170	1.627	148.706
	P	1.029	2.647	1.363	1.219	1.738	126.662
COS/DBN/1-propanol	R	1.790	0.985	2.977	1.152	1.562	177.962
	TS	1.464	1.073	1.870	1.170	1.627	148.513
	P	1.029	2.642	1.363	1.219	1.738	126.782
COS/DBN/1-butanol	R	1.789	0.987	3.176	1.152	1.563	177.836
	TS	1.460	1.074	1.872	1.171	1.627	148.594
	P	1.030	2.612	1.362	1.219	1.739	127.008
COS/DBN/1-pentanol	R	1.886	0.980	3.005	1.153	1.561	178.431
	TS	1.469	1.068	1.862	1.171	1.628	148.235
	P	1.030	2.608	1.363	1.219	1.738	127.050
COS/DBN/1-hexanol	R	1.929	0.978	3.030	1.152	1.561	178.500
	TS	1.468	1.070	1.856	1.172	1.629	147.881
	P	1.030	2.608	1.363	1.219	1.738	127.119
Geometric parameter		H31-N1	H31-O26	C25-O26	C25-O27	C25-S28	O27-C25-S28

Table 4.1. (cont'd) Geometrical parameters, which comprise the bond lengths in Å and the bond angles in degrees, for the reactant, the transition state (TS), and the product structures of the systems used to capture the COS. The numbering scheme for these atoms is given in Figures 4.2–4.25).

System		Geometric parameter					
		H31-N1	H31-O26	C25-O26	C25-O27	C25-S28	O27-C25-S28
COS/BTMG/methanol	R	1.801	0.990	2.987	1.152	1.563	177.694
	TS	1.438	1.090	1.902	1.170	1.623	149.821
	P	1.018	1.927	1.379	1.219	1.726	128.209
COS/BTMG/ethanol	R	1.799	0.990	2.991	1.152	1.562	177.759
	TS	1.483	1.075	1.859	1.171	1.627	148.328
	P	1.018	1.976	1.381	1.219	1.726	127.682
COS/BTMG/1-propanol	R	1.806	0.986	2.931	1.152	1.562	177.936
	TS	1.496	1.077	1.837	1.174	1.629	146.716
	P	1.025	2.493	1.363	1.220	1.735	127.378
COS/BTMG/1-butanol	R	1.796	0.990	3.071	1.152	1.562	177.989
	TS	1.431	1.088	1.919	1.169	1.622	150.334
	P	1.019	1.858	1.383	1.218	1.726	128.176
COS/BTMG/1-pentanol	R	1.747	0.991	2.917	1.152	1.562	177.615
	TS	1.436	1.088	1.905	1.170	1.623	150.016
	P	1.019	1.868	1.383	1.218	1.726	128.190
COS/BTMG/1-hexanol	R	1.752	0.990	2.920	1.152	1.562	177.563
	TS	1.435	1.089	1.906	1.170	1.623	150.014
	P	1.019	1.866	1.385	1.218	1.725	128.230
Geometric parameter		H31-N1	H31-O26	C25-O26	C25-O27	C25-S28	O27-C25-S28
COS/TBD/methanol	R	1.751	0.992	3.818	1.151	1.564	178.778
	TS	1.041	1.716	2.382	1.155	1.586	164.284
	P	1.017	1.887	1.373	1.216	1.731	127.857
COS/TBD/ethanol	R	1.790	0.985	2.986	1.152	1.563	177.996
	TS	1.486	1.065	1.885	1.168	1.628	149.041
	P	1.014	2.009	1.368	1.217	1.735	127.904
COS/ TBD /1-propanol	R	1.848	0.983	2.919	1.151	1.563	177.921
	TS	1.428	1.090	1.889	1.169	1.625	149.075
	P	1.023	2.695	1.360	1.219	1.741	126.735
COS/ TBD /1-butanol	R	1.814	0.985	2.899	1.151	1.564	177.760
	TS	1.503	1.061	1.852	1.171	1.629	148.275
	P	1.023	2.723	1.360	1.219	1.742	126.661
COS/ TBD /1-pentanol	R	1.829	0.985	2.954	1.152	1.563	178.260
	TS	1.503	1.062	1.850	1.171	1.629	148.231
	P	1.022	2.717	1.360	1.219	1.742	126.775
COS/ TBD /1-hexanol	R	1.837	0.983	2.913	1.151	1.564	177.781
	TS	1.516	1.057	1.836	1.172	1.630	147.790
	P	1.019	2.599	1.359	1.219	1.740	127.184

In the geometrical parameters, the above-mentioned changes to all of the systems that were investigated herein proved that while the termolecular reactions were taking place, the following also occurred: 1) the hydrogen atom was transferred from the alcohol to the amine, 2) H31-O26 bond cleavage took place, 3) formation of a new H31-N1 bond took place, and, since the COS had a strong interaction with the

deprotonated alcohols ($R-CH_2-O^-$), 4) a new C25-O26 covalent bond was formed. Consequently, the amine-alcohol mixture captured the COS, which is clearly depicted in Figures 4.2−4.25.

Some atoms experienced partial charges because they were located around the region of the reaction, and this meant that they were exposed to significant changes. This provided an opportunity to examine the electron transfer that occurs when a chemical reaction takes place. Mulliken [86] and Hirshfeld [87] analyzed such changes, which are mentioned in Table 4.2. Mulliken found that the charges were more negative in the case of negatively-charged species, which confirmed the findings mentioned in the literature. However, the Hirshfeld analysis was followed herein, as have some other researchers [88]. Since there was an alcohol-anime H_2 (H31) transfer, and the formation of a new C25-O26 bond between deprotonated alcohol and the COS, the negative charge distribution was observed to have changed significantly, which specifically took place in the C25, O26, O27, and S28 atoms. Moreover, on the Hirshfeld scheme, it could be observed that, on the O27 atom, an increase occurred in the negative charge in the reactant, from –0.127, –0.148, –0.137 and –0.150 *e* to –0.373, –0.379, –0.383 and –0.374 e in the product. On the other hand, the S28 negative charge in the reactant was observed to have increased significantly, from –0.047, –0.042, –0.046 *e* and –0.034 e to –0.522, –0.576, –0.537 and –0.511 *e* in the product for the COS/DBU/methanol system, the COS/DBN/methanol system, the COS/BTMG/methanol system, and the COS/TBD/methanol system respectively. Moreover, at the same time, the positive charge on the C25 atom was observed to have reduced from the reactant to the product between 0.069 *e* (for the COS/BTMG/methanol system: from 0.216 to 0.147) and 0.060 *e* (for the COS-DBN-1-hexanol system: from 0.214 to 0.154 *e*) for all of the systems investigated, which occurred as a result of to the newly-formed C25-O26 bond. The charges on the C25, O27, and S28 atoms significantly changed because they had bond elongation between the C25-S28 and C25-O27 atoms. The C25-O27 elongation was observed from 1.152, 1.152, 1.152 and 1.151 Å (in the reactants) to 1.220, 1.218, 1.219 and 1.216 Å (in the products). The elongation of the C25-S28 bond in the COS-DBU-methanol system, the COS/DBN/methanol system, COS/BTMG/methanol system and

COS/TBD/methanol system ranged from 1.563, 1.562, 1.563 and 1.564 Å, in the reactants, to 1.723, 1.726, 1.726 and 1.731 Å in the products.

In the COS/DBU/methanol system, the COS/DBN/methanol system, the COS/BTMG/methanol system and the COS/TBD/methanol system on the O26 atom, the negative charge diminished from –0.317*e*, –0.307*e*, –0.292*e* and –0.311e (in the reactants) to –0.139e, –0.133e, –0.125e and –0.131e (in the products). Considering all of the systems, on the O26 atom, the negative charge reduced between 0.18*e* (–0.318*e* to –0.138*e* for the COS-DBU-1-pentanol system) and 0.14*e* (–0.282*e* to –0.142*e* for COS-BTMG-1-propanol system), which originated because of the transfer of the H31 atom from the O26 atom of the alcohol group to the N1 atoms in the amine. On the other hand, in the Mulliken population analysis, it was observed that a stronger diminishment in the negative charge on the O26 atom, of approximately 0.4 *e*. In the majority of the products, an observation was made that the O26 atom had a positive charge, as can be seen in Table 4.2.

Table 4.2. Partial charges, in e, of the atoms that were in the reaction region, which were obtained via the Mulliken and Hirshfeld population analysis. The numbering scheme for these atoms is given in Figures 4.2–4.25).

Mulliken charges										
System		Atom								
		O26	O27	S28	C25	H31	N1	C6	N2	N3
COS/DBU/methanol	R	–0.487	–0.091	–0.055	0.173	0.470	–0.405	–0.091	0.141	----
	P	–0.083	–0.314	–0.532	–0.263	0.418	–0.125	–0.111	0.147	----
COS/DBU/ethanol	R	–0.428	–0.034	–0.033	0.127	0.418	–0.402	–0.205	0.149	----
	P	–0.018	–0.288	–0.599	–0.302	0.434	–0.142	–0.153	0.146	----
COS/DBU/1-propanol	R	–0.406	–0.021	–0.061	0.1418	0.418	–0.381	–0.157	0.132	----
	P	0.004	–0.271	–0.638	–0.224	0.454	–0.141	–0.246	0.156	----
COS/DBU/1-butanol	R	–0.363	–0.045	–0.001	0.210	0.429	–0.218	–0.323	0.191	----
	P	0.034	–0.259	–0.677	–0.182	0.473	–0.142	–0.293	0.150	----
COS/DBU/1-pentanol	R	–0.353	–0.035	–0.002	0.215	0.427	–0.215	–0.345	0.193	----
	P	0.049	–0.250	–0.657	–0.176	0.486	–0.128	–0.348	0.152	----
COS/DBU/1-hexanol	R	–0.349	–0.021	–0.018	0.221	0.425	–0.203	–0.325	0.206	----
	P	0.057	–0.246	–0.672	–0.148	0.490	–0.124	–0.371	0.154	----
System		O26	O27	S28	C25	H31	N1	C6	N2	N3
COS/DBN/methanol	R	–0.475	–0.106	0.008	0.080	0.416	–0.369	–0.154	0.168	----
	P	–0.108	–0.364	–0.561	–0.085	0.422	–0.209	0.080	0.148	----
COS/DBN/ethanol	R	–0.414	–0.100	0.031	0.078	0.345	–0.366	–0.320	0.193	----
	P	–0.003	–0.360	–0.480	–0.063	0.170	0.253	–0.823	0.232	----
COS/DBN/1-propanol	R	–0.368	–0.085	0.042	0.065	0.321	–0.326	–0.528	0.221	----
	P	0.026	–0.356	–0.504	–0.063	0.174	0.247	–0.751	0.237	----
COS/DBN/1-butanol	R	–0.398	–0.065	–0.051	0.163	0.448	–0.302	–0.367	0.165	----
	P	0.030	–0.357	–0.507	–0.065	0.181	0.242	–0.690	0.237	----
COS/DBN/1-pentanol	R	–0.305	–0.100	–0.041	0.207	0.357	–0.254	–0.579	0.175	----
	P	0.042	–0.354	–0.510	–0.053	0.184	0.242	–0.681	0.241	----
COS/DBN/1-hexanol	R	–0.277	–0.088	–0.021	0.191	0.301	–0.173	–0.759	0.245	----
	P	0.046	–0.351	–0.509	–0.047	0.182	0.254	–0.670	0.238	----
System		O26	O27	S28	C25	H31	N1	C6	N2	N3

Table 4.2. (cont'd) Partial charges, in e, of the atoms that were in the reaction region, which were obtained via the Mulliken and Hirshfeld population analysis. The numbering scheme for these atoms is given in Figures 4.2–4.25).

Mulliken charges										
System		Atom								
		O26	O27	S28	C25	H31	N1	C6	N2	N3
COS/BTMG/methanol	R	–0.425	–0.083	–0.017	0.126	0.336	–0.151	–1.295	–0.032	0.078
	P	–0.086	–0.339	–0.512	–0.151	0.363	–0.062	–0.675	–0.049	0.091
COS/BTMG/ethanol	R	–0.379	–0.060	–0.066	0.168	0.399	–0.062	–1.360	–0.017	0.096
	P	0.013	–0.314	–0.403	–0.332	0.377	–0.171	–0.666	–0.027	0.090
COS/BTMG/1-propanol	R	–0.351	–0.097	0.011	0.139	0.495	0.207	–1.836	–0.030	0.243
	P	0.108	–0.338	–0.438	–0.149	0.203	0.516	–2.108	0.086	0.247
COS/BTMG/1-butanol	R	–0.319	–0.036	–0.056	0.164	0.481	–0.053	–1.441	0.003	0.111
	P	0.038	–0.294	–0.507	–0.215	0.427	–0.117	–0.938	–0.036	0.167
COS/BTMG/1-pentanol	R	–0.318	–0.050	0.043	0.055	0.346	–0.134	–1.34	0.050	0.086
	P	0.036	–0.289	–0.512	–0.213	0.440	–0.125	–0.937	–0.033	0.171
COS/BTMG/1-hexanol	R	–0.310	–0.043	0.036	0.057	0.343	–0.129	–1.342	0.047	0.098
	P	0.037	–0.282	–0.511	–0.209	0.444	–0.120	–0.959	–0.028	0.177
System		O26	O27	S28	C25	H31	N1	C6	N2	N3
COS/TBD/methanol	R	-0.469	-0.081	0.082	-0.011	0.405	-0.363	-0.247	-0.227	0.036
	P	-0.150	-0.365	-0.499	-0.034	0.423	-0.229	0.066	0.008	-0.064
COS/TBD/ethanol	R	-0.409	-0.067	0.020	0.060	0.339	-0.444	-0.242	-0.096	0.018
	P	-0.101	-0.366	-0.472	-0.072	0.327	-0.091	-0.179	0.036	-0.009
COS/TBD/1-propanol	R	-0.303	-0.125	0.034	0.136	0.287	-0.268	-0.338	-0.205	0.112
	P	0.116	-0.339	-0.503	-0.064	0.169	0.172	-0.413	-0.026	0.093
COS/TBD/1-butanol	R	-0.326	-0.109	0.007	0.171	0.354	-0.340	-0.424	-0.105	0.166
	P	0.139	-0.324	-0.517	-0.054	0.176	0.193	-0.428	-0.030	0.090
COS/TBD/1-pentanol	R	-0.294	-0.077	-0.006	0.168	0.214	-0.307	-0.462	-0.129	0.198
	P	0.143	-0.318	-0.515	-0.071	0.182	0.206	-0.447	-0.012	0.095
COS/TBD/1-hexanol	R	-0.303	-0.107	0.023	0.137	0.338	-0.265	-0.495	-0.118	0.200
	P	0.143	-0.297	-0.421	-0.218	0.210	0.061	-0.276	0.076	0.114

Table 4.2. (cont'd) Partial charges, in e, of the atoms that were in the reaction region, which were obtained via the Mulliken and Hirshfeld population analysis. The numbering scheme for these atoms is given in Figures 4.2–4.25).

Hirshfeld Charges										
System		Atom								
		O26	O27	S28	C25	H31	N1	C6	N2	N3
COS/DBU/methanol	R	–0.317	–0.127	–0.047	0.217	0.097	–0.223	0.127	–0.087	----
	P	–0.139	–0.373	–0.522	0.150	0.117	–0.079	0.184	–0.042	----
COS/DBU/ethanol	R	–0.311	–0.127	–0.047	0.217	0.096	–0.222	0.127	–0.087	----
	P	–0.140	–0.360	–0.522	0.153	0.115	–0.080	0.183	–0.043	----
COS/DBU/1-propanol	R	–0.310	–0.126	–0.046	0.218	0.097	–0.224	0.128	–0.087	----
	P	–0.140	–0.358	–0.519	0.154	0.116	–0.080	0.183	–0.043	----
COS/DBU/1-butanol	R	–0.319	–0.132	–0.024	0.220	0.097	–0.225	0.127	–0.087	----
	P	–0.140	–0.359	–0.520	0.153	0.115	–0.080	0.183	–0.043	----
COS/DBU/1- pentanol	R	–0.318	–0.131	–0.024	0.220	0.098	–0.225	0.127	–0.087	----
	P	–0.138	–0.359	–0.517	0.154	0.113	–0.080	0.183	–0.043	----
COS/DBU/1-hexanol	R	–0.317	–0.132	–0.024	0.220	0.099	–0.225	0.127	–0.087	----
	P	–0.139	–0.358	–0.514	0.154	0.113	–0.080	0.183	–0.044	----
System		O26	O27	S28	C25	H31	N1	C6	N2	N3
COS/DBN/methanol	R	–0.307	–0.148	–0.042	0.215	0.098	–0.245	0.120	–0.081	----
	P	–0.133	–0.379	–0.576	0.148	0.109	–0.079	0.180	–0.042	----
COS/DBN/ethanol	R	–0.299	–0.149	–0.043	0.215	0.100	–0.244	0.121	–0.082	----
	P	–0.143	–0.381	–0.508	0.154	0.094	–0.092	0.179	–0.040	----
COS/DBN/1- propanol	R	–0.297	–0.150	–0.043	0.215	0.101	–0.244	0.121	–0.082	----
	P	–0.142	–0.381	–0.507	0.154	0.094	–0.092	0.180	–0.040	----
COS/DBN/1-butanol	R	–0.315	–0.133	–0.049	0.218	0.098	–0.228	0.122	–0.085	----
	P	–0.141	–0.382	–0.508	0.153	0.094	–0.091	0.180	–0.040	----
COS/DBN/1- pentanol	R	–0.294	–0.147	–0.064	0.214	0.106	–0.260	0.124	–0.079	----
	P	–0.141	–0.381	–0.507	0.153	0.094	–0.091	0.180	–0.041	----
COS/DBN/1-hexanol	R	–0.296	–0.146	–0.066	0.214	0.108	–0.253	0.124	–0.079	----
	P	–0.141	–0.380	–0.505	0.154	0.094	–0.091	0.180	–0.041	----
System		O26	O27	S28	C25	H31	N1	C6	N2	N3

Table 4.2. (cont'd) Partial charges, in e, of the atoms that were in the reaction region, which were obtained via the Mulliken and Hirshfeld population analysis. The numbering scheme for these atoms is given in Figures 4.2–4.25).

Hirshfeld Charges										
System		Atom								
		O26	O27	S28	C25	H31	N1	C6	N2	N3
COS/BTMG/methanol	R	–0.292	–0.137	–0.046	0.216	0.104	–0.221	0.165	–0.095	–0.088
	P	–0.125	–0.383	–0.537	0.147	0.098	–0.100	0.208	–0.063	–0.055
COS/BTMG/ethanol	R	–0.287	–0.134	–0.045	0.217	0.104	–0.221	0.165	–0.095	–0.088
	P	–0.140	–0.373	–0.537	0.149	0.096	–0.102	0.207	–0.062	–0.054
COS/BTMG/1-propanol	R	–0.282	–0.153	–0.051	0.213	0.106	–0.213	0.169	–0.095	–0.092
	P	–0.142	–0.384	–0.503	0.152	0.089	–0.099	0.209	–0.063	–0.054
COS/BTMG/1-butanol	R	–0.288	–0.131	–0.041	0.217	0.044	–0.220	0.166	–0.095	–0.087
	P	–0.123	–0.372	–0.540	0.150	0.096	–0.099	0.208	–0.063	–0.056
COS/BTMG/1-pentanol	R	–0.290	–0.140	–0.048	0.217	0.100	–0.212	0.166	–0.095	–0.088
	P	–0.123	–0.372	–0.538	0.150	0.096	–0.100	0.208	–0.063	–0.055
COS/BTMG/1-hexanol	R	–0.289	–0.140	–0.047	0.217	0.100	–0.211	0.166	–0.096	–0.089
	P	–0.124	–0.370	–0.532	0.150	0.097	–0.100	0.208	–0.063	–0.055
System		O26	O27	S28	C25	H31	N1	C6	N2	N3
COS/TBD/methanol	R	-0.311	-0.150	-0.034	0.220	0.099	-0.246	0.157	-0.152	-0.101
	P	-0.131	-0.374	-0.511	0.152	0.102	-0.109	0.208	-0.116	-0.067
COS/TBD/ethanol	R	-0.300	-0.146	-0.037	0.214	0.101	-0.265	0.154	-0.149	-0.101
	P	-0.132	-0.377	-0.522	0.152	0.108	-0.109	0.209	-0.109	-0.066
COS/TBD/1-propanol	R	-0.294	-0.159	-0.056	0.214	0.102	-0.265	0.164	-0.139	-0.098
	P	-0.154	-0.377	-0.499	0.154	0.092	-0.111	0.208	-0.104	-0.063
COS/TBD/1-butanol	R	-0.298	-0.155	-0.059	0.214	0.100	-0.259	0.167	-0.136	-0.092
	P	-0.153	-0.376	-0.497	0.155	0.093	-0.112	0.208	-0.105	-0.064
COS/TBD/1-pentanol	R	-0.301	-0.153	-0.064	0.213	0.099	-0.258	0.167	-0.135	-0.091
	P	-0.153	-0.375	-0.496	0.155	0.095	-0.111	0.208	-0.105	-0.064
COS/TBD/1-hexanol	R	-0.295	-0.157	-0.058	0.214	0.101	-0.262	0.167	-0.139	-0.089
	P	-0.159	-0.369	-0.516	0.153	0.104	-0.101	0.211	-0.101	-0.066

Table 4.2. (cont'd) Partial charges, in e, of the atoms that were in the reaction region, which were obtained via the Mulliken and Hirshfeld population analysis. The numbering scheme for these atoms is given in Figures 4.2–4.25).

Natural Population Analysis Charges										
System	Atom									
		O26	O27	S28	C25	H31	N1	C6	N2	N3
COS/DBU/methanol	R	–0.823	–0.468	–0.012	0.475	0.504	–0.673	0.533	–0.521	----
	P	–0.632	–0.712	–0.578	0.615	0.450	–0.577	0.614	–0.447	----
COS/DBU/ethanol	R	–0.835	–0.466	–0.014	0.478	0.507	–0.671	0.533	–0.520	----
	P	–0.645	–0.715	–0.574	0.616	0.451	–0.579	0.614	–0.448	----
COS/DBU/1-propanol	R	–0.829	–0.466	–0.012	0.478	0.506	–0.671	0.534	–0.520	----
	P	–0.643	–0.713	–0.572	0.616	0.451	–0.578	0.614	–0.448	----
COS/DBU/1-butanol	R	–0.820	–0.461	0.012	0.454	0.504	–0.669	0.529	–0.522	----
	P	–0.643	–0.712	–0.572	0.616	0.452	–0.579	0.614	–0.448	----
COS/DBU/1- pentanol	R	–0.819	–0.461	0.012	0.455	0.504	–0.668	0.529	–0.522	----
	P	–0.643	–0.711	–0.571	0.616	0.453	–0.580	0.614	–0.449	----
COS/DBU/1-hexanol	R	–0.817	–0.462	0.013	0.455	0.504	–0.667	0.529	–0.523	----
	P	–0.644	–0.710	–0.569	0.615	0.453	–0.580	0.614	–0.449	----
System		O26	O27	S28	C25	H31	N1	C6	N2	N3
COS/DBN/methanol	R	–0.818	–0.462	–0.007	0.466	0.500	–0.675	0.529	–0.507	----
	P	–0.632	–0.706	–0.594	0.622	0.459	–0.580	0.602	–0.435	----
COS/DBN/ethanol	R	–0.825	–0.461	–0.010	0.470	0.499	–0.678	0.530	–0.508	----
	P	–0.623	–0.709	–0.579	0.640	0.446	–0.608	0.620	–0.445	----
COS/DBN/1- propanol	R	–0.822	–0.461	–0.011	0.471	0.500	–0.678	0.530	–0.508	----
	P	–0.620	–0.708	–0.577	0.641	0.446	–0.608	0.620	–0.444	----
COS/DBN/1-butanol	R	–0.827	–0.462	–0.013	0.472	0.502	–0.675	0.529	–0.507	----
	P	–0.619	–0.708	–0.578	0.643	0.446	–0.608	0.620	–0.444	----
COS/DBN/1- pentanol	R	–0.811	–0.464	–0.004	0.466	0.496	–0.676	0.524	–0.514	----
	P	–0.620	–0.707	–0.578	0.642	0.446	–0.608	0.620	–0.445	----
COS/DBN/1-hexanol	R	–0.807	–0.463	–0.005	0.466	0.496	–0.671	0.521	–0.519	----
	P	–0.620	–0.706	–0.575	0.642	0.447	–0.608	0.620	–0.445	----
System		O26	O27	S28	C25	H31	N1	C6	N2	N3

Table 4.2. (cont'd) Partial charges, in e, of the atoms that were in the reaction region, which were obtained via the Mulliken and Hirshfeld population analysis. The numbering scheme for these atoms is given in Figures 4.2–4.25).

Natural Population Analysis Charges										
System	Atom									
		O26	O27	S28	C25	H31	N1	C6	N2	N3
COS/BTMG/methanol	R	–0.826	–0.461	–0.014	0.477	0.510	–0.716	0.720	–0.562	–0.519
	P	–0.626	–0.710	–0.590	0.625	0.448	–0.671	0.786	–0.499	–0.461
COS/BTMG/ethanol	R	–0.838	–0.464	–0.010	0.476	0.514	–0.716	0.721	–0.562	–0.519
	P	–0.637	–0.712	–0.585	0.619	0.450	–0.678	0.783	–0.495	–0.459
COS/BTMG/1-propanol	R	–0.829	–0.462	–0.013	0.473	0.507	–0.699	0.713	–0.560	–0.528
	P	–0.622	–0.712	–0.581	0.638	0.455	–0.698	0.776	–0.499	–0.466
COS/BTMG/1-butanol	R	–0.836	–0.463	–0.005	0.472	0.515	–0.716	0.721	–0.562	–0.519
	P	–0.641	–0.708	–0.585	0.628	0.452	–0.668	0.787	–0.498	–0.468
COS/BTMG/1-pentanol	R	–0.839	–0.465	–0.013	0.481	0.514	–0.703	0.721	–0.562	–0.525
	P	–0.642	–0.708	–0.585	0.628	0.452	–0.670	0.787	–0.498	–0.466
COS/BTMG/1-hexanol	R	–0.838	–0.465	–0.013	0.480	0.514	–0.700	0.720	–0.563	–0.526
	P	–0.642	–0.707	–0.582	0.627	0.453	–0.671	0.789	–0.499	–0.466
System		O26	O27	S28	C25	H31	N1	C6	N2	N3
COS/TBD/methanol	R	-0.827	-0.448	-0.020	0.474	0.501	-0.721	0.690	-0.676	-0.539
	P	-0.625	-0.699	-0.568	0.635	0.446	-0.632	0.740	-0.656	-0.484
COS/TBD/ethanol	R	-0.825	-0.462	-0.007	0.472	0.497	-0.721	0.689	-0.672	-0.539
	P	-0.635	-0.703	-0.581	0.641	0.446	-0.632	0.740	-0.648	-0.485
COS/TBD/1-propanol	R	-0.820	-0.459	-0.023	0.479	0.499	-0.719	0.684	-0.658	-0.535
	P	-0.610	-0.705	-0.583	0.638	0.440	-0.645	0.745	-0.628	-0.488
COS/TBD/1-butanol	R	-0.822	-0.459	-0.023	0.478	0.500	-0.715	0.687	-0.66	-0.537
	P	-0.610	-0.705	-0.585	0.640	0.440	-0.645	0.746	-0.629	-0.489
COS/TBD/1-pentanol	R	-0.826	-0.458	-0.014	0.469	0.500	-0.714	0.687	-0.662	-0.535
	P	-0.610	-0.704	-0.584	0.639	0.440	-0.643	0.746	-0.631	-0.489
COS/TBD/1-hexanol	R	-0.820	-0.458	-0.025	0.479	0.499	-0.714	0.685	-0.664	-0.533
	P	-0.611	-0.705	-0.588	0.630	0.442	-0.629	0.741	-0.639	-0.489

Mulliken and Hirshfeld conducted population analyses, which are given in Table 4.3. The Mulliken charge for the negatively charged species was excessively negative. Additionally, the positive species were excessively positive when compared to the Hirshfeld charges, which are also given in Table 4.3. The COS/DBU/1-pentanol, COS/DBU/1-hexanol, and COS/DBU/1-butanol systems were perhaps the most interesting examples, because their fragments charged above ±1. The Hirshfeld scheme showed a systematic reduction in the negative as well as positive charges using the linear alcohols for the COS/DBU/1-pentanol system, the COS/DBU/1-hexanol system, and COS/DBU/1-butanol system. The COS/BTMG/ethanol system was the only exception, which showed that the fragment charges slightly increased when compared to the COS/BTMG/methanol system, no trend was observed in the Mulliken scheme for the systematic analysis. The structures of the product of the COS/DBU/methanol system, the COS/DBN/methanol system, the COS/BTMG/methanol system and the COS/TBD/methanol system resulted in fragments that consisted of: $DBU - H^+$, $DBN - H^+$, $BTMG - H^+$, $TBD - H^+$ They had 0.757*e*, 0.810*e*, 0.773*e* and 0.730*e* Hirshfeld partial charges and $CH_3 - O - COS^-$ fragments for the systems, which had – 0.757*e*, –0.810*e*, –0.773*e* and – 0.730*e* partial charges. The COS/TBD/methanol systems (– 0.730, 0.730*e*) exhibited the lowest Hirshfeld fragment charges, while the highest fragment charges were seen with the COS/DBN/methanol system, at –0.810 and 0.810 *e*. The mixture of these 4 amines with the studied linear alcohols brought about the same $amine - H^+$ and $R - O - COS^-$ trend as the fragment charge distribution. Table 4.3 shows the findings that the products of the Zwitterionic complex were formed as a result of the single-step reaction and Eq. (2.8) suggests the mechanism, which was given above in the COS reaction process.

Table 4.3. Charges, in e, that were on the product fragments, which were obtained via the Mulliken and Hirshfeld analyses, which comprised amine–H+ and R–O–COS–.

System		Fragment	
		$DBU - H^+$	$CH_3 - O - COS^-$
COS/DBU/methanol	Mulliken	0.949	– 0.949
	Hirshfeld	0.757	– 0.757
	NPA	0.966	– 0.966
		$DBU - H^+$	$CH_3 - O - COS^-$
COS/DBU/ethanol	Mulliken	0.983	– 0.983
	Hirshfeld	0.746	– 0.746
	NPA	0.963	– 0.963
		$DBU - H^+$	$CH_3 - O - COS^-$

Table 4.3. (cont'd) Charges, in e, that were on the product fragments, which were obtained via the Mulliken and Hirshfeld analyses, which comprised amine–H+ and R–O–COS–.

System		Fragment	
		$DBU-H^+$	$CH_3-O-COS^-$
COS/DBU/1-propanol	Mulliken	0.997	– 0.997
	Hirshfeld	0.746	– 0.746
	NPA	0.964	– 0.964
		$DBU-H^+$	$CH_3-O-COS^-$
COS/DBU/1-butanol	Mulliken	1.001	– 1.001
	Hirshfeld	0.746	– 0.746
	NPA	0.963	– 0.963
		$DBU-H^+$	$CH_3-O-COS^-$
COS/DBU/1-pentanol	Mulliken	1.009	– 1.009
	Hirshfeld	0.742	– 0.742
	NPA	0.962	– 0.962
		$DBU-H^+$	$CH_3-O-COS^-$
COS/DBU/1-hexanol	Mulliken	1.014	– 1.014
	Hirshfeld	0.739	– 0.739
	NPA	0.961	– 0.961
		$DBN-H^+$	$CH_3-O-COS^-$
COS/DBN/methanol	Mulliken	0.878	– 0.878
	Hirshfeld	0.810	– 0.810
	NPA	0.965	– 0.965
		$DBN-H^+$	$CH_3-O-COS^-$
COS/DBN/ethanol	Mulliken	0.770	– 0.770
	Hirshfeld	0.757	– 0.757
	NPA	0.920	– 0.920
		$DBN-H^+$	$CH_3-O-COS^-$
COS/DBN/1-propanol	Mulliken	0.823	– 0.823
	Hirshfeld	0.755	– 0.755
	NPA	0.920	– 0.920
		$DBN-H^+$	$CH_3-O-COS^-$
COS/DBN/1-butanol	Mulliken	0.847	– 0.847
	Hirshfeld	0.752	– 0.752
	NPA	0.921	– 0.921
		$DBN-H^+$	$CH_3-O-COS^-$
COS/DBN/1-pentanol	Mulliken	0.864	– 0.864
	Hirshfeld	0.751	– 0.751
	NPA	0.879	– 0.879
		$DBN-H^+$	$CH_3-O-COS^-$
COS/DBN/1-hexanol	Mulliken	0.865	– 0.865
	Hirshfeld	0.748	– 0.748
	NPA	0.918	– 0.918
		$BTMG-H^+$	$CH_3-O-COS^-$
COS/BTMG/methanol	Mulliken	0.863	– 0.863
	Hirshfeld	0.773	– 0.773
	NPA	0.957	– 0.957
		$BTMG-H^+$	$CH_3-O-COS^-$
COS/BTMG/ethanol	Mulliken	0.891	– 0.891
	Hirshfeld	0.783	– 0.783
	NPA	0.959	– 0.959
		$BTMG-H^+$	$CH_3-O-COS^-$

Table 4.3. (cont'd) Charges, in e, that were on the product fragments, which were obtained via the Mulliken and Hirshfeld analyses, which comprised amine–H+ and R–O–COS–.

System		Fragment	
		$DBU-H^+$	$CH_3-O-COS^-$
COS/BTMG/1-propanol	Mulliken	0.745	– 0.745
	Hirshfeld	0.770	– 0.770
	NPA	0.926	– 0.926
		$BTMG-H^+$	$CH_3-O-COS^-$
COS/BTMG/1-butanol	Mulliken	0.887	– 0.887
	Hirshfeld	0.766	– 0.766
	NPA	0.954	– 0.954
		$BTMG-H^+$	$CH_3-O-COS^-$
COS/BTMG/1-pentanol	Mulliken	0.900	– 0.900
	Hirshfeld	0.766	– 0.766
	NPA	0.954	– 0.954
		$BTMG-H^+$	$CH_3-O-COS^-$
COS/BTMG/1-hexanol	Mulliken	0.906	– 0.906
	Hirshfeld	0.760	– 0.760
	NPA	0.952	– 0.952
		$TBD-H^+$	$CH_3-O-COS^-$
COS/TBD/methanol	Mulliken	0.841	– 0.841
	Hirshfeld	0.730	– 0.730
	NPA	0.910	– 0.910
		$TBD-H^+$	$CH_3-O-COS^-$
COS/TBD/ethanol	Mulliken	0.825	– 0.825
	Hirshfeld	0.749	– 0.749
	NPA	0.920	– 0.920
		$TBD-H^+$	$CH_3-O-COS^-$
COS/TBD/1-propanol	Mulliken	0.711	– 0.711
	Hirshfeld	0.763	– 0.763
	NPA	0.923	– 0.923
		$TBD-H^+$	$CH_3-O-COS^-$
COS/TBD/1-butanol	Mulliken	0.696	– 0.696
	Hirshfeld	0.751	– 0.751
	NPA	0.920	– 0.920
		$TBD-H^+$	$CH_3-O-COS^-$
COS/TBD/1-pentanol	Mulliken	0.733	– 0.733
	Hirshfeld	0.750	– 0.750
	NPA	0.920	– 0.920
		$TBD-H^+$	$CH_3-O-COS^-$
COS/TBD/1-hexanol	Mulliken	0.813	– 0.813
	Hirshfeld	0.777	– 0.777
	NPA	0.935	– 0.935

It is worth mentioning that, generally, chemical reactions exhibit aspects that are both thermodynamic and kinetic; hence, the thermodynamics and kinetics were also analyzed to investigate the reactionary energetics, in addition to analyzing the structures and population. The standard Gibbs free reactionary energy (ΔG°_{rxn}), reaction rate constant (k) and free activation energy ($\Delta^{\ddagger}G^{\circ}$) values are given in Table

4.4. Eyring [89] presented a postulate to calculate reaction rate constants. In Table 4.4, the ΔG°_{rxn} values were an indication that all of these COS capturing reactions that were investigated herein had an exergonic nature, which means that all of these reactions were thermodynamically feasible and spontaneous. Here, the ΔG°_{rxn} values kept changing between –8.57 kcal/mol, in the COS/DBU/1-hexanol system, and –18.87, in the COS/TBD/1-propanol system. The next lowest after the COS/TBD/1-propanol system was the COS/BTMG/methanol system, with a ΔG°_{rxn} value of –18.12 kcal/mol. Among all of the systems that were investigated, the COS/BTM/methanol system was determined to have the activation energy value that was the lowest, which was 8.49 kcal/mol, when an investigation of the reaction barriers was conducted via calculation of the standard Gibbs free-energy activation values. Because the activation energy had an influence on the reaction rate constant, and so the activation energy value of the COS/BTMG/methanol system, which was low, and is shown in Figure 4.3., thus brought about the highest reaction rate constant value, which was 37.34×10^5 s^{-1}. The COS/TBD/1-propanol system exhibited the 2nd-best performance with regard to the COS absorption, which can be seen in Figure 4.4. It can be observed that the $\Delta^{\ddagger}G^{\circ}$ value was 8.71 kcal/mol, while the k value was 25.39×10^5 s^{-1}. Activation energy yields of below 10 kcal/mol were also obtained with the other systems, such as the COS/DBU/methanol system, with a value of 9.23 kcal/mol, as shown in Figure 4.5. and COS/BTMG/1-pentanol system, with a value of 9.07 kcal/mol, as shown in Figure 4.6. The rate constants for these were determined to be 14.02×10^5 s^{-1} and 10.57×10^5 s^{-1}, respectively. Rather than using BTMG or DBU as a base, when DBN and TBD was used, the same reactionary performance was achieved for all of the COS/DBN/alcohols and COS/TBD/alcohols. The activation energy and rate constant were observed to fluctuate for the both systems. Such as, (10.61 kcal/mol and 1.032×10^5 s^{-1}) and (10.13 kcal/mol and 2.329×10^5 s^{-1}) for COS/DBN/1-propanol and COS/TBD/methanol system, respectively, while for the COS/DBN/1-butanol and COS/TBD/1-hexanol systems these values were (11.64 kcal/mol and 0.181×10^5 s^{-1}) and (12.49 kcal/mol and 0.043×10^5 s^{-1}) respectively. In fact, the COS capturing performance using the COS/DBN/alcohol and COS/TBD/alcohol processes, Figures (4.8–4.13), (4.20–4.25) was generally an intermediate-level performance.

The mixture of BTMG and 1-propanol should be avoided while capturing COS because it exhibited the reaction rate constant that was the lowest, at 0.829×10^3 s^{-1}, and the reaction barrier that was the highest, at13.47 kcal/mol.

Table 4.4. Tabulation of the kinetic and thermodynamic properties of the systems used to capture the COS.

Thermodynamic & kinetic properties	System			
	COS/DBU/methanol	COS/DBN/methanol	COS/BTMG/methanol	COS/TBD/methanol
ΔG°_{rxn} *(kcal/mol)*	–12.61	–12.74	–18.17	–16.28
$\Delta^{\ddagger}G^{\circ}$ *(kcal/mol)*	9.23	10.71	8.49	10.13
k (s⁻¹)	10.57×10^5	0.876×10^5	37.34×10^5	2.33×10^5
	COS/DBU/ethanol	COS/DBN/ethanol	COS/BTMG/ethanol	COS/TBD/ethanol
ΔG°_{rxn} *(kcal/mol)*	–13.05	–13.99	–16.50	–17.45
$\Delta^{\ddagger}G^{\circ}$ *(kcal/mol)*	8.83	11.24	10.97	11.12
k (s⁻¹)	21.07×10^5	0.359×10^5	0.568×10^5	0.44×10^5
	COS/DBU/1-propanol	COS/DBN/1-propanol	COS/BTMG/1-propanol	COS/TBD/1-propanol
ΔG°_{rxn} *(kcal/mol)*	–10.93	–15.01	–18.12	–18.87
$\Delta^{\ddagger}G^{\circ}$ *(kcal/mol)*	10.06	10.61	13.47	8.71
k (s⁻¹)	2.635×10^5	1.032×10^5	0.829×10^3	25.39×10^5
	COS/DBU/1-butanol	COS/DBN/1-butanol	COS/BTMG/1-butanol	COS/TBD/1-butanol
ΔG°_{rxn} *(kcal/mol)*	–10.16	–13.16	–16.23	–16.69
$\Delta^{\ddagger}G^{\circ}$ *(kcal/mol)*	11.68	11.64	10.37	11.90
k (s⁻¹)	0.171×10^5	0.181×10^5	1.555×10^5	0.117×10^5
	COS/DBU/1-pentanol	COS/DBN/1-pentanol	COS/BTMG/1-pentanol	COS/TBD/1-pentanol
ΔG°_{rxn} *(kcal/mol)*	–9.40	–13.66	–14.49	–16.55
$\Delta^{\ddagger}G^{\circ}$ *(kcal/mol)*	12.54	10.97	9.07	11.88
k (s⁻¹)	0.040×10^5	0.560×10^5	14.02×10^5	0.121×10^5
	COS/DBU/1-hexanol	COS/DBN/1-hexanol	COS/BTMG/1-hexanol	COS/TBD/1-hexanol
ΔG°_{rxn} *(kcal/mol)*	–8.57	–13.87	–14.11	–16.12
$\Delta^{\ddagger}G^{\circ}$ *(kcal/mol)*	12.69	10.62	10.48	12.49
k (s⁻¹)	0.031×10^5	1.013×10^5	1.293×10^5	0.043×10^5

For various organic liquids, when the reaction barriers to COS capture were compared to the findings available in the literature, it can be claimed that the findings presented in the research herein are promising. First, Hinderaker and Sandall [4], and later,

Amararene and Bouallou [3], conducted experiments to investigate COS capturing through the application of aqueous diethanol amine solution, which showed reaction barriers of around 12.5 and 11.5 kcal/mol, respectively. Cabaço et al. determined barrier heights between 15.1 to 27.3 kcal/mol for a reaction in which COS and imidazole-2-ylidene carbene species were used at the B3LYP/6-31+(d,p):MQZVP(S) theoretical level [90]. The stopped-flow technique was used by Alper et al., from 278 K to 298 K, using monoethanolamine, diethanolamine, diglycolamine, 2-amino-2-methyl-1-propanol, morpholine, and 2-(methylamino)ethanol, and di-isopropanolamine in their research study of COS reaction kinetics in the solutions, such as propylene glycol, ethylene glycol, isopropanol, and methanol. The activation energies were in the range of 11.1–19.7 kcal/mol [46]. According to our knowledge, in a recently conducted computational study related to COS capture using ionic liquids, the barriers with the lowest values were determined to be in 1-ethyl-3-methylimidazolium acetate (7.4 kcal/mol) at a B3LYP/6-31+(d,p):MQZVP(S) theoretical level [6]. In the current research study conducted herein, all of the reaction barrier values were determined to be less than or nearly equal to both the theoretical and the experimental values that have been previously reported in the literature for the different organic liquids. The results showed that most amine alcohol mixtures, which were investigated in this study, can be used for capturing COS.

In summary, the theoretical findings determined within the context of this research proved that as a guanidine base, such as BTMG when mixed with the methanol and TBD when mixed with the 1-propanol, exhibited the kinetically fastest reactions. Hence, this means that they were thermodynamically the most viable options for use in the capture of COS. Furthermore, when an amidine base, such as DBN or DBU, was utilized after having been mixed with a linear alcohol, comprising the methanol to 1-hexanol, DBU/methanol, or DBU/ethanol, and DBN/1-propanol mixture, it was observed that the systems effectively captured COS.

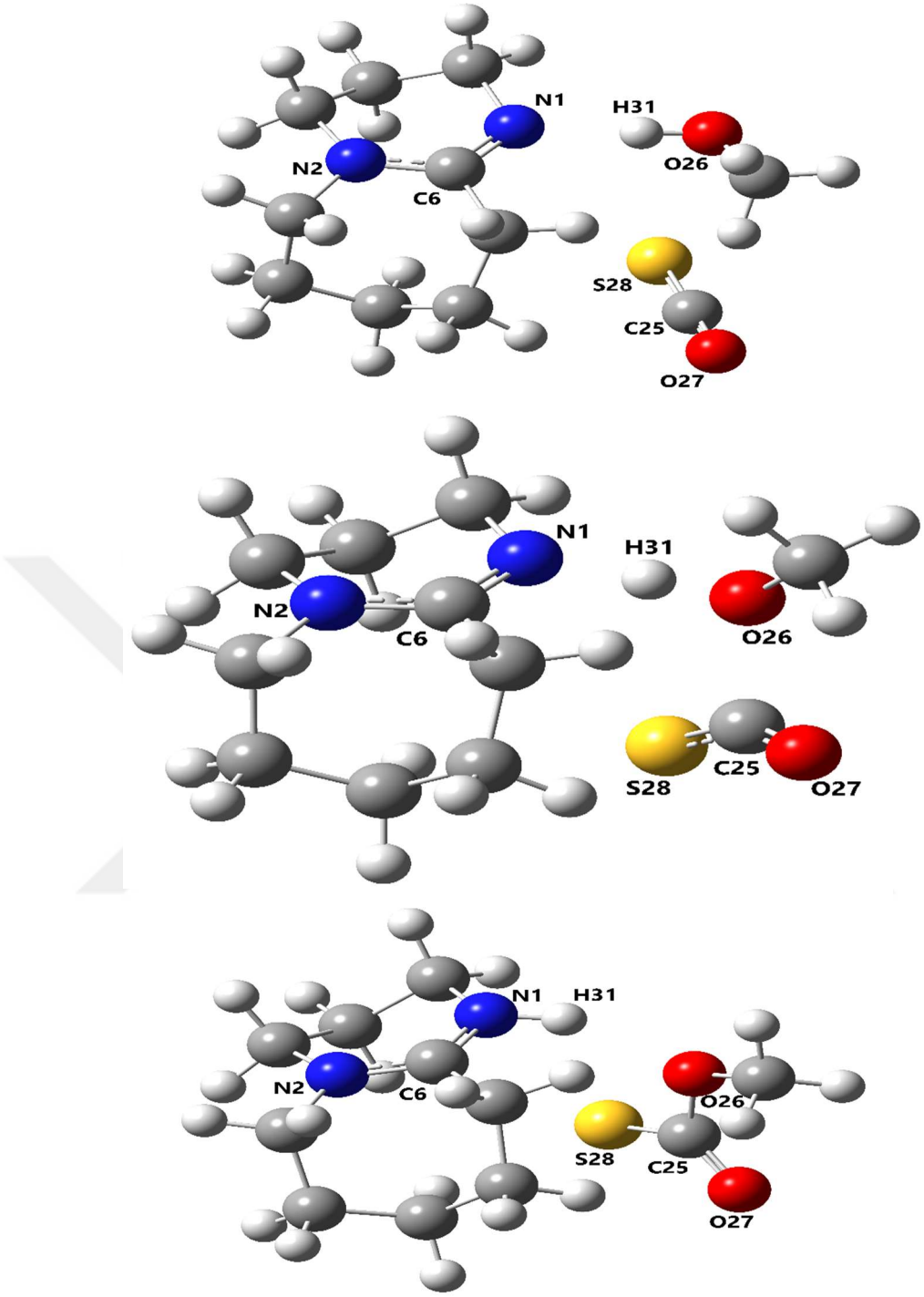

Figure 4.2. R (top), TS (middle), and P (bottom) structures of the COS/DBU/methanol system.

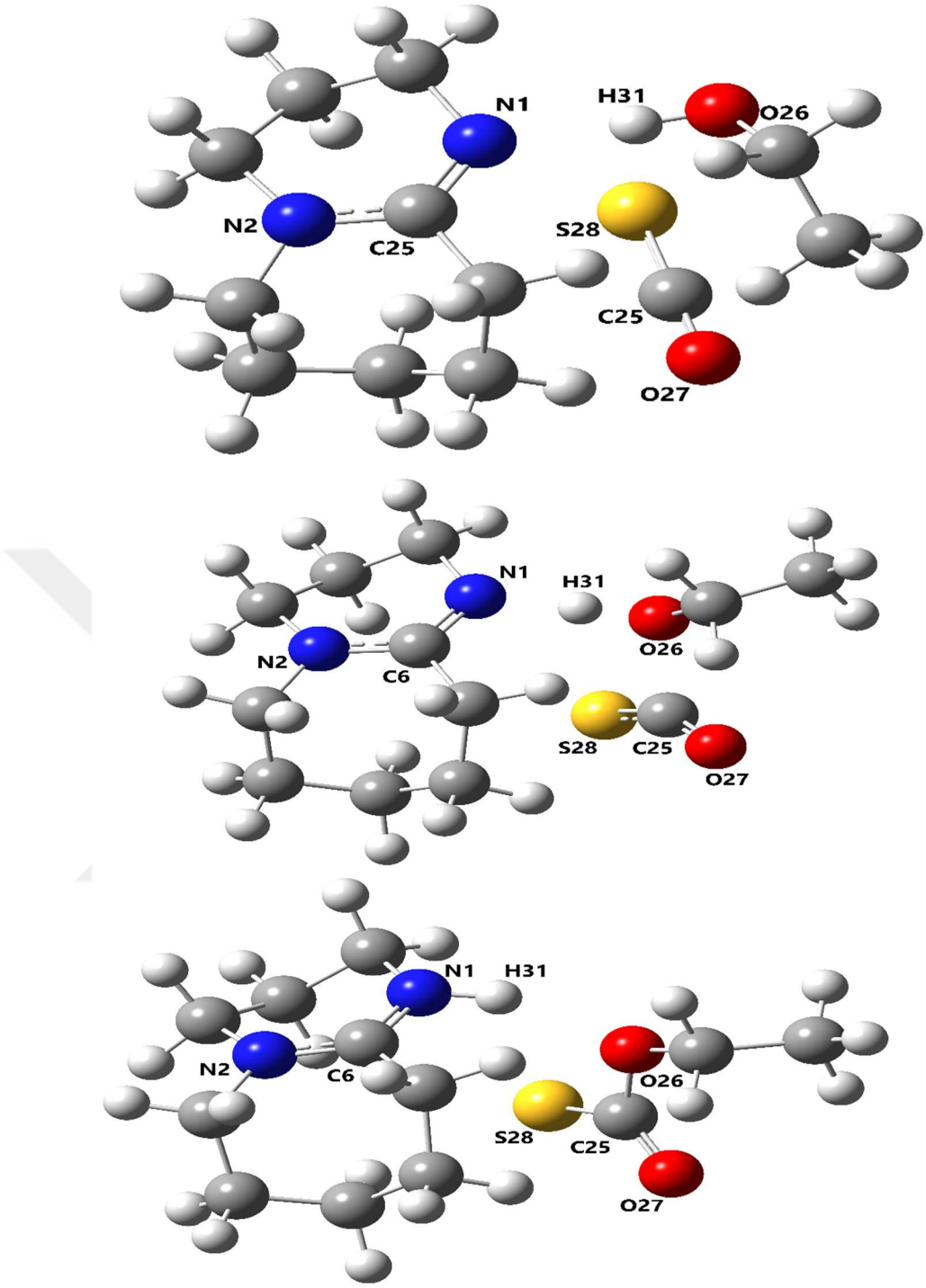

Figure 4.3. R (top), TS (middle), and P (bottom) structures of the COS/DBU/ethanol system.

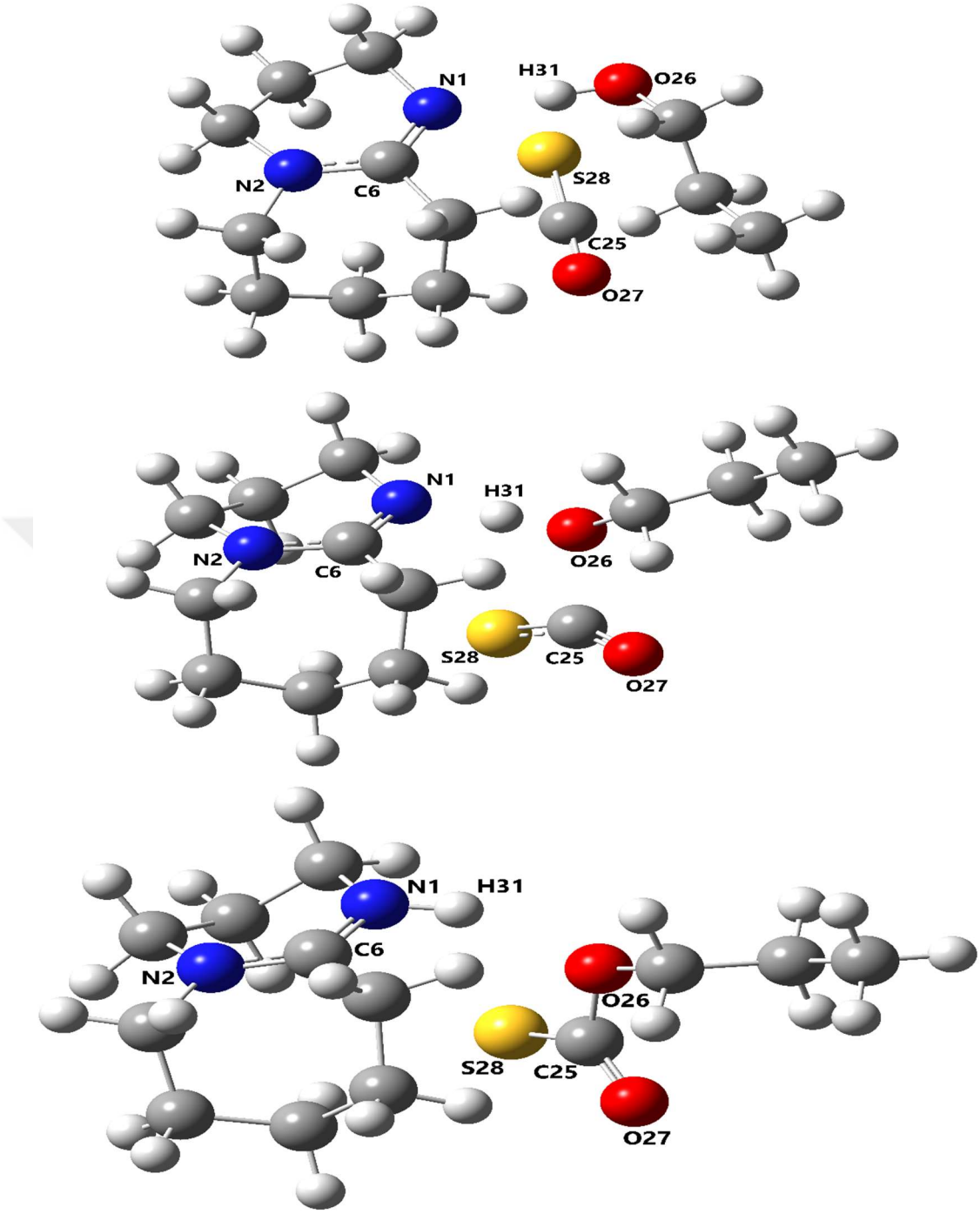

Figure 4.4. R (top), TS (middle), and P (bottom) structures of the COS/DBU/1-propanol system.

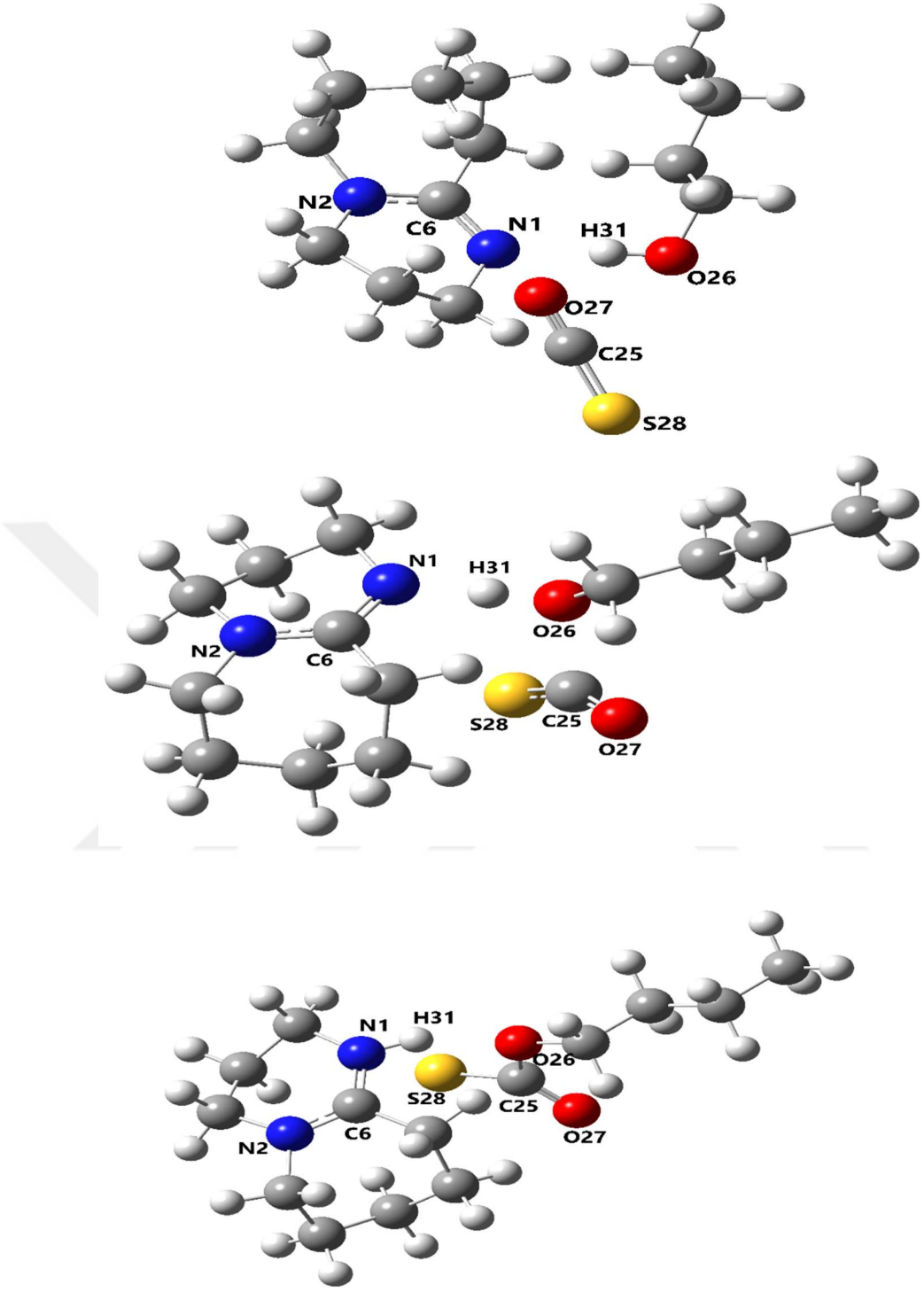

Figure 4.5. R (top), TS (middle), and P (bottom) structures of the COS/DBU/1-butanol system.

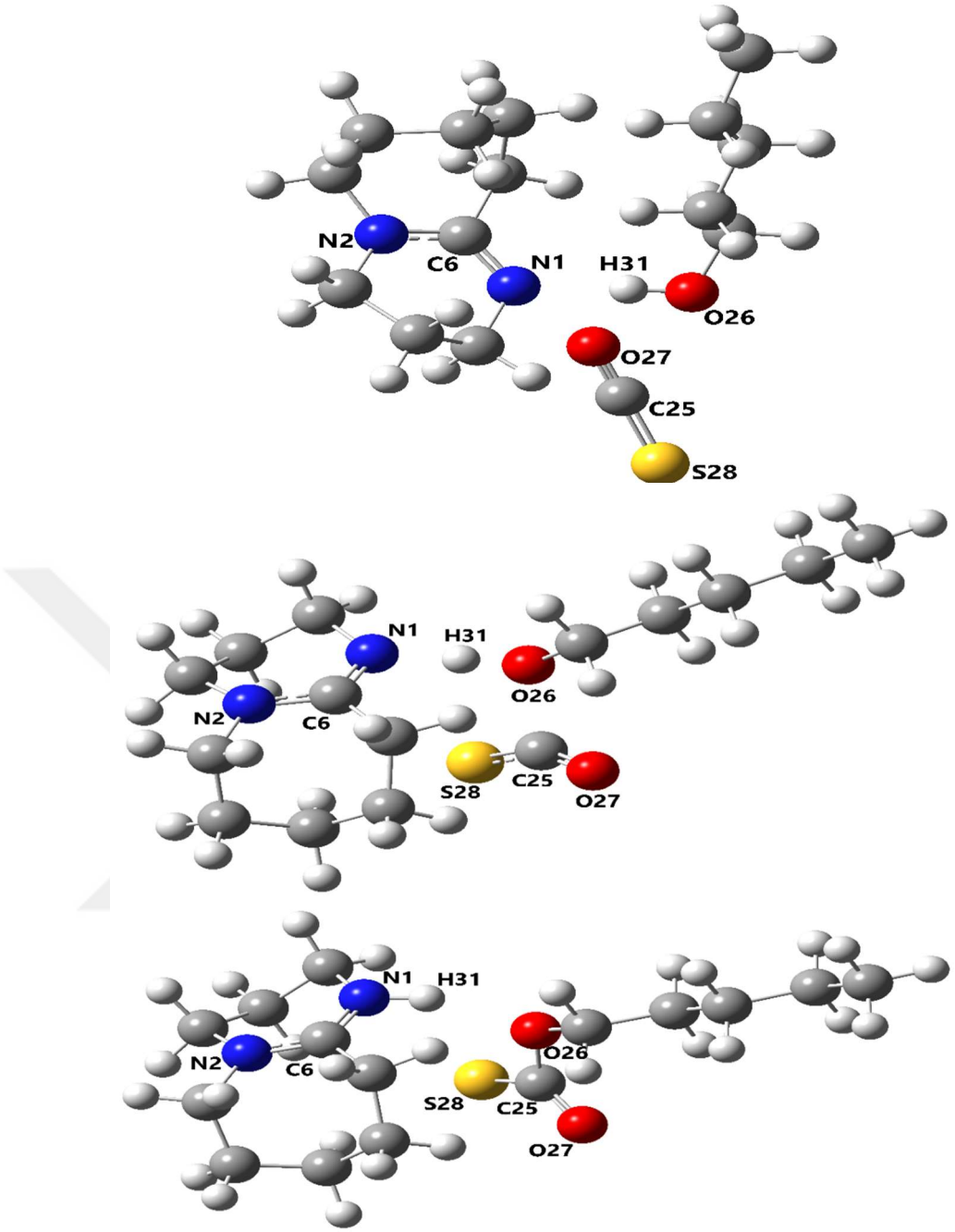

Figure 4.6. R (top), TS (middle), and P (bottom) structures of the COS/DBU/1-pentanol system.

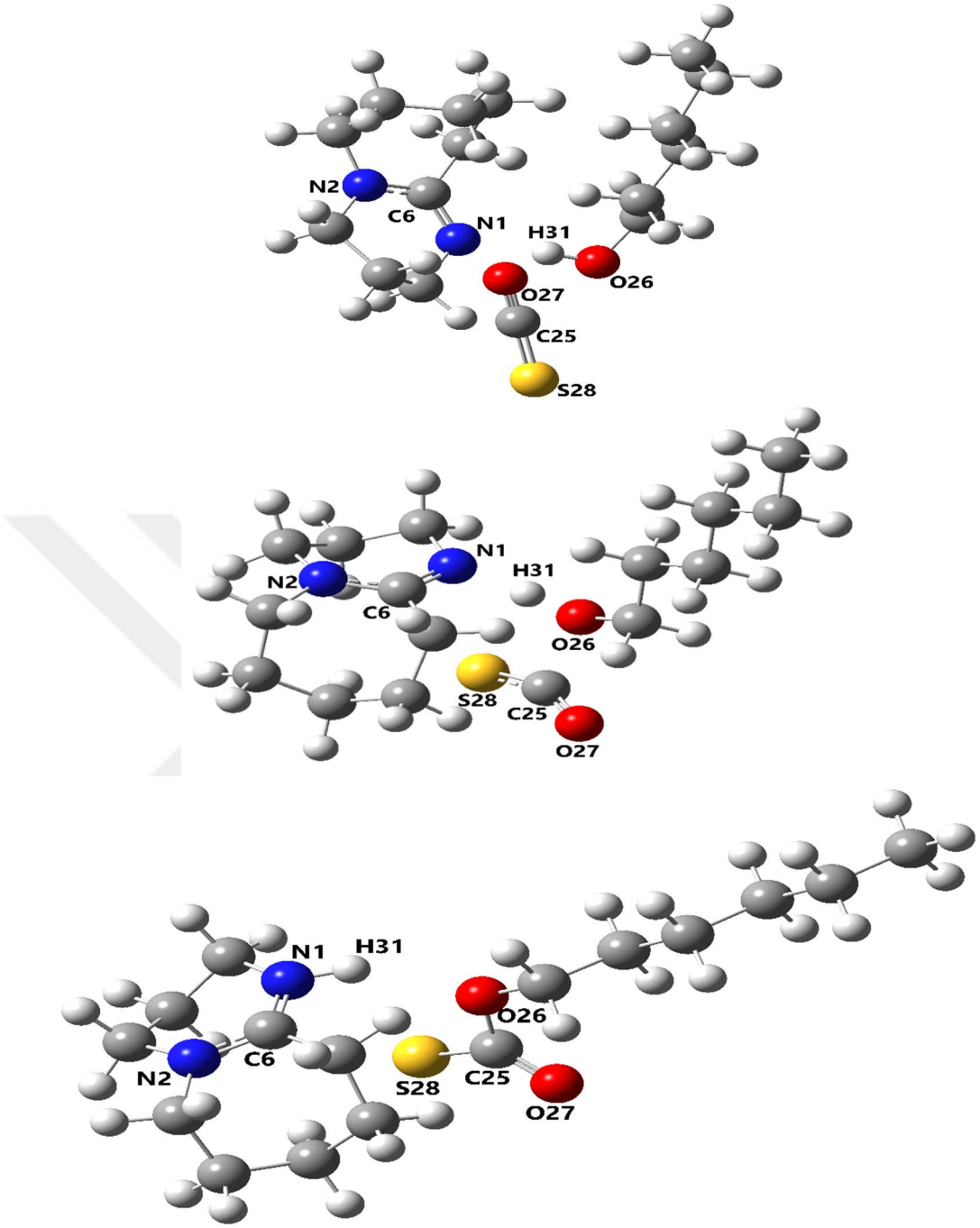

Figure 4.7. R (top), TS (middle), and P (bottom) structures of the COS/DBU/1-hexanol system.

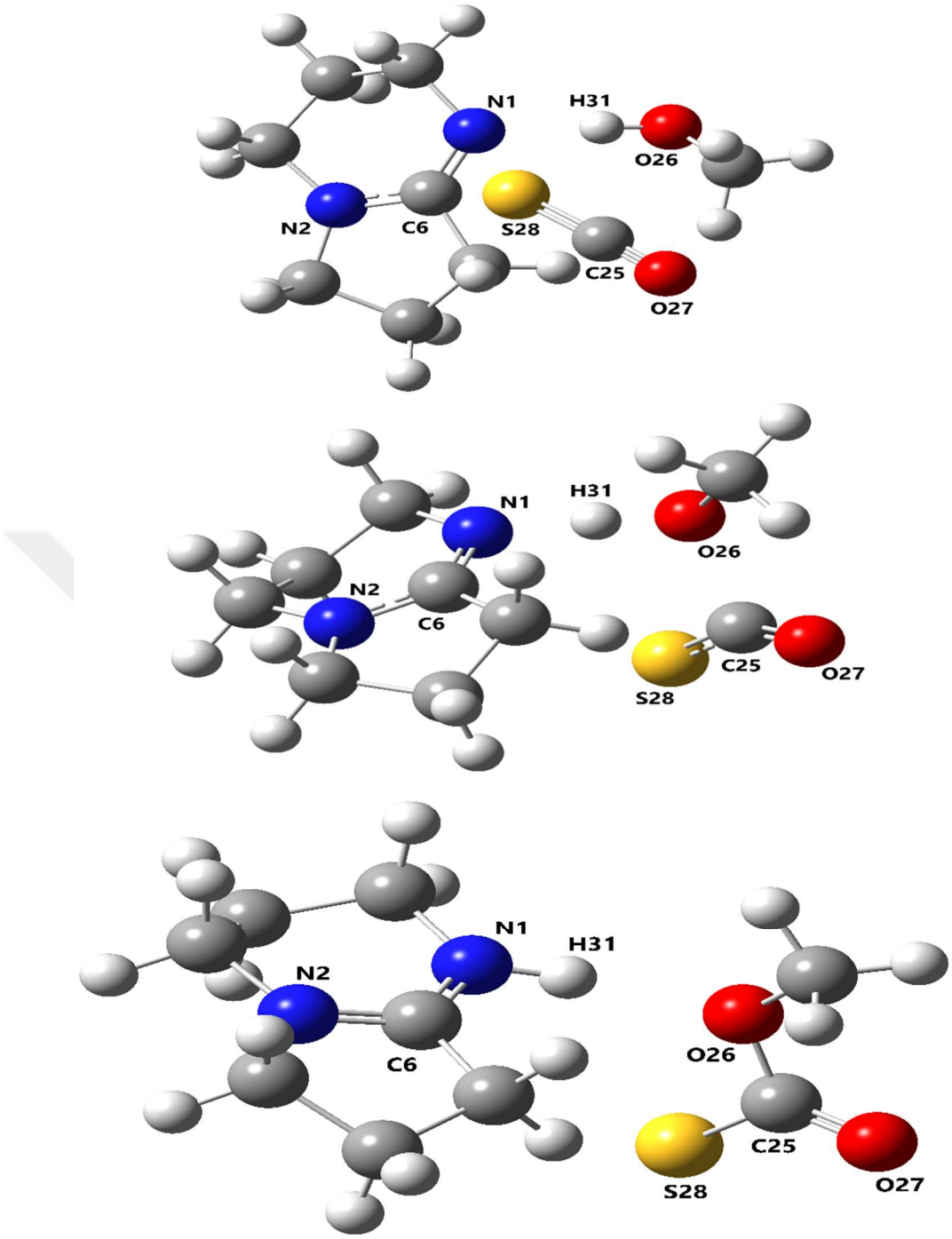

Figure 4.8. R (top), TS (middle), and P (bottom) structures of the COS/DBN/methanol system.

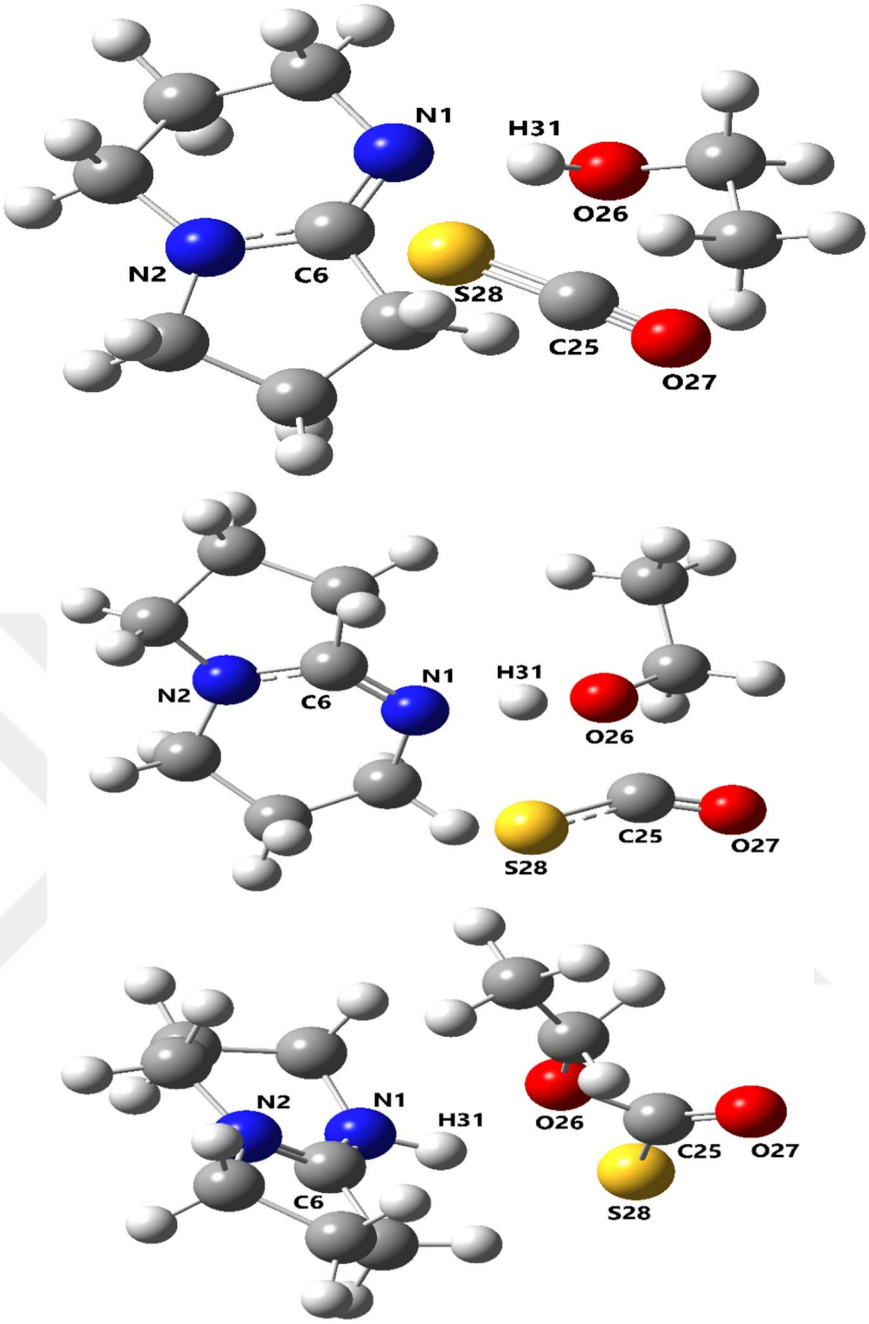

Figure 4.9. R (top), TS (middle), and P (bottom) structures of the COS/DBN/ethanol system.

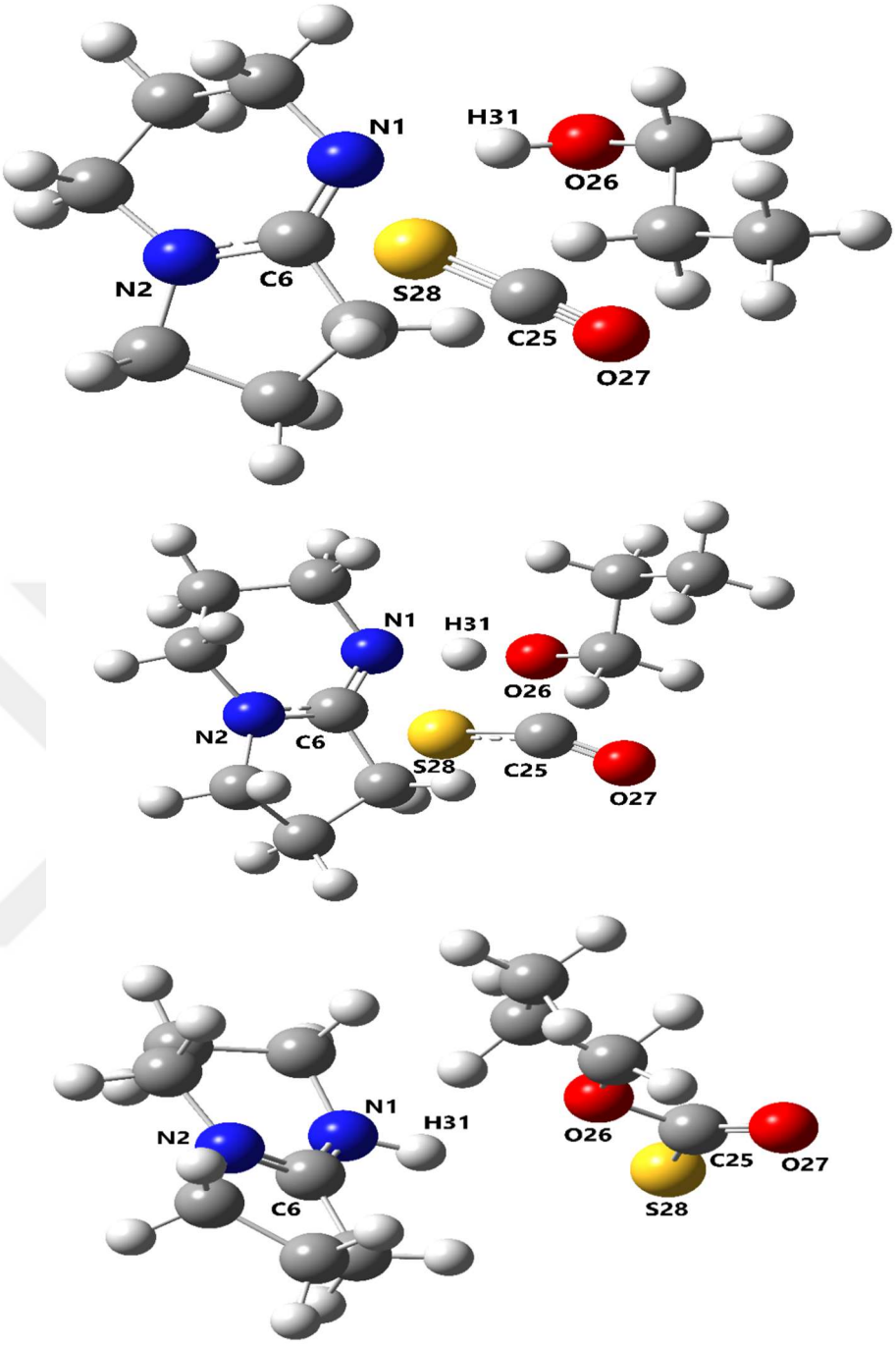

Figure 4.10. R (top), TS (middle) and P (bottom) structures of the COS/DBN/1-propanol system.

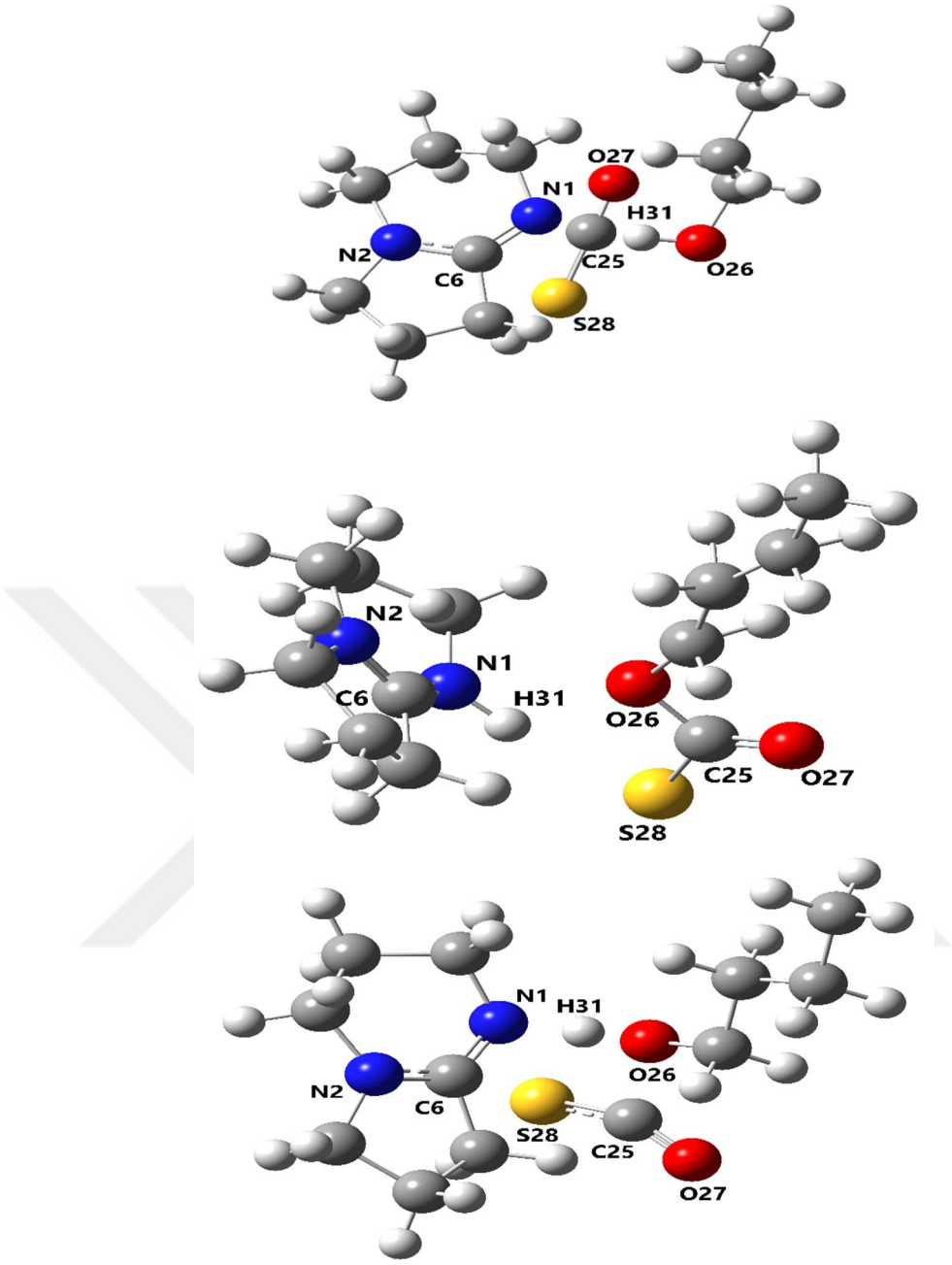

Figure 4.11. R (top), TS (middle) and P (bottom) structures of the COS/DBN/1-butanol system.

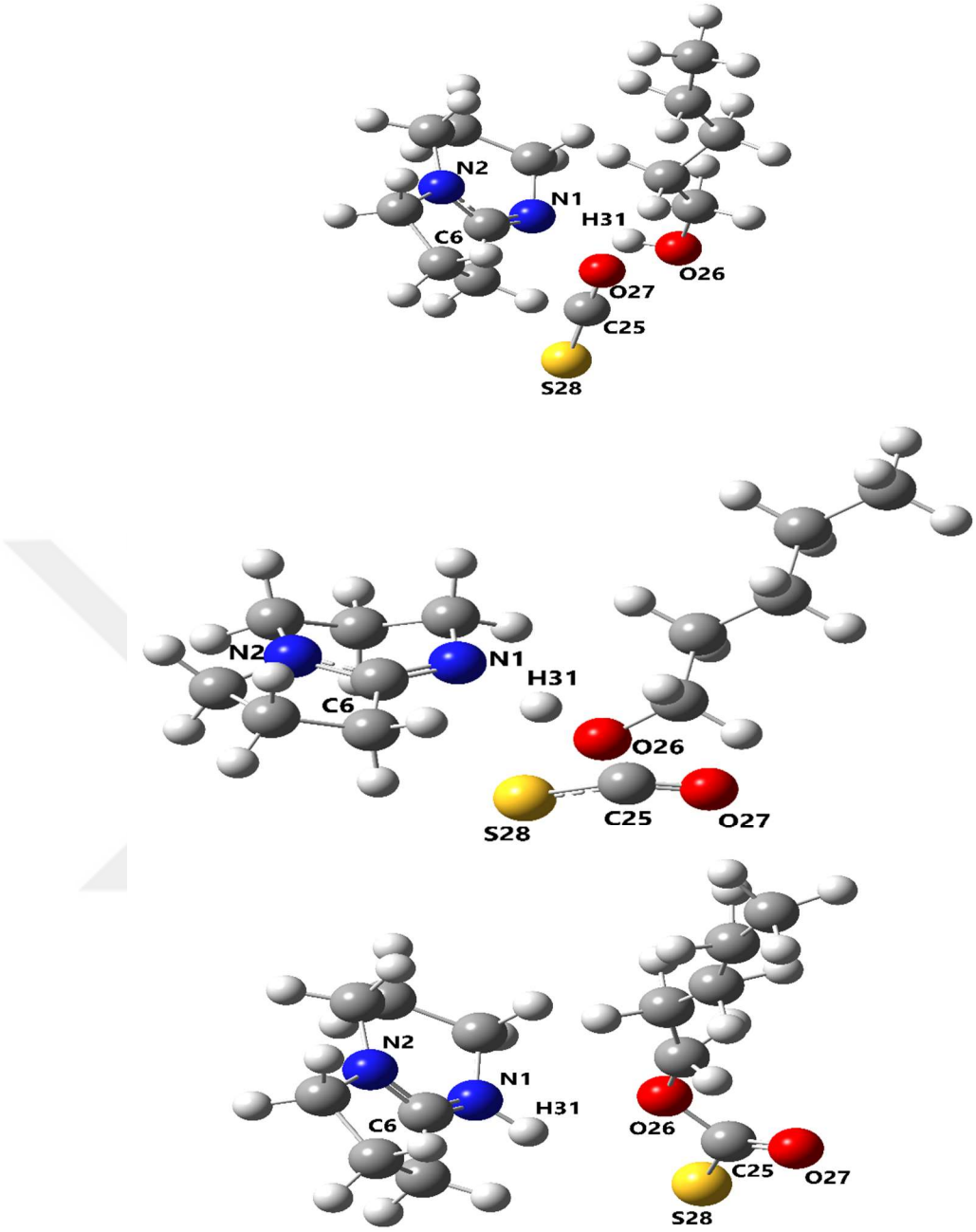

Figure 4.12. R (top), TS (middle), and P (bottom) structures of the COS/DBN/1-pentanol system.

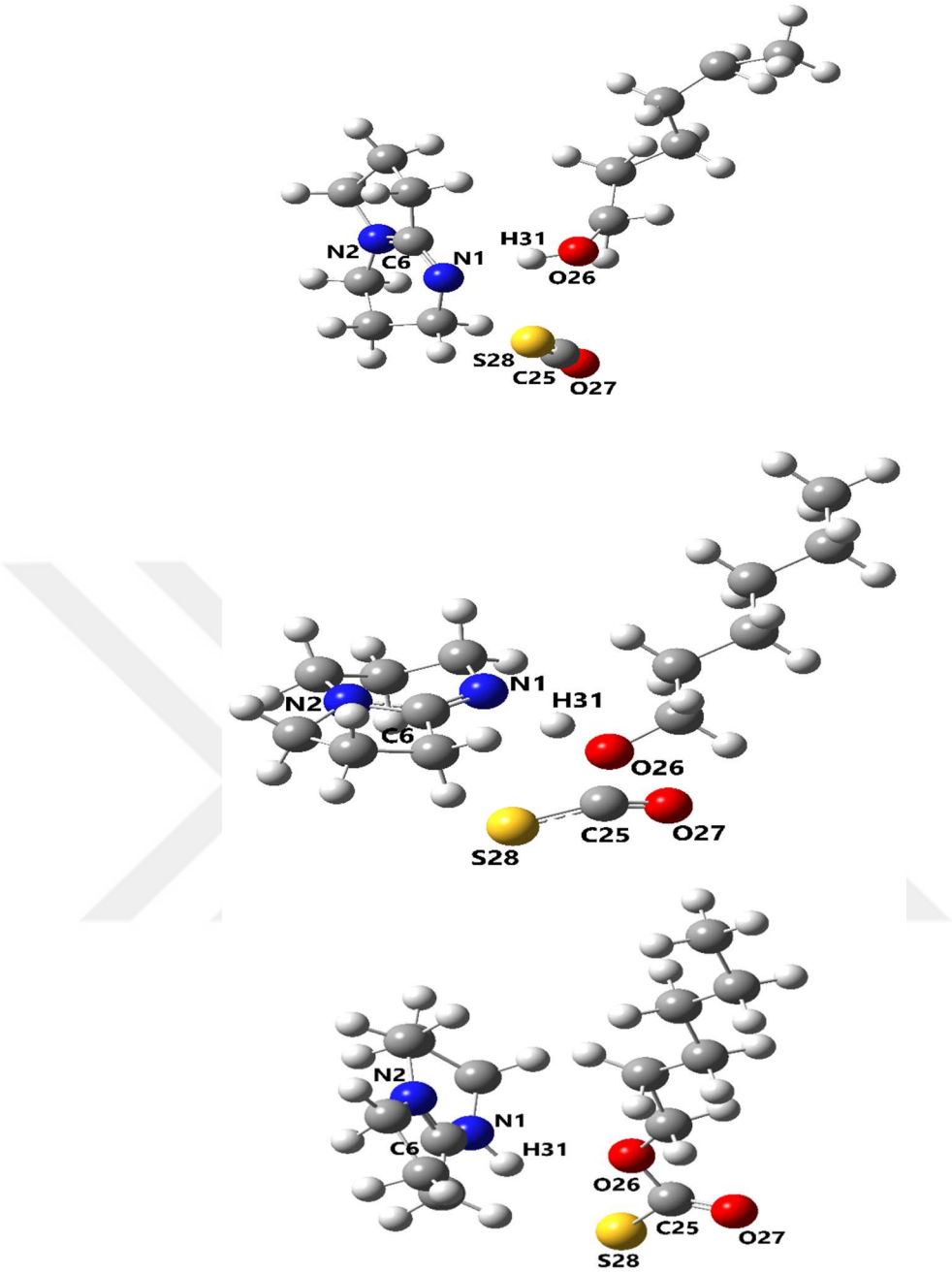

Figure 4.13. R (top), TS (middle), and P (bottom) structures of the COS/DBN/1-hexanol system.

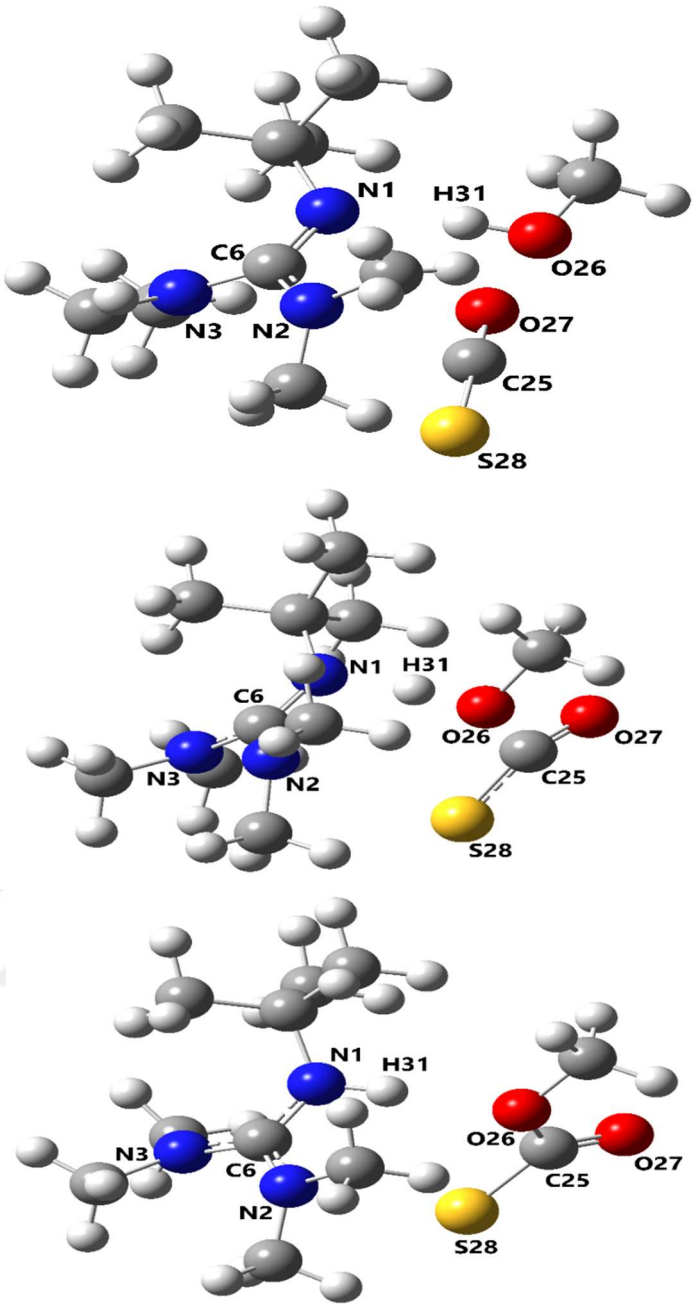

Figure 4.14. R (top), TS (middle), and P (bottom) structures of the COS/BTMG/methanol system.

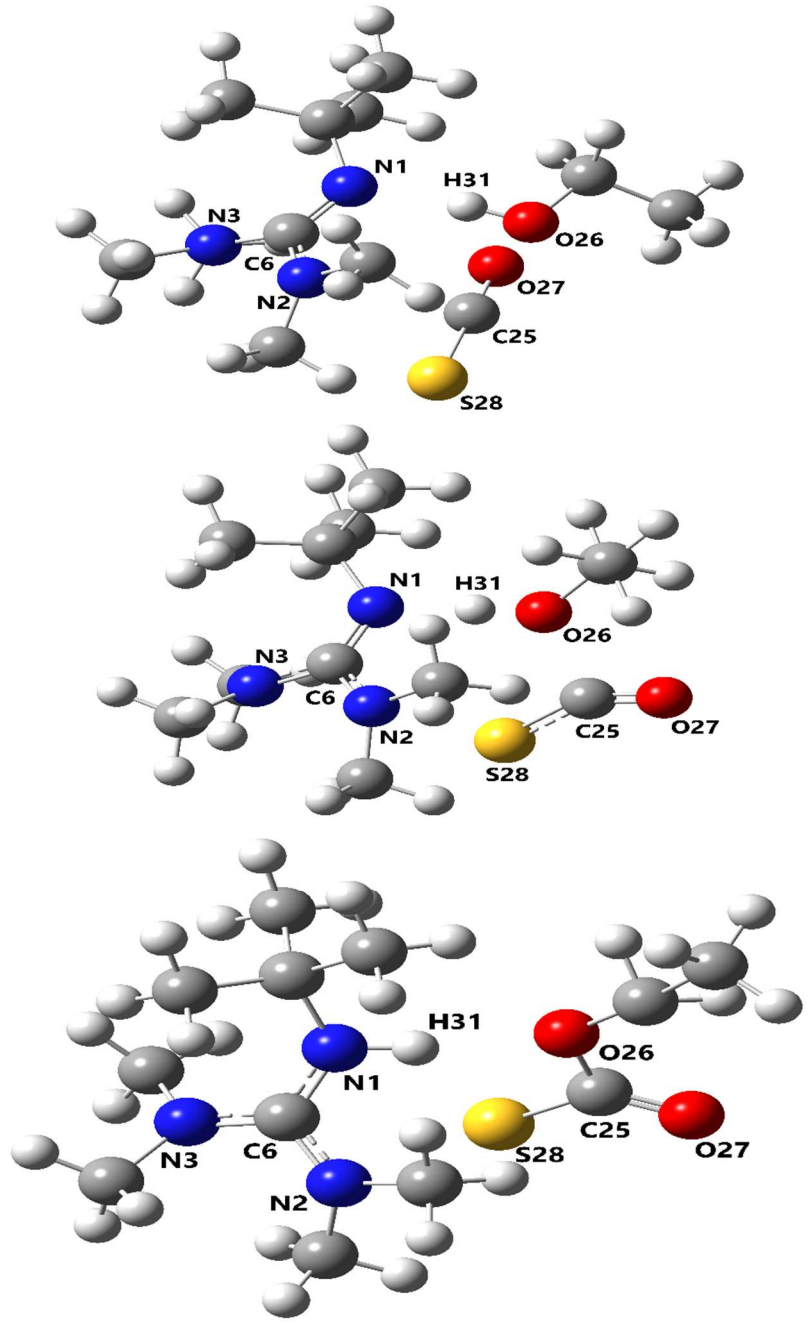

Figure 4.15. R (top), TS (middle), and P (bottom) structures of the COS/BTMG/ethanol system.

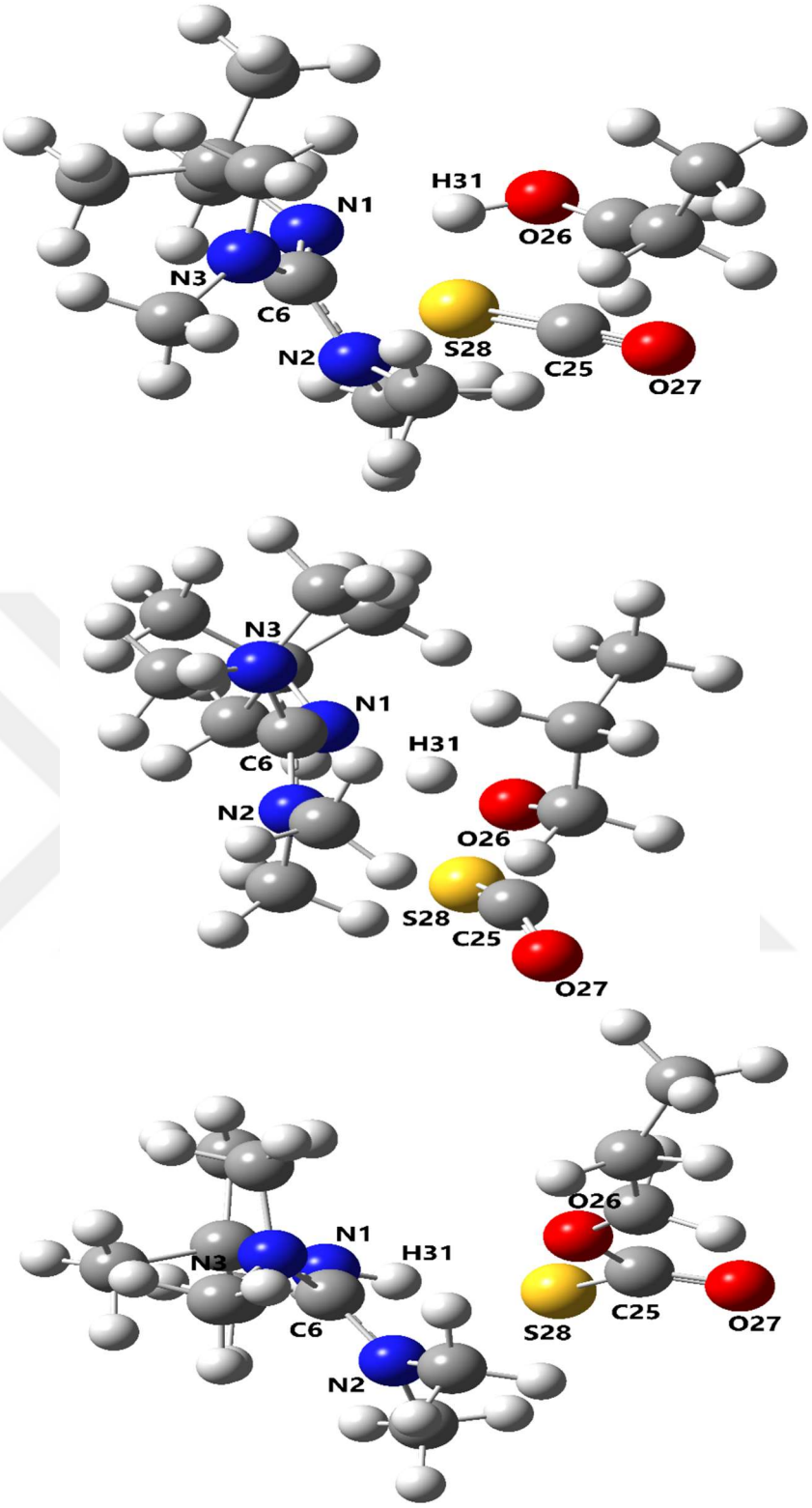

Figure 4.16. R (top), TS (middle), and P (bottom) structures of the COS/BTMG/1-propanol system.

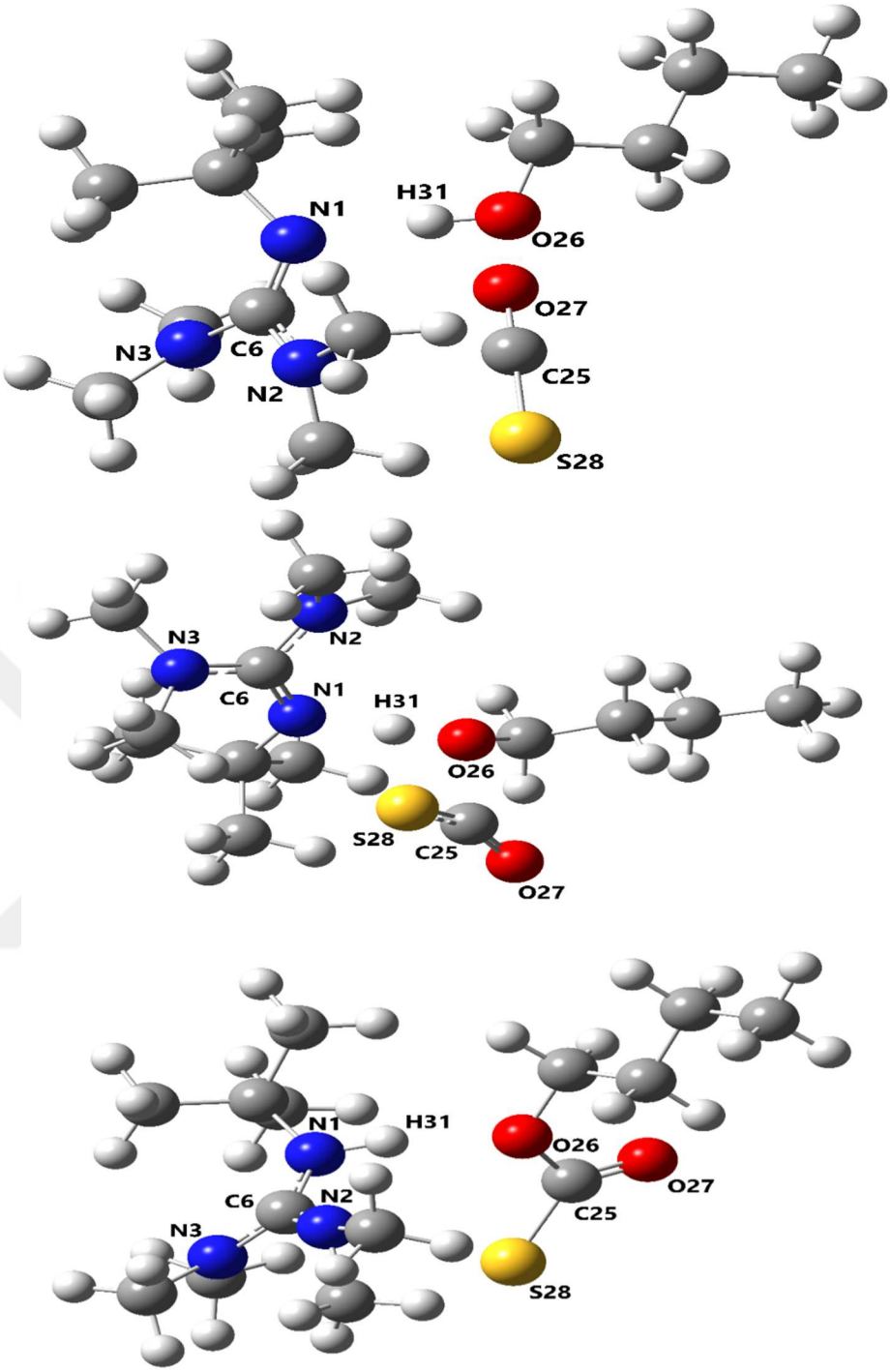

Figure 4.17. R (top), TS (middle), and P (bottom) structures of the COS/BTMG/1-butanol system.

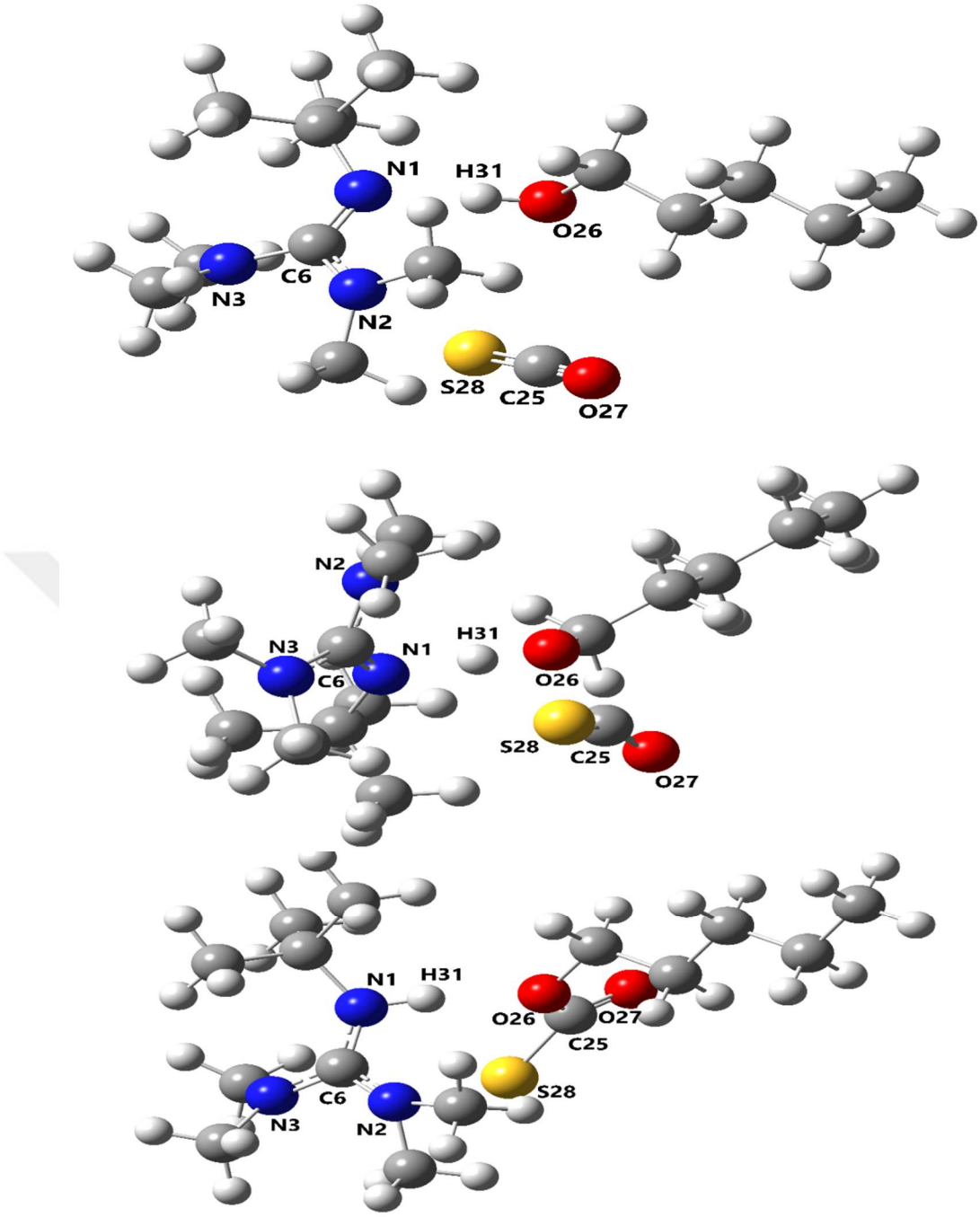

Figure 4.18. R (top), TS (middle), and P (bottom) structures of the COS/BTMG/1-pentanol system.

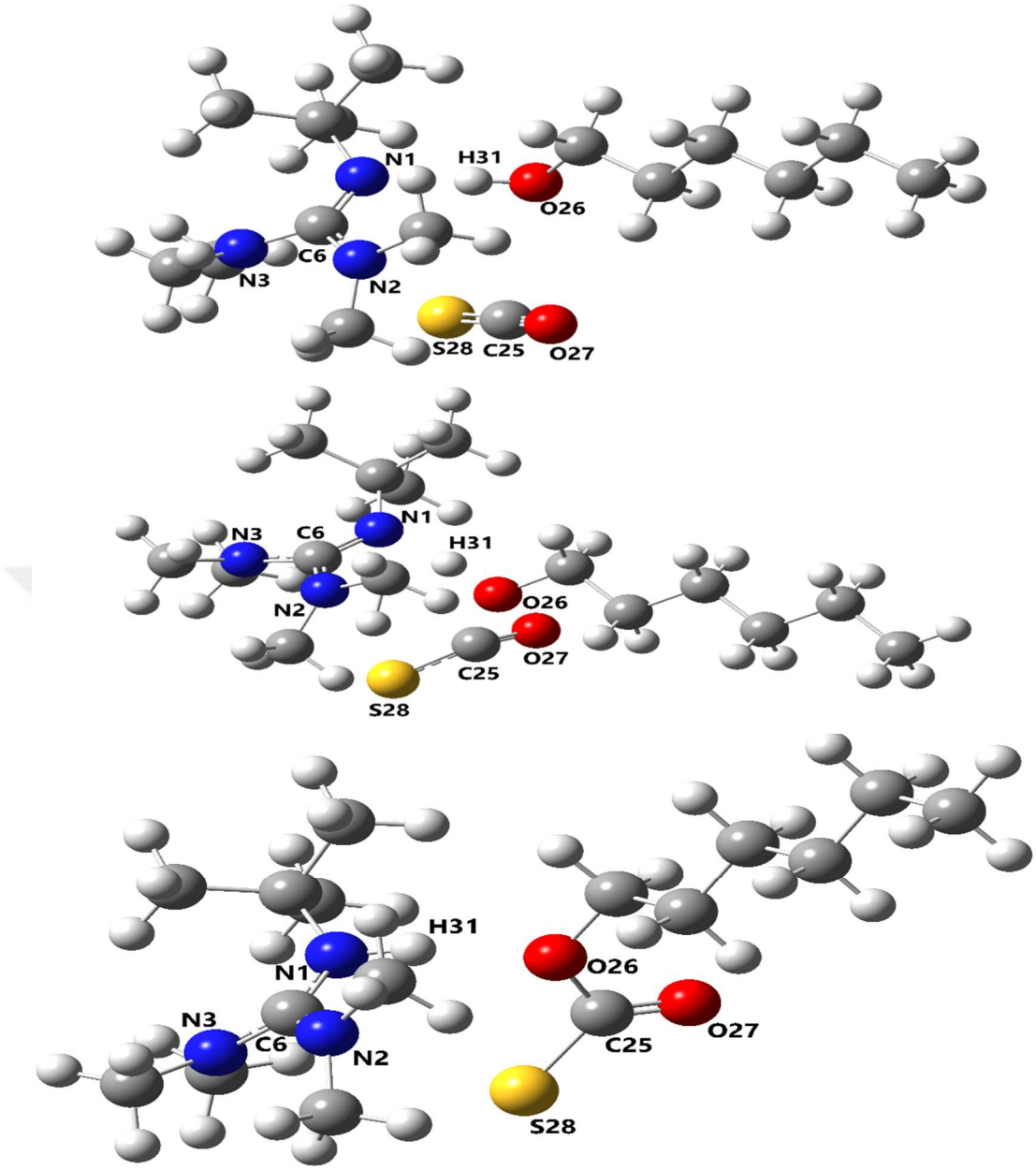

Figure 4.19. R (top), TS (middle), and P (bottom) structures of the COS/BTMG/1-hexanol system.

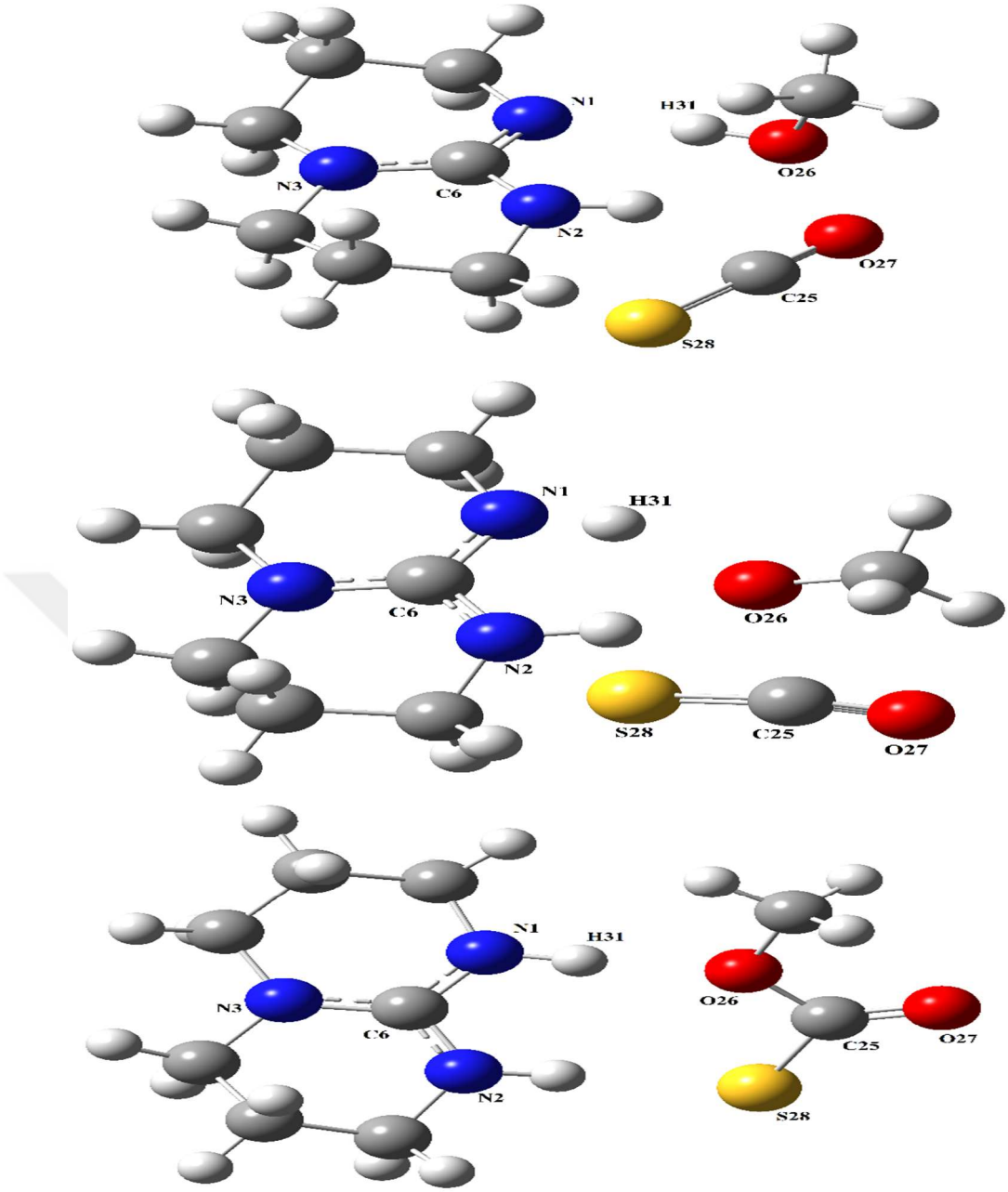

Figure 4.20. R (top), TS (middle), and P (bottom) structures of the COS/TBD/methanol system.

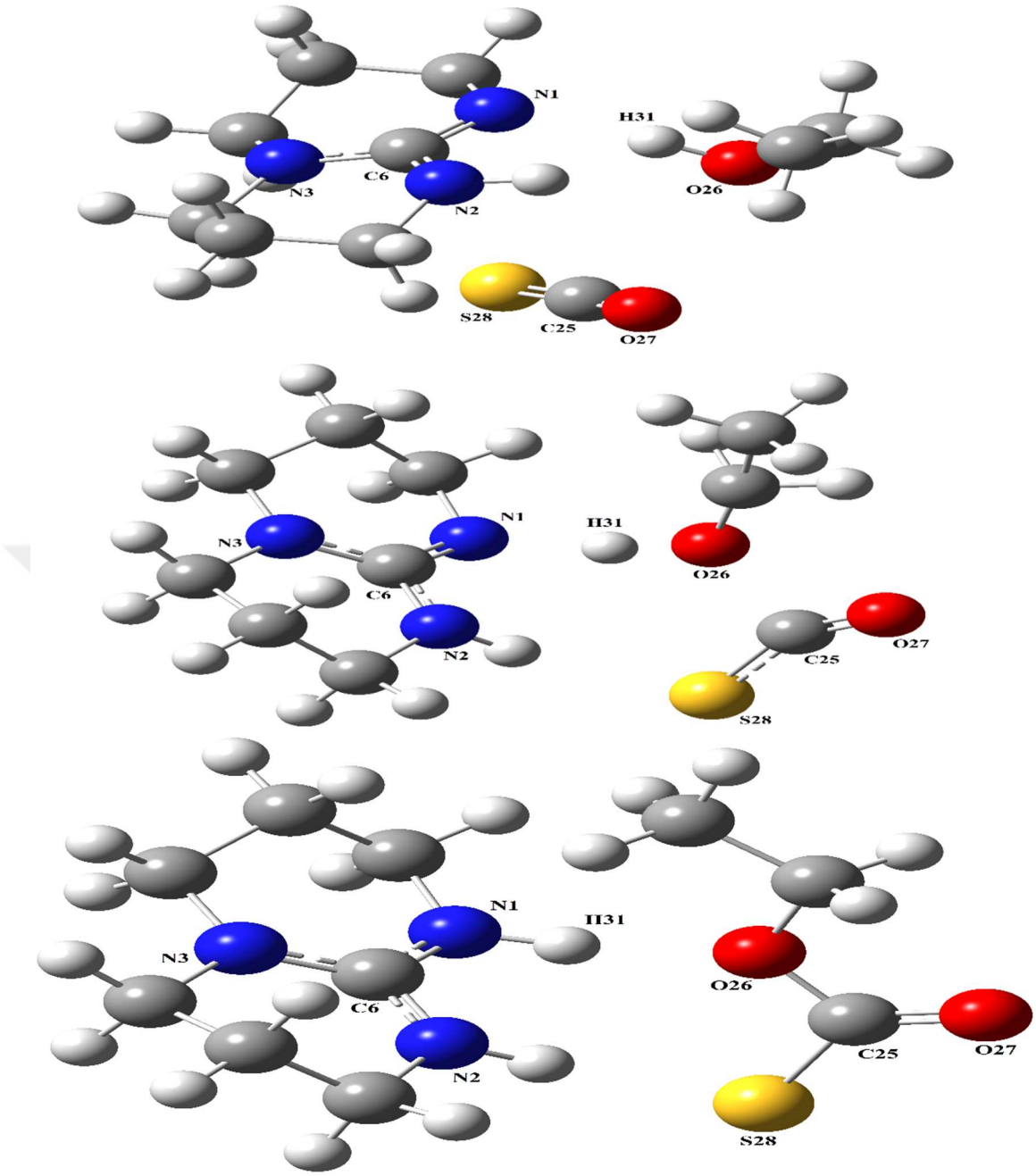

Figure 4.21. R (top), TS (middle), and P (bottom) structures of the COS/TBD/ethanol system.

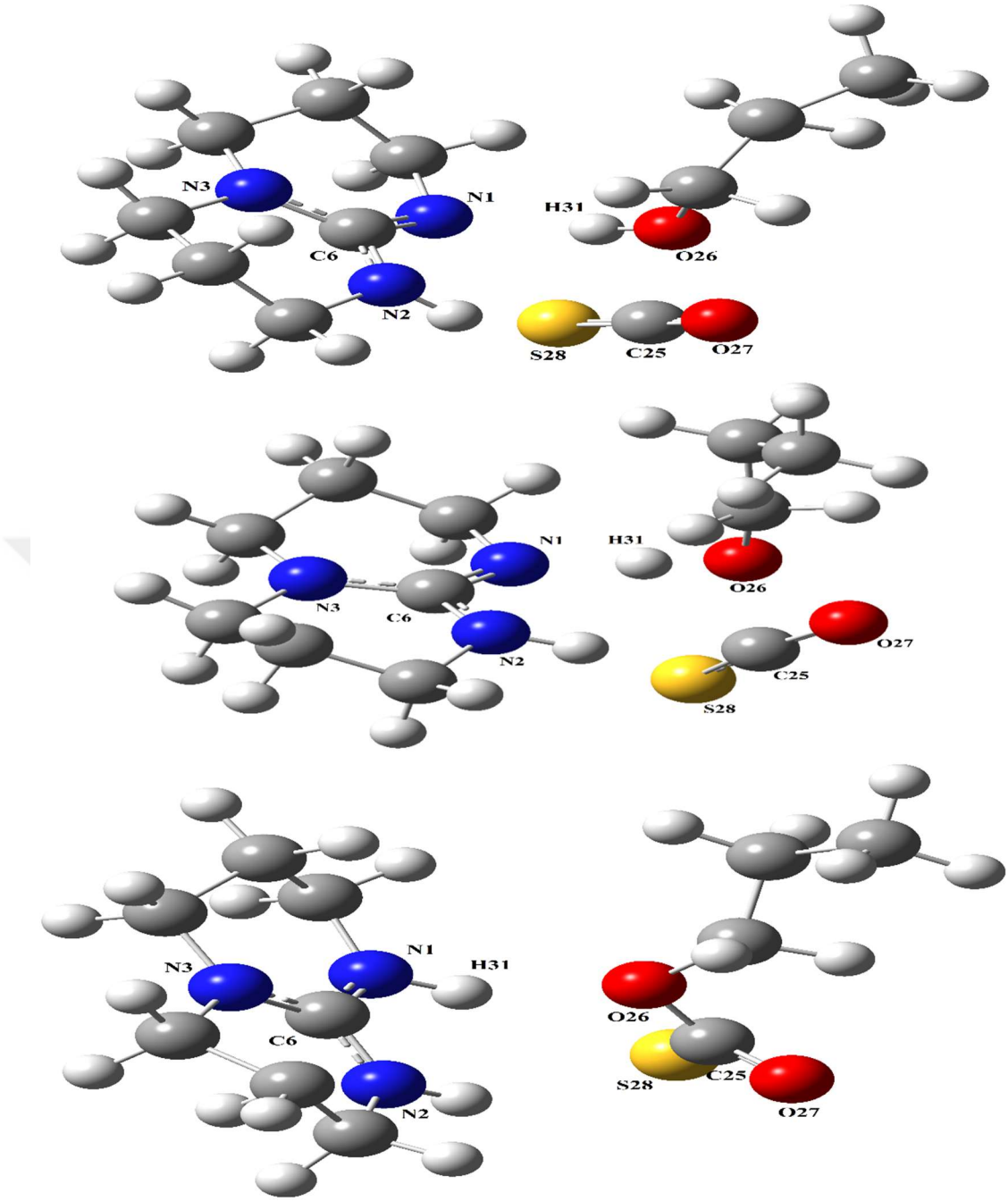

Figure 4.22. R (top), TS (middle), and P (bottom) structures of the COS/TBD/1-propanol system.

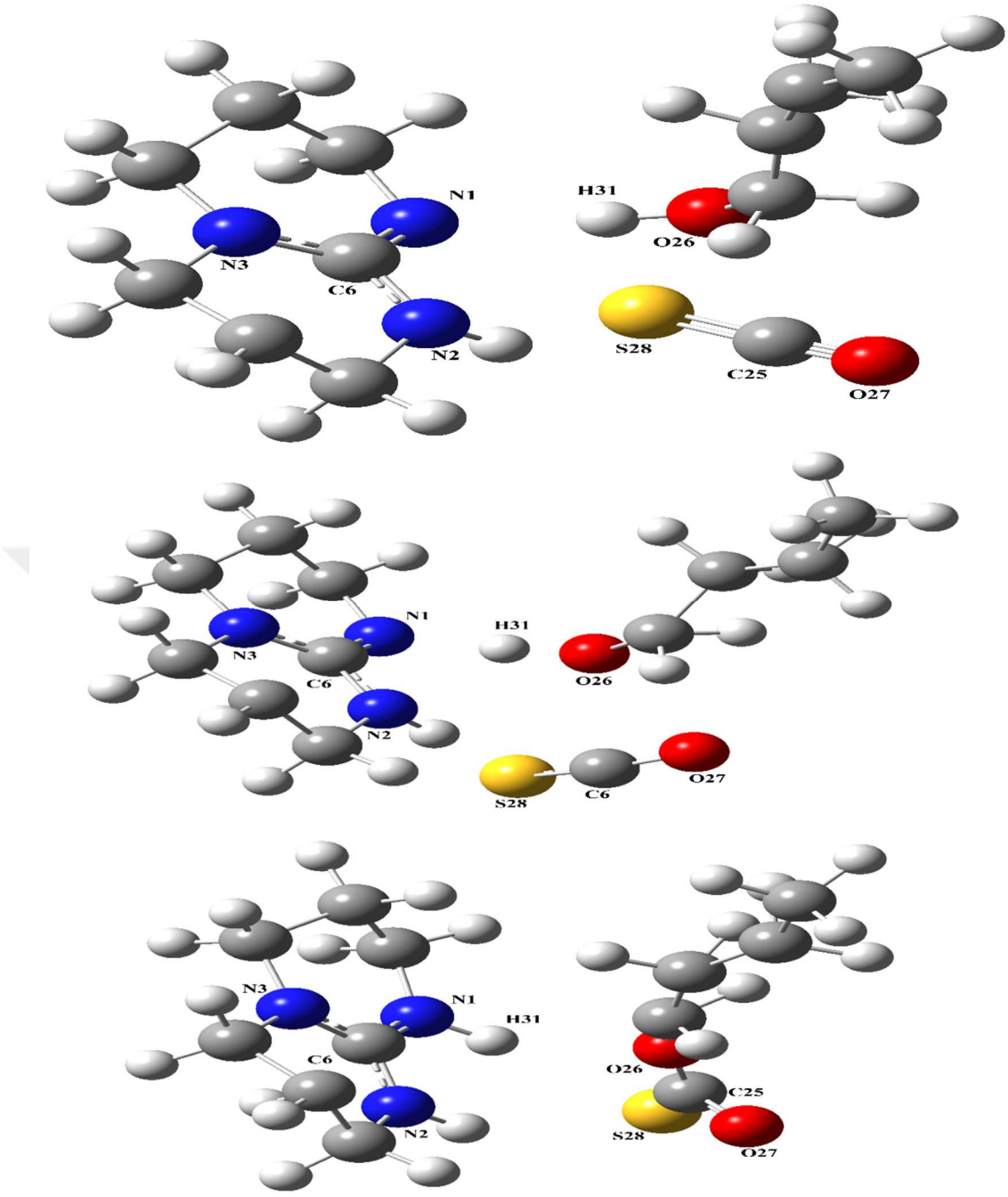

Figure 4.23. R (top), TS (middle), and P (bottom) structures of the COS/TBD/1-butanol system.

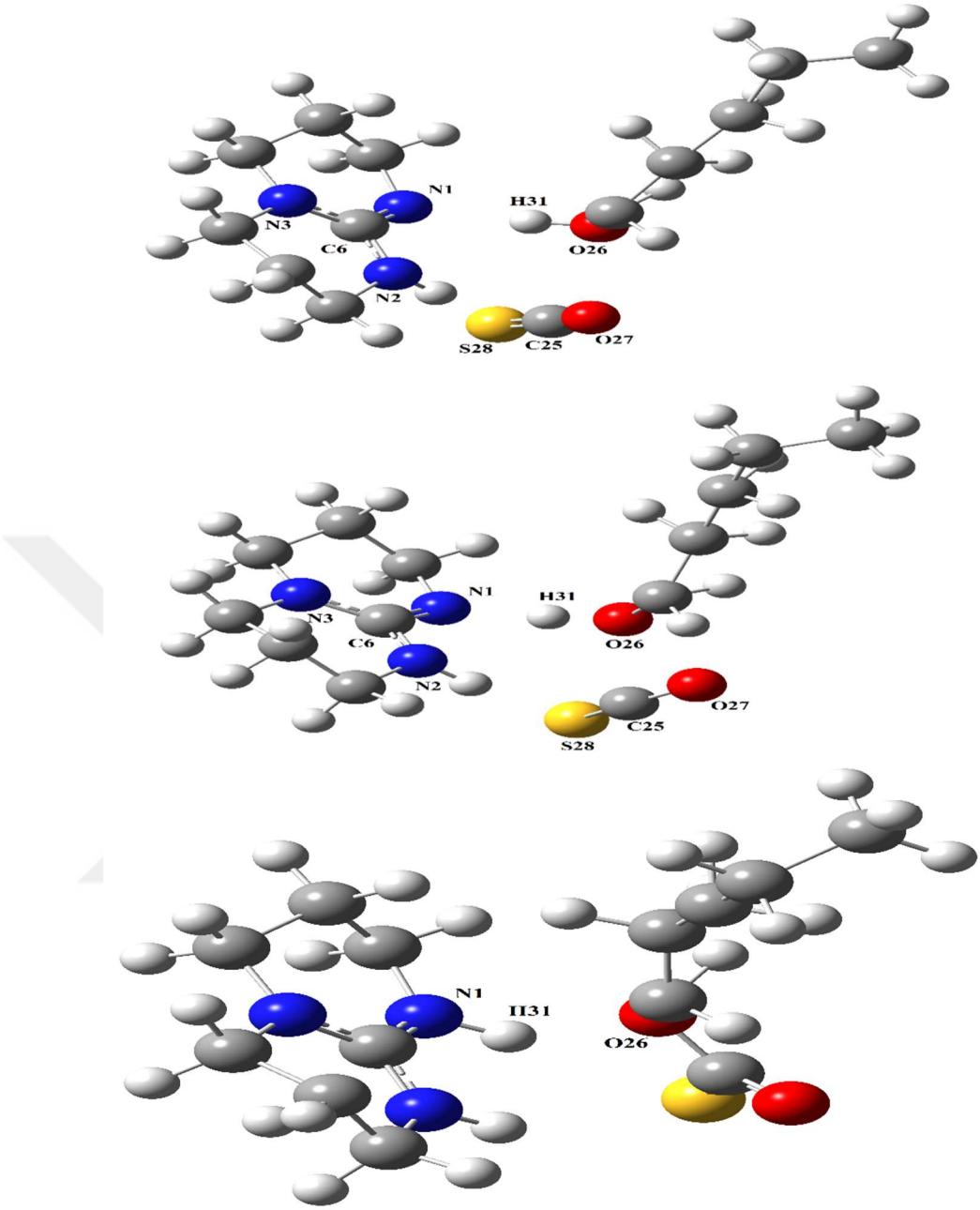

Figure 4.24. R (top), TS (middle), and P (bottom) structures of the COS/TBD/1-pentanol system.

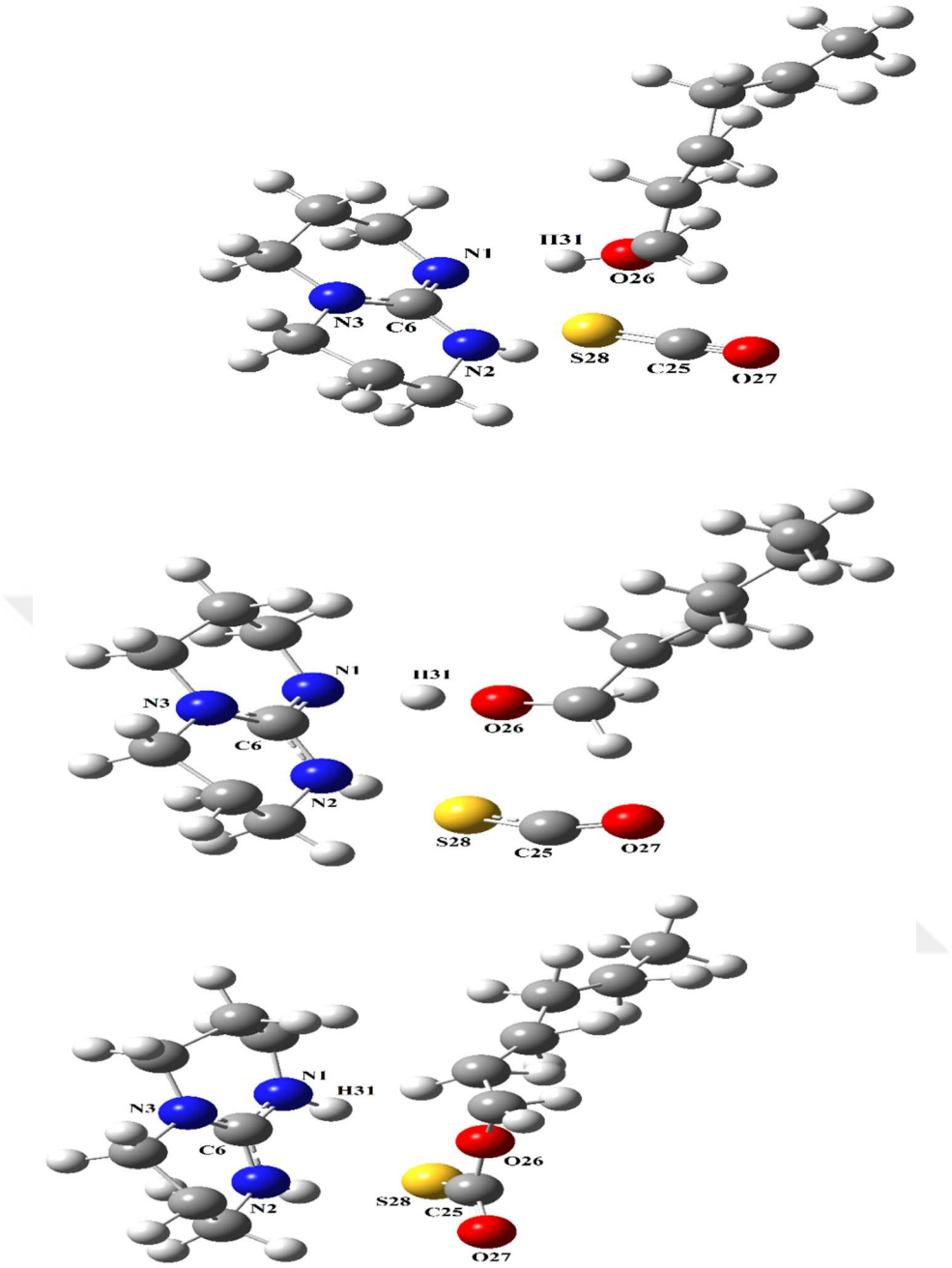

Figure 4.25. R (top), TS (middle), and P (bottom) structures of the COS/TBD/1-hexanol system.

CHAPTER 5

CONCLUSIONS

Quantum chemical calculations were performed to investigate the potential uses of twenty-four organic liquid mixture systems consist of guanidine, such as BTMG and TBD or amidine, such as DBU and DBN, bases and the linear alcohols, which included methanol, ethanol, 1-propanol, 1-butanol, 1-pentanol and 1-hexanol in the capture of COS.

These above-mentioned ωB97X-D3/6-311++G(d,p) calculations included the polarizable continuum model, which proved that the single-step termolecular reaction mechanism that was proposed herein was thermodynamically feasible. In fact, findings of this study also proved both the theoretical and experimental findings, which were obtained for capturing CO_2 with similar organic liquid mixtures mentioned in previous studies [53-55], and were also congruent with the results, i.e., B3LYP/6-31G(d), that were previously reported by Wang et al., in a theoretical study that they conducted in order to investigate the CO_2/DBU/1-propanol system [85].

Based on the findings that were obtained in the research conducted herein, the BTMG/methanol exhibited the reaction barrier that was the lowest. This meant that the organic liquid mixture that had the highest reaction rate constant is the best and the most suitable one among the twenty-four organic mixture systems for the capture of COS investigated here. After this system, the TBD/1-propanol system is the second most appropriate choice according to the theoretical findings obtained. Both ethanol and methanol showed better kinetic and thermodynamic results when DBU was used as the amidine. Moreover, 1-propanol was the most appropriate alcohol option with DBN.

RECOMMENDATIONS

In many ways, these investigations might be continued. Some suggestions for future study work are provided below.

- Modeling different systems of amines.
- Integrate the models with commercial simulation tools such as ASPEN PLUS, ASPEN HYSYS and simulate the acid gas process.
- It is extremely necessary to measure the physical characteristics of the loaded amine alcohol solutions within the temperature range of industrial applications. Few investigations on the physical properties of solvents used to remove acid gas from the process of amine-based acid.

REFERENCES

[1] A. Barreau, E. Blanchon Le Bouhelec, K. N. Habchi Tounsi, P. Mougin and F. Lecomte, "Absorption of H_2S and CO_2 in Alkanolamine Aqueous Solution: Experimental Data and Modelling with the Electrolyte-NRTL Model", *Oil & Gas Science and Technology*, vol. 61, no. 3, pp. 345–361, 2006.

[2] K. Othmer, "Metathesis" in *Encyclopedia of Chemical Technology*, vol. 26. J. Peters, Ed. New York: McGraw-Hill, 2005, pp. 920–958.

[3] F. Amararene and C. Bouallou, "Kinetics of Carbonyl Sulfide (COS) Absorption with Aqueous Solutions of Diethanolamine and Methyldiethanolamine", *Industrial and Engineering Chemistry Research*, vol. 43, no. 19, pp. 6136–6141, 2004.

[4] G. Hinderaker and O.C. Sandall, "Absorption of Carbonyl Sulfide in Aqueous Diethanolamine", *Chemical Engineering Science*, vol. 55, no. 23, pp. 5813–5818, 2000.

[5] S.C. Lee, M.J. Snodgrass, M.K. Park and O.C. Sandall, "Kinetics of Removal of Carbonyl Sulfide by Aqueous Monoethanolamine", *Environmental Science and Technology*, vol. 35, no. 11, pp. 2352–2357, 2001.

[6] F. Yan, R. Kakuchi, K. Takahashi and H.J. Kim, "CS_2 Capture in the Ionic Liquid 1-alkyl-3-methylimidazolium Acetate: Reaction Mechanism and Free Energetics", *Physical Chemistry Chemical Physics*, vol. 20, no. 29, pp. 19339–19349, 2018.

[7] P.D. Vaidya and E.Y. Kenig, "Kinetics of Carbonyl Sulfide Reaction with Alkanolamines: A review", *Chemical Engineering Journal*, vol. 148, no. 2–3. pp. 207–211, 2009.

[8] S. Francisco, N. Technical Monitor and A. Aden, (2009, Mar.), "Survey and Down-selection of Acid Gas Removal Systems for the Thermochemical Conversion of Biomass to Ethanol with A detailed Analysis of an MDEA System Task 1: Acid Gas Removal Technology Survey and Screening for Thermochemical Ethanol Synthesis." *National Renewable Energy Laboratory*, [Online], Available: http://www.osti.gov/bridge [Dec. 1, 2019].

[9] S. Bishnoi and G.T. Rochelle, “Absorption of Carbon Dioxide into Aqueous Piperazine: Reaction Kinetics, Mass Transfer and Solubility”, *Chemical Engineering Science*, vol. 55, no. 22, pp. 5531–5543, 2000.

[10] R. Cadours, D. Roquet and G. Perdu, “Competitive Absorption-desorption of Acid Gas into Water-DEA Solutions”, *Industrial and Engineering Chemistry Research*, vol. 46, no. 1, pp. 233–241, 2007.

[11] I.Kim, H.F. Svendsen and E. Børresen, “Ebulliometric Determination of Vapor-Liquid Equilibria for Pure Water, Monoethanolamine, N-methyldiethanolamine, 3-(methylamino)-propylamine, and their Binary and Ternary Solutions”, *Journal of Chemical and Engineering Data*, vol. 53, no. 11, pp. 2521–2531, 2008.

[12] Y.A. Anufrikov, G.L. Kuranov and N.A. Smirnova, “Solubility of CO_2 and H_2S in Alkanolamine-Containing Aqueous Solutions”, *Russian Journal of Applied Chemistry*, vol. 80, no. 4. pp. 515–527, 2007.

[13] H. Oediger, F. Moller and K. Eiter, “Bicyclic Amidines as Reagents in Organic Syntheses”, *Reagents for Organic Synthesis*, vol. D-5090, pp. 591–598, 1972.

[14] M.P. Coles, “Bicyclic-Guanidines, -Guanidinates and -Guanidinium Salts: Wide Ranging Applications from a Simple Family of Molecules”, *Chemical Communications*, no. 25, pp. 3659–3676, 2009.

[15] T, Ishikawa, *Superbases for Organic Synthesis: Guanidines, Amidines and Phosphazenes and Related Organocatalysts*. John Wiley & Sons, 2009.

[16] R.G.S. Berlinck A.E. Trindade-Silva and M.F.C. Santos, “The Chemistry and Biology of Organic Guanidine Derivatives”, *Natural Product Reports*, vol. 27, no. 12. pp. 1871–1907, 2010.

[17] T. Ishikawa, “Guanidine Chemistry”, *Chemical and Pharmaceutical Bulletin*, vol. 58, no. 12, pp. 1555–1564, 2010.

[18] X. Fu and C.H. Tan, “Mechanistic Considerations of Guanidine-Catalyzed Reactions”, *Chemical Communications*, vol. 47, no. 29, pp. 8210–8222, 2011.

[19] K.T. Leffek, P. Pruszynski and K. Thanapaalasingham, “Basicity of Substituted 2-phenyl-1,1,3,3-tetramethylguanidines and other Bases in Acetonitrile Solvent”, *Canadian Journal of Chemistry*, vol. 67, no. 4, 590–595, 2011.

[20] S.E. Denmark and G.L. Beutner, “Lewis Base Catalysis in Organic Synthesis”, *Angewandte Chemie - International Edition*, vol. 47, no. 9. pp. 1560–1638, 2008.

[21] S. Dong, X. Feng and X. Liu, “Chiral Guanidines and their Derivatives in Asymmetric Synthesis,” *Chemical Society Reviews*, vol. 47, no. 23, pp. 8525–8540, 2018.

[22] N. Ghosh, “DBU (1,8-diazabicyclo[5.4.0]undec-7-ene) - A nucleophillic Base”, *Synlett*, no. 3, pp. 574–575, 2004.

[23] R.J. Ferm, “The Chemistry of Carbonyl Sulfide”, *Chemical Reviews*, vol. 57, no. 4, pp. 621–640, 1957.

[24] E. Wilhelm, R. Battino and R.J. Wilcock, “Low-Pressure Solubility of Gases in Liquid Water”, *Chemical Reviews*, vol. 77, no. 2, pp. 219–262, 1977.

[25] J.S. Muenter, “Electric Dipole Moment of Carbonyl Sulfide”, *Journal of Chemical Physics*, vol. 48, no. 10, pp. 4544–4547, 1968.

[26] P.L. Hanst, L.L. Spiller, D.M. Watts, J.W. Spence and M.F. Miller, “Infrared Measurement of Fluorocarbons, Carbon Tetrachloride, Carbonyl Sulfide, and other Atmospheric Trace Gases”, *Journal of the Air Pollution Control Association*, vol. 25, no. 12, pp. 1220–1226, 1975.

[27] M. Chin and D.D. Davis, “A reanalysis of Carbonyl Sulfide as A source of Stratospheric Background Sulfur Aerosol”, *Journal of Geophysical Research: Atmospheres*, vol. 100, no. D5, pp. 8993–9005, 1995.

[28] M.A.K. Khalil and R.A. Rasmussen, “Atmospheric Methane in the Recent and Ancient Atmospheres' Concentrations, Trends, and Interhemispheric Gradient”, *Journal of Geophysical Research: Atmospheres*, vol. 89, no. D7, pp. 599–605, 1984.

[29] N. Hewitt and B.M. Davison, “The lifetimes of Organosulphur Compounds in the Troposphere”, *Applied Organometallic Chemistry*, vol. 2, no. 5, pp. 407–415, 1988.

[30] D.J. Kleber, J. Jiao, R.P. Kiene and T.S. Bates, “Impact of Dimethyl Sulfide Photochemistry on Methyl Sulfur Cycling in the Equatorial Pacific Ocean”, *Journal of Geophysical Research C: Oceans*, vol. 101, no. C2, pp. 3715–3722, 1996.

[31] L.M. Goshman, R.P. Smith, and H.C. Hodge, *Clinical Toxicology of Commercial Products*, 5th ed., vol. 74. Published by Elsevier Inc., 1985.

[32] R. Houriet and D. Louvier, "Emission of Toxic Sulfur Gases from Polymers Coming in Contact with Food Products and with Infants", *Analusis*, vol. 27, no. 4, pp. 369–372, 1999.

[33] W. Braker and A. Mossman, *Matheson Gas Data Book*. East Rutherford, NJ, 1971, pp. 574.

[34] P.D.N. Svoronost and T.J. Bruno, "Carbonyl Sulfide: A review of its Chemistry and Properties", *Industrial and Engineering Chemistry Research*, vol. 41, no. 22. pp. 5321–5336, 2002.

[35] M. von Hobe, T. Kenntner, F.H. Helleis, L. Sandoval-Soto and M.O. Andreae, "Cryogenic Trapping of Carbonyl Sulfide without Expendable Cryogens", *Analytical Chemistry*, vol. 72, no. 21, pp. 5513–5515, 2000.

[36] W.R. Ernst, M.S.K. Chen and D.L. Mitchell, "Hydrolysis of Carbonyl Sulfide: Comparison to Reactions of Isocyanates", *Canadian Journal of Chemical Engineering*, vol. 68, no. 2, pp. 319–323, 1990.

[37] E. Alper and W. Bouhamra, "Kinetics and Mechanism of the Reaction Between Carbonyl Sulphide and Primary and Secondary Amines in Aqueous Solutions", *Doga Turkish Journal of Chemistry*, vol. 17, pp. 7–7, 1993.

[38] S.C. Lee, M.J. Snodgass, M.K. Park and O.C. Sandall, "Kinetics of Removal of Carbonyl Sulfide by Aqueous Methanolamine", *Environmental Science and Technology*, vol. 35, pp. 2352, 2001.

[39] R. Rivera-Tinoco and C. Bouallou, "Reaction kinetics of Carbonyl Sulfide (COS) with Diethanolamine in Methanolic Solutions", *Industrial and Engineering Chemistry Research*, vol. 47, no. 19, pp. 7375–7380, 2008.

[40] M.M. Sharma, "Kinetics of Reactions of Carbonyl Sulphide and Carbon Dioxide with Amines and Catalysis by Bronsted Bases of the Hydrolysis of COS", *Transactions of the Faraday Society*, vol. 61, pp. 681–688, 1965.

[41] R.J. Littel, G.F. Versteeg and W.P.M. van Swaaij, "Kinetics of COS Amines with Primary and Secondary in Aqueous Solutions", *AIChE Journal*, vol. 38, no. 2, pp. 244–250, 1992.

[42] M. Singh and J.A. Bullin, “Determination of Rate Constants for the Reaction Between Diglycolamine and Carbonyl Sulphide”, *Gas Separation and Purification*, vol. 2, no. 3, pp. 131–137, 1988.

[43] H.A. Al-Ghawas, G. Ruiz-Ibanez and O.C. Sandall, “Absorption of Carbonyl Sulfide in Aqueous Methyldiethanolamine”, *Chemical Engineering Science*, vol. 44, no. 3, pp. 631–639, 1989.

[44] R.J. Littel, G.F. Versteeg and Wim P.M. van Swaaij, “Kinetic Study of COS with Tertiary Alkanolamine Solutions. 1. Experiments in an Intensely Stirred Batch Reactor”, *Industrial and Engineering Chemistry Research*, vol. 31, no. 5, pp. 1262–1269, 1992.

[45] R.J. Littel, G.F. Versteeg and W.P.M. van Swaaij, “Kinetic Study of COS with Tertiary Alkanolamine Solutions. 2. Modeling and Experiments in A stirred Cell Reactor”, *Industrial and Engineering Chemistry Research*, vol. 31, no. 5, pp. 1269–1274, 1992.

[46] E. Alper, M. Al-Roweih and W. Bouhamra, “Reaction Kinetics of COS with Primary and Secondary Amines in Alcoholic Solutions”, *Chemical Engineering Journal and Biochemical Engineering Journal*, vol. 55, no. 1–2, pp. 53–59, 1994.

[47] P.D. Vaidya and E.Y. Kenig, “Kinetics of Carbonyl Sulfide Reaction with Alkanolamines: A review”, *Chemical Engineering Journal*, vol. 148, no. 2–3, pp. 207–211, 2009.

[48] M. Caplow, “Kinetics of Carbamate Formation and Breakdown”, *Journal of the American Chemical Society*, vol. 90, no. 24, pp. 6795–6803, 1968.

[49] P.V. Danckwerts, “The Reaction of CO_2, with Ethanolamines”, *Chemical Engineering Science*, vol. 34, no. 4, pp. 443–446, 1979.

[50] E. Alper and W. Bouhamra, “Reaction Kinetics of Carbonyl Sulfide with Aqueous Ethylenediamine and Diethylenetriamine”, *Gas Separation and Purification*, vol. 8, no. 4, pp. 237–240, 1994.

[51] E. Alper, “Reaction Mechanism and Kinetics of Aqueous Solutions of 2-amino-2 methyl-1,3-propanediol and Carbonyl Sulphide”, *Turkish Journal of Chemistry*, vol. 25, no. 2, pp. 209–214, 2001.

[52] J.E. Crooks and J.P. Donnellan, “Kinetics and Mechanism of the Reaction Between Carbon Dioxide and Amines in Aqueous Solution”, *Chemical Engineering Science*, vol. 45, no. 12, pp. 3407–3415, 1990.

[53] H. Tankal, O.Y. Orhan, E. Alper, T. Ozdoğan and H. Kayi, “Experimental and Theoretical Investigation of the Reaction Between CO_2 and Carbon Dioxide Binding Organic Liquids”, *Turkish Journal of Chemistry*, vol. 40, no. 5, pp. 706–719, 2016.

[54] O.Y. Orhan, H. Tankal, H. Kayi and E. Alper, “Kinetics of CO_2 Capture by Carbon Dioxide Binding Organic Liquids: Experimental and Molecular Modelling Studies”, *International Journal of Greenhouse Gas Control*, vol. 49, pp. 379–386, 2016.

[55] O.Y. Orhan, H. Tankal, H. Kayi and E. Alper, “Innovative Carbon Dioxide-Capturing Organic Solvent: Reaction Mechanism and Kinetics”, *Chemical Engineering and Technology*, vol. 40, no. 4, pp. 737–744, 2017.

[56] S. Miertus, E. Scrocco and J. Tomasi, “Electrostatic Interaction of A solute with Acontinuum. A direct Utilizaion of AB initio Molecular Potentials for the Prevision of Solvent Effects”, *Chemical Physics*, vol. 55, no. 1, pp. 117–129, 1981.

[57] S. Miertus and J. Tomasi, “Approximate Evaluations of the Electrostatic Free Energy and Internal Energy Changes in Solution Processes”, *Chemical Physics*, vol. 65, no. 2, pp. 239–245, 1982.

[58] J.L. Pascual-Ahuir, E. Silla and I. Tunon, “GEPOL: An Improved Description of Molecular Surfaces. 111. A new Algorithm for the Computation of A solvent-excluding Surface”, *Journal of Computational Chemistry*, vol. 15, no. 10, pp. 1127–1138, 2004.

[59] E.F. da Silva and H.F. Svendsen, “Computational Chemistry Study of Reactions, Equilibrium and Kinetics of Chemical CO_2 Absorption”, *International Journal of Greenhouse Gas Control*, vol. 1, no. 2, pp. 151–157, 2007.

[60] C.J. Cramer, *Essentials of Computational Chemistry: Theories and Models*. John Wiley & Sons, 1961, pp. 581.

[61] R.D. Crouch, “The Molecular Modeling Workbook for Organic Chemistry (by Warren J. Hehre, Alan J. Shusterman, and Janet E. Nelson)”, *Journal of Chemical Education*, vol. 76, no. 9, pp. 1193, 1999.

[62] F. Jensen, *Introduction to Computational Chemistry*. Wiley, 2016, pp. 664.

[63] R.G. Parr, "Density Functional Theory of Atoms and Molecules", In: Fukui K., Pullman B. (eds) Horizons of Quantum Chemistry. *Académie Internationale Des Sciences Moléculaires Quantiques / International Academy of Quantum Molecular Science*, vol 3. Springer, Dordrecht. 1980.

[64] W. Koch and M.C. Holthausen, *A chemist's Guide to Density Functional Theory*. Wiley-VCH, 2001.

[65] E.F. da Silva, "Computational Chemistry Study of Solvents for Carbon Dioxide Absorption." Ph.D. thesis, *Fakultet for Naturvitenskap Og Teknologi*, 2005.

[66] J.A. Pople and R.K. Nesbet, "Self-consistent Orbitals for Radicals" *Journal of Chemical Physics*, vol. 22, no. 3. pp. 571–572, 1954.

[67] S. Bell, T.J. Dines, B.Z. Chowdhry and R. Withnall, (2007, Aug.) "Computational Chemistry using Modern Electronic Structure Methods", *Journal of Chemical Education,* [Online], 84(8), pp. 1364–1370. Available: www.JCE.DivCHED.org [Dec. 1, 2020].

[68] I.N. Levine, *Quantum Chemistry*. Prentice Hall, 2000, pp. 739–1564.

[69] P. Hohenberg and W. Kohn, "Inhomogeneous Electron Gas," *Physical Review*, vol. 136, pp. B864–B871, 1964.

[70] W. Kohn and L.J. Sham, "Self-consistent Equations Including Exchange and Correlation Effects," *Physical Review*, vol. 140, pp. A1133–A1138, 1965.

[71] H. Jacobsen and L. Cavallo, "Directions for use of Density Functional Theory: A short Instruction Manual for Chemists," in *Handbook of Computational Chemistry*, Springer International Publishing, pp. 225–267, 2017.

[72] J.D. Whitfield, "At the Intersection of Quantum Computing and Quantum Chemistry." Ph.D. thesis, Cambridge, Massachusetts, 2011.

[73] W.J. Hehre, R.F. Stewart and J.A. Pople, "Self-consistent Molecular-orbital Methods. I. Use of Gaussian Expansions of Slater-type Atomic Orbitals," *The Journal of Chemical Physics*, vol. 51, no. 6, pp. 2657–2664, 1969.

[74] A.D. McLean and G.S. Chandler, “Contracted Gaussian Basis Sets for Molecular Calculations. I. Second Row Atoms, Z=11-18,” *The Journal of Chemical Physics*, vol. 72, no. 10, pp. 5639–5648, 1980.

[75] T.H. Dunning, “Gaussian Basis Sets for use in Correlated Molecular Calculations. I. The Atoms Boron Through Neon and Hydrogen,” *The Journal of Chemical Physics*, vol. 90, no. 2, pp. 1007–1023, 1989.

[76] A.D. Becke, “Density-functional Exchange-energy Approximation with Correct Asymptotic Behavior,” *Physical Review. A, General Physics*, vol. 38, no. 6, pp. 3098–3100, 1988.

[77] C. Lee, W. Yang and R.G. Parr, “Development of the Colic-salvetti Correlation-energy Formula into A functional of the Electron Density,” *Physical Review B: Condensed Matter*, vol. 37, no. 2, pp. 785–789, 1988.

[78] A.D. Becke, “Density-functional Thermochemistry. III. The Role of Exact Exchange,” *The Journal of Chemical Physics*, vol. 98, pp. 5648–5652, 1993.

[79] J.P. Perdew, P. Ziesche and H. Eschrig, “*Electronic Structure of Solids’ 91*”, vol. 11. Berlin: Akademie Verlag, 1991.

[80] L. Goerigk, A. Hansen, C. Bauer, S. Ehrlich, A. Najibi and S. Grimme, “A look at the Density Functional Theory Zoo with the Advanced GMTKN55 Database for General Main Group Thermochemistry, Kinetics and Noncovalent Interactions,” *Physical Chemistry Chemical Physics*, vol. 19, no. 48, pp. 32184–32215, 2017.

[81] R. Krishnan, J.S. Binkley, R. Seeger and J.A. Pople, “Self-consistent Molecular Orbital Methods. XX. A basis Set for Correlated Wave Functions,” *The Journal of Chemical Physics*, vol. 72, no. 1, pp. 650–654, 1980.

[82] M.J. Frisch, G.W. Trucks, H.B. Schlegel, G.E. Scuseria, M.A. Robb, J.R. Cheeseman et al., “Gaussian 09, Revision D. 01.” Gaussian, Inc.: Wallingford CT, 2009.

[83] R. Dennington, T. Keith and J. Millam, “GaussView, Version 5.0.9.” Semichem Inc.: Shawnee Mission KS, 2009.

[84] P. Venkateswarlu and W. Gordy, “Methyl Alcohol. II. Molecular Structure,” *The Journal of Chemical Physics*, vol. 23, no. 7, pp. 1200–1202, 1955.

[85] Y. Wang, Q. Han and H. Wen, “Theoretical Discussion on the Mechanism of Binding CO_2 by DBU and Alcohol,” *Molecular Simulation*, vol. 39, no. 10, pp. 822–827, 2013.

[86] R.S. Mulliken, “Electronic Population Analysis on LCAO-MO Molecular Wave Functions. II. Overlap Populations, Bond Orders, and Covalent Bond Energies,” *The Journal of Chemical Physics*, vol. 23, no. 10, pp. 1841–1846, 1955.

[87] F.L. Hirshfeld, “Bonded-atom Fragments for Describing Molecular Charge Densities,” *Theoretica Chimica Acta*, vol. 44, no. 2, pp. 129–138,1977.

[88] A. Galliot, A. Gil and M.J. Calhorda, “Effects of the Oxygenation in the Intercalation of 1,10-phenanthroline-5,6/4,7-dione between DNA Base Pairs: Acomputational Study,” *Physical Chemistry Chemical Physics*, vol. 19, pp. 16638–16649, 2017.

[89] H. Eyring, “The Activated Complex in Chemical Reactions,” *The Journal of Chemical Physics*, vol. 3, no. 2, pp. 107–115, 1935.

[90] M.I. Cabaço, M. Besnard, F.V. Chávez, N. Pinaud, P.J. Sebastião, J.A. Coutinho et al., “Understanding Chemical Reactions of CO_2 and its Isoelectronic Molecules with 1-butyl-3-methylimidazolium Acetate by Changing the Nature of the Cation: The Case of CS2 in 1-butyl-1-methylpyrrolidinium Acetate Studied by NMR Spectroscopy and Density Functional Theory Calculations,” *Journal of Chemical Physics*, vol. 140, no. 24, 2014.

APPENDICES

Appendix A: Thermochemistry Calculations

Free Energy of the Reaction:

The free energies of the reactions can be determined by the deduction of the sum of the free energies of the reactants from the sum of the free energies of the products.

The free energies can be calculated for each chemical species within the model based on the frequencies of the resulting optimized species. This is derived from the thermochemical portion of the outputs.

$$\Delta G^{\circ}_{rxn} = [\Delta G_{(products)}] - [\Delta G_{(reactants)}]$$

Free Energy of Activation:

The free energies of the activation ($\Delta^{\neq}G^{o}$) are determined from the difference in the free energies of the reactants and the transition state. The free energies can be measured from the frequency calculations of the optimized individual chemical species, as well as the TS. All of the computations are performed using the same algorithm mentioned above.

$$\Delta^{\neq}G^{\circ} = [\Delta G_{(transition\ state)}] - [\Delta G_{(reactants)}]$$

Using the value of the free energy of the activation in the Eyring equation, the rates for the reaction from the ground state to the activated state can be easily determined. This allows for the measurement of the concentration of the products formed by the reaction in the reaction rate constants.

Activation Energy:

The activation energies are determined by deduction of the free electronic energies of the individual reactants, and the electronic energies of the transition state.

$$\Delta E^{\neq} = [\Delta E_{(transition\ state)}] - [\Delta E_{(reactants)}]$$